The tidal streams in southern Start Bay.

Perring, M. E.

Award date:
1976

Awarding institution:
University of Bath

THE TIDAL STREAMS IN SOUTHERN START BAY

submitted by MICHAEL EDWIN PERRING

for the degree of Ph.D.

of the University of Bath

1976.

M Perring

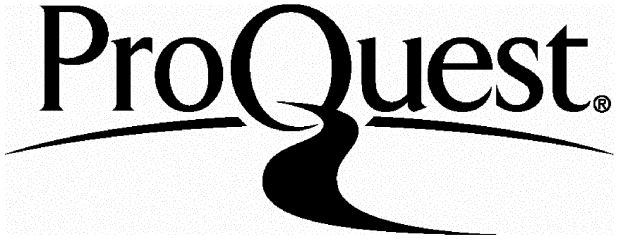

ERRATA

page 12, line 13 should read ...
"the direction readings emanating from the 'compass-carrying' Braystoke"

page 18, line 8 should read ...
"give the time of recording. (The receiving apparatus is shown in figures"

page 25, line 12 should read ...
"speed in metres per second."

page 25, line 22 should read ...
"minute interval, for each sensor, and then forming the arithmetic mean of"

page 26, line 18 should read ...
"current speed and direction emanating from all the positions where data is"

page 34, line 21 should read ...
"transformations 4.3.1 to overcome the effects of tidal range upon the time-"

page 35, line 5 should read ...
" $t_3 = -0.41\ Z + 4.52$ hours"

page 36, line 23 should read ...
"to a tidal range of 3.6 metres (broken curve). Sea-trial data collected at"

page 39, line 16 should read ...
"from that of Acton in that the concept of a principal axis has not been"

page 48, last line should read ...
"s' will be of order unity."

page 60, line 5 should read ...
"shown in the bottom right of figure 7.1. This enabled the water level to be"

page 61, line 10 should read ...
"to the unidirectional and uniform water flow. For each of the five incident"

page 63, line 5 should read ...
"given in the last column."

page 65, table 7.2
The model predicted value for position N should be " <0.40 m/s"

page 70, table 7.4
The model predicted value for position N should be " <0.40 m/s"

page 72, line 19 should read ...
"scale both the dependant and independant variables. The empirical"

page 80, last line should read ...
"is reduced considerably if not virtually eliminated."

page 98, line 14 should read ...
"HYDROGRAPHER, The (1942). English and Bristol Channels, pocket tidal"

SUMMARY

The work presented in this thesis concerns the procuring of maps of the tidal streams in southern Start Bay, a region of particular interest as the existence of the shallow Skerries Bank results in considerable variation of the water depth in the area.

The first step taken towards achieving this intention involves the accumulation, by sea-trials, of considerable sea-trial data. For this data (collected at different times and therefore different states of the tide) to be compared, empirical relationships are presented to allow all tidal stream results to be adjusted to refer to a chosen reference spring tidal range.

Use is then made of these comparisons to deduce the approximate hydrodynamic equations describing the tidal flow over the region, taken as a whole. In the light of these equations, an argument against employing mathematical modelling as a means of obtaining the tidal stream maps in this particular region is put forward.

Instead of mathematical modelling, a simple hydraulic model is used and it's predictive results are presented in cartographic form. The resulting maps are compared to sea-trial data and discussed.

Finally, the results emanating from this work are summarized, conclusions drawn from them and some suggestions made for future work.

THE TIDAL STREAMS IN SOUTHERN START BAY

submitted by MICHAEL EDWIN PERRING

for the degree of Ph.D.

of the University of Bath

1976.

M Perring

SUMMARY

The work presented in this thesis concerns the procuring of maps of the tidal streams in southern Start Bay, a region of particular interest as the existence of the shallow Skerries Bank results in considerable variation of the water depth in the area.

The first step taken towards achieving this intention involves the accumulation, by sea-trials, of considerable sea-trial data. For this data (collected at different times and therefore different states of the tide) to be compared, empirical relationships are presented to allow all tidal stream results to be adjusted to refer to a chosen reference spring tidal range.

Use is then made of these comparisons to deduce the approximate hydrodynamic equations describing the tidal flow over the region, taken as a whole. In the light of these equations, an argument against employing mathematical modelling as a means of obtaining the tidal stream maps in this particular region is put forward.

Instead of mathematical modelling, a simple hydraulic model is used and it's predictive results are presented in cartographic form. The resulting maps are compared to sea-trial data and discussed.

Finally, the results emanating from this work are summarized, conclusions drawn from them and some suggestions made for future work.

ERRATA AND ADDENDA

In Figure Appendix 1.1, Braystroke should read Braystoke.

During the preparation of this thesis, the Unit of Coastal Sedimentation at Taunton has become the Institute of Oceanographic Sciences (Taunton).

ACKNOWLEDGEMENTS

The author would first like to thank Professor W D Chesterman, Head of School during this work, and Dr J R Acton for providing the initial impetus for this work. To Dr J R Acton a special debt is owed. As supervisor his constant enthusiasm and advice has proved invaluable.

Many thanks are extended to the Captain, Britannia Royal Naval College, Dartmouth for providing the facilities which made many of the sea-trials possible. A special mention must be made of the kindness of Mr J Barlee, Oceanographer at the College, who gave generously of his leisure time and experience to assist in many of the initial sea-trials.

For providing the author with ship time on many occasions, Dr J Hails, Unit of Coastal Sedimentation, Taunton, is most gratefully thanked.

The Ministry of Agriculture, Fisheries and Food, Trinity House, The Department of Trade and Industry, The Chamber of Shipping and The Royal Yachting Association's agreement to allow the author's unconventional anchored system to be laid in Start Bay is gratefully acknowledged. In particular, many thanks are extended to Mr Williams, Plymouth, and Mr Worden, Brixham - local representatives for the Ministry of Agriculture, Fisheries and Food - for their advice and help in ensuring that the author's sea-trials in no way interfered with the local fisherman's livelihood.

For allowing their lighthouse at Start Point to be used as a receiving station, the author gratefully thanks Trinity House. The active assistance of Mr Smith, head lighthouse keeper, and his companions is gratefully acknowledged.

To the fisherman at Hallsands, who actively helped in some of the sea-trials (notably the first sea-trial conducted on the shallow and exposed Skerries Bank) and conveyed knowledge gained from a lifetime's experience of fishing in southern Start Bay, a great debt is owed.

Thanks are also due to members of the Physics staff who have given generously of their time and help: Mr Brian Ring, Chief Technician; Mrs C M Dyer, Mr Brian Gay, Mr Richard Curtis and other members of the Geophysics Group.

The writer gratefully acknowledges the assistance of the University Computer Unit, under it's Director, Dr A Nicholls, and the staff of the University Library.

Finally, he is deeply indebted to Janet Musson who has typed this thesis with great skill and much patience.

CONTENTS

CHAPTER 1 INTRODUCTION

Start Bay, in southern Devon, has a considerable history of scientific investigation.

The first published paper concerning scientific work performed in this bay appears to be that of Pengelly (1869). During severe winter storms, sand is removed from the beach at Blackpool by the action of the breaking waves. Pengelly observed that occasionally, after such storms, semi-fossilised remains of an ancient forest, submerged when the sea level rose after the last ice-age, were visible.

In 1897, during the building of Devonport dockyards, it was found necessary to acquire vast quantities of shingle. Attention was turned to the sea in an effort to locate such a supply. The foreshore at Hallsands appeared an admirable supply ground, for it was argued that the relatively small quantity of shingle removed would soon be replenished by the sea's 'infinite' storehouse.

Amongst others Hansford Worth, a noted scientist of the time, argued against this; his argument being that the sea would not replenish the shingle removed. This would, in turn, endanger the fishing village of Hallsands itself. However, despite objections, a local contractor obtained permission from the Board of Trade in 1897 to exploit this ready supply of shingle. This exploitation ended in 1902 but by this time nearly half a million cubic yards of shingle had been removed. A survey of the beach level two years later (Hansford Worth 1904) showed that Hallsands beach had been lowered by as much as twelve feet throughout it's length. A subsequent survey (Hansford Worth 1909) showed little change in this situation.

It was in January 1917 that the folly of this removal of shingle became tragically apparent. A severe north easterly gale, coinciding with a spring tidal high water, resulted in mountainous swell with waves

exceeding 30 feet in height. These waves, upon approaching Hallsands, finding the natural defences drastically lowered, smashed their way into the village. The result was almost total destruction of this village and worse, tragic loss of life.

A third survey of Hallsands beach, carried out by Hansford Worth (1923) showed the beach to have suffered even greater reduction in elevation. In 1956, Robinson (1961) resurveyed this beach using Hansford Worth's transients. His findings showed that little increase in elevation had taken place since Hansford Worth's investigations. Indeed, in some parts, the beach had become even lower.

The tidal streams in Start Bay came under investigation - by the Admiralty - in 1951. Two tidal cycles of data were collected at each of three positions and presented, in tabular form, on the hydrographic chart of this bay (Hydrographer 1953). It was not until 1970 that further tidal stream data was collected. In that year, Acton (1972) recorded tidal stream data at four more positions in the bay. These, and later results obtained with the writer in 1971, were used by him to work out a mathematical mapping procedure and apply it to the tidal streams in central Start Bay.

Acton's tidal stream maps were initially intended to be used to see if any correlation between sand-waves, in this region, and the overlying tidal currents existed. However, to compliment an extensive geophysical survey of Start Bay being conducted by the Unit of Coastal Sedimentation located at Taunton, from about 1971 onwards, it was agreed that Bath University would produce tidal stream maps of the entire bay for inclusion in a symposium to be held in 1975 (Acton and Dyer, 1975).

It was at this stage that the writer expressed his concern about applying mathematical modelling techniques to southern Start Bay. From

the very start of this work the writer felt that an eddy would be present north of Start Point during the flood half cycle. This feeling was supported by an examination of the 1970 and 1971 sea-trial results, obtained by the writer, Acton and the Unit of Coastal Sedimentation. Here a rapid change in the tidal current vector with space was observed, suggesting that the non-linear advection terms in the equations of motion may well be important in this region. Over the southern region of Start Bay with it's radical topographical variations, however, the inclusion of these non-linear advection terms in the equations of motion present problems to mathematical modelling (as suggested by Acton, 1972, Appendices 2.1 and 2.2).

It was, therefore, decided that, although mathematical modelling of the tidal streams in this region would be continued by Acton, a second and independant mapping technique would be advantageous for comparison with the mathematically modelled results. The aim of this work is the procuring of these tidal stream maps.

In striving towards this goal, the first step taken involved collecting as much tidal stream data as possible. Chapter 2 details the sea-trials undertaken and the techniques employed to obtain this data. Some of this Chapter, together with Appendix 1, is devoted to the description of an anchored current monitoring system designed and constructed by the writer for use in shallow water of depth less than 10 metres. This enabled vital measurements to be made near the coast allowing a definitive answer as to whether an eddy exists during the flood half-cycle.

The raw sea-trial data is put into a more convenient form as a result of Chapter 3. Here Van Veen's (1936) formula is assumed to apply to Start Bay. This enables vertical integration of the tidal stream data to be performed. However, although in a more convenient form, evidence is presented at the end of this Chapter which suggests that this recorded tidal

stream data is also affected significantly by the value of the prevailing tidal range.

Accordingly, Chapter 4 is devoted to an investigation of how the prevailing tidal range influences the tidal stream parameters. Empirical formulae are presented. They allow all the data to be referred to a standard tidal range. The sea-trial results are thus brought into a comparable form; a basic pre-requisite for mapping.

With the sea-trial data in a form ready to be used for mapping, the tidal streams in southern Start Bay, consideration is then turned to finding a modelling method capable of realising this.

This is initiated by a consideration of the hydrodynamic equations of motion and continuity in their vertically integrated form. These are introduced in Chapter 5 where, by applying a space-averaging technique, the orders of magnitude of the various terms in these equations are deduced. This allows the approximate hydrodynamic equations describing the flow to be, in turn, deduced. From these equations it is concluded that southern Start Bay is something of an 'oddity' in the sense that the second order advection terms dominate the equations of motion.

Chapter 6 considers the implication of this upon mathematical modelling and shows this approach to be undesirable. Hydraulic modelling is suggested as an alternative to allow tidal stream maps to be procured in this region.

The hydraulic model used to test this suggestion is detailed in Chapter 7. It's predictive results are presented in tabular and pictorial form and compared to the sea-trial data. (A discussion of these results is deferred until Appendix 3, where an appreciation of the magnitude of the tidal streams over the shallow Skerries Bank is obtained).

Finally, a summary of the results obtained, together with the conclusions drawn from them, is presented in Chapter 8. This Chapter ends by suggesting possible lines for future research.

CHAPTER 2 SEA TRIALS IN START BAY

This Chapter describes the sea trials performed in Start Bay, Devon from 1971 to 1973 inclusive. The trials overlap with and are a continuation of the work described by Acton (1972). (Due to this some duplication will occur).

2.1 Introduction

The first published tidal stream surveys in Start Bay appear to be those quoted on the Admiralty chart of the area (Hydrographer 1953). These surveys were performed in 1951 using H.M.S. Seagull, the positions being A, B and C in Figure 2.1. The procedure adopted by the Admiralty surveyors is detailed in "Tides and tidal streams" (Hydrographer 1969), a more concise description of the method being given by Acton ...

"The Admiralty surveyors were particularly interested in the water speeds in the top 30 ft.of sea, since their prime concern was the effect of currents upon vessels up to this draught. The method of measurement was elegantly adapted to this end. At half-hourly intervals a 30 ft pole, weighted so as to be upright and almost completely submerged, was released from the anchored vessel, and carried away by the tidal stream. A light tethering cable was drawn out by the pole, and the current magnitude directly calculated from the time taken to draw out a measured length of line. Current direction was measured by sighting along the line to the pole, which carried a lamp at night. Readings were taken every half-hour for a fortnight so that figures for both spring and neap tides were obtained".

During 1970 eight sorties were made by Acton, a total of four positions (D, E, F and G in Figure 2.1) being visited. These trials are detailed in Chapter 3 of his thesis.

The procedure adopted involved cycling a Dentan (also called Toho) meter at half-hourly intervals taking readings of the tidal current speed and direction at six feet from the surface, at half depth and at six feet from the bottom.

When the present work started, therefore, there were tidal current results from seven positions in Start Bay (A - G in Figure 2.1), only two of which were in the southern region. It was decided that every effort would be made to remedy this sparcity of data in a region where the tidal currents were, according to the local inhabitants, believed to reach six knots over the Skerries Bank and through 'the race'.

This work was given a very good start by an expedition organised by the newly formed Unit of Coastal Sedimentation (U.C.S.) located at Taunton. A Bath team was invited to sail, in addition to a U.C.S. team, on one of the three vessels used; the 'Sara Lena', a trawler having a crew experienced in survey work. Simultaneously, current measurements were made by the U.C.S. team on the other two vessels, the 'Waterwitch' and the 'Sarsia', at three positions chosen after consultation with the University. Between one and two tidal cycles were obtained at each of the locations D', H, J, K and L (Figure 2.1).

Subsequent trials, many under the direction of the writer, have resulted in an increase from two to nine data positions in the southern region of Start Bay, and from seven to seventeen data positions over the entire bay. Figure 2.1 shows the locations, each given a code letter, where surveys have been carried out. The precise latitudes and longitudes of these positions are given in table 2.1.

Table 2.1

Latitude and Longitude of stations shown in Figure 2.1

Position	Latitude	Longitude
A	50° 13.00'N	3° 37.00'W
B	50° 17.00'N	3° 35.00'W
C	50° 20.20'N	3° 33.40'W
(D)	50° 15.90'N	3° 37.90'W
D'	50° 15.80'N	3° 37.70'W
(E)	50° 18.50'N	3° 33.40'W
F	50° 16.20'N	3° 33.80'W
G	50° 19.70'N	3° 31.80'W
(H)	50° 19.60'N	3° 30.45'W
(J)	50° 15.20'N	3° 34.15'W
K	50° 13.60'N	3° 37.90'W
L	50° 18.00'N	3° 34.90'W
(M)	50° 18.63'N	3° 36.50'W
(N)	50° 14.10'N	3° 39.10'W
O	50° 13.93'N	3° 36.43'W
(P)	50° 14.33'N	3° 37.07'W
(Q)	50° 15.28'N	3° 35.94'W

Table 2.2a sets out all the positions visited by the Bath team during the work. It will be seen that the writer visited eight positions (bracketed) and was chief observer for six of them.

Table 2.2a

Trial No.	Date	Location	Boat	Captain	Chief Observer	Duration of trial (hrs)
9	9.5.71	(H)	Sara Lena	J.Rae	J.Acton	16
9	11.5.71	(J)	Sara Lena	J.Rae	J.Acton	13½
10	29.5.71	(D)	R.N.K.R.	J.Barlee	J.Acton & M.Perring	6½
11	30.5.71	(E)	R.N.K.R.	J.Barlee	J.Acton & M.Perring	8½
12	30.6.72	(M)	Anchored System	-	M.Perring	41½
13	2.10.72	(N)	Anchored System	-	M.Perring	27
14	29.4.73	(P))	Enterprise	J.Trout	M.Perring	8½
14	1.5.73	(P))				
15	15.5.73	(Q)	R.V.Jane	P.Davis	M.Perring	12½

Four positions were surveyed during this time by U.C.S., the offer of this data being gratefully accepted. These are set out in Table 2.2b.

Table 2.2b

Date	Location	Boat	Duration of Trial (cycles)
9.5.71	K	Waterwitch	2
9.5.71	L	Sarsia	2
9.5.71	H	Sara Lena	2
11.5.72	J	Sara Lena	2
11.5.72	D'	Waterwitch	2
22.6.72	O	Anchored System	71

2.2 Experimental Procedure

All measurements which had previously been obtained by Acton were at positions chosen for their convenience from the point of view of seamanship. For example, the trials at positions E, F and G involved securing the small boat used to navigational buoys. Right from the start of this work, however, the decision was taken to visit positions which, although less convenient, were considered to be of more interest. Some of these trials involved using an 'anchored current monitoring system', designed and constructed by the writer; these trials being detailed in section 2.3. Most of the results were, however, performed whilst working off a boat: the experimental procedure used in these sorties will now be described.

The trials were initiated by the U.C.S./Bath University trial of May 1971. Here the Bath teams method of obtaining tidal current speed and direction measurements varied dramatically from the method used in trials D to G inclusive and the similar method adopted by the U.C.S. team of cycling one meter every half-hour.

Braystoke current meters were used instead of the Dentan (or Toho). These meters are of an integrating type incorporating a reed switch which opens and closes once every revolution of the impeller. The pulse produced operates an electro-magnetic counter, which is situated in a convenient position on the boat. As the impeller has a helix of one foot, then every pulse or count, registered by the counter, corresponds to one foot of water travel. Hence, the number of counts registered in, say 10 minutes allows the average tidal current speed, during this period, to be calculated.

The Braystoke current meter has the advantage over the Dentan, or similar 'direct reading' instruments, of smoothing out the turbulent fluctuations in the tidal current speed. In this way, the subjective element in the reading of this speed is removed. The meters, all having been calibrated by the 'Hydraulics Research Station' at Wallingford, were considered accurate to $\pm$ 2% above a water speed of 0.024m/s. Below this speed the makers advised that the readings be treated with caution, presumably because of the increased influence of friction and the decreasing effectiveness of the fins in aligning the meter with the tidal current.

These meters were exclusively used throughout the work undertaken by the writer.

Further, rather than cycling one meter up and down, a tiresome task to perform manually, especially in deep water, two Braystokes were used at fixed depths of 1/3rd. and 2/3rds. the average depth of water. This average depth of water was computed from the datum depths from the Admiralty Chart No 1634 (Hydrographer 1953) by adding an allowance for tidal elevation of 8 feet. By bringing two P.V.C. markers, fixed to the suspension cables prior to the trial, in line with the surface, the correct meter depths were ensured; a method devised and used by Acton.

Figure 2.2 shows the experimental arrangement. Each Braystoke had its own weight ($\sim$10kg) and was supported by its own suspension cable.

In this way, once the meters were lowered into position they remained so until the end of the trial, a considerable saving in physical effort over the cycling process. Furthermore, readings of the tidal current speed could then be taken more frequently; every 5 or 10 minutes. This resulted in a more detailed speed cycle than had been obtained before, when readings were taken every 30 minutes.

Directions were obtained by a method related to the Admiralty technique (see Figure 2.2). A one foot cube sheet metal box is suspended from a surface float. By partially filling this box with bricks it is maintained at approximately half depth, the tendency for it to stream upwards being reduced. The metal box was designed to give high enough drag, even in slow currents, so that the effect of wind on the surface float would have negligible effect on the reading of the tidal current direction. A light tethering rope is attached between the boat and the float, the float being allowed to stream away some 60 metres with the current. By sighting along the line from the boat to the float using a hand-held compass, the tidal current directions were obtained. These were recorded every 5 to 10 minutes. The compass readings were checked by two methods to allow correction, if needed, to the readings due to metallic fittings etc. on the boat used. Firstly, fixes were taken on distant landmarks and secondly by checking against the ships heading using the 'corrected' bridge compass.

It was found that for the Sara Lena, when constantly operating from the stern of the vessel, the compass readings needed the standard correction on the ebb to give the tidal current directions as referred to true north but required 8 degrees adding, rather than subtracting, when the currents were on the flood.

This technique for direction measurement was found to be more accurate than relying on the magnetic readings from (say) a Dentan meter which has inherent errors of, at best, $\pm 5^{o}$. (Acton 1972, Appendix 1.4). The consistency of the readings obtained at positions H and J using this direction technique were dramatic. For some four hours on the ebb at each position,

the direction readings, given by the hand-held compass, varied by no more than $\pm 3^{o}$ about the mean value.

An equally dramatic comparison between the direction readings obtained by this drogue method and by the readings obtained from a 'compass carrying' Braystoke, kindly lent by Mr J Barlee, resulted from trials 10 and 11 at positions D and E. During this time the sea-state approached the limit of safety in the small boat used due to a 10 knot wind, the use of a hand-held compass being made very difficult. However, as shown in Table 2.3, during a two hour period close to the maximum flood speed, on trial 11, the 25 readings of tidal current direction taken by the writer, using the hand-held compass and drogue, varied only from 57^{o} to 60^{o}, a range of just 3^{o}. This suggests that the error of the mean is less than $\pm 1^{o}$. By comparison the direction readings eminating from the 'compass-carrying' Braystoke during this time varied from 0^{o} to 110^{o}, a range of 110^{o}. A later investigation of this meter by the manufacturers resulted in no fault being found. (Personal correspondance with Mr J Barlee).

Trials 9, 10 and 11 seem, therefore, to provide convincing evidence of the superiority of direction measurements made by this drogue technique over methods using existing small 'compass carrying' instruments such as the Dentan.

This experimental technique for measuring the tidal current direction remained unchanged throughout the rest of the trials, although a sextant was used to measure the angle between the float and a prominent landmark at position Q (trial 15) as the boat used (R.V. Jane) was constructed almost exclusively of iron. The use of iron-hulled vessels had, up to this time, been carefully avoided due to the adverse effects on the hand-held compass readings.

Table 2.3

Direction measurements at position E

Time	Drogue measured directions	Braystoke measured directions			
		1st	2nd	3rd	Mean
11.00	57°				
11.05	57°	30°	30°	30°	30°
11.10	58°				
11.15	59°	70°	70°	70°	70°
11.20	58°				
11.25	59°	70°	70°	40°	60°
11.30	59°				
11.35	58°	30°	60°	80°	57°
11.40	59°				
11.45	58°	50°	70°	70°	63°
11.50	58°				
11.55	58°	60°	50°	30°	47°
12.00	57°				
12.05	59°	80°	30°	30°	47°
12.10	58°				
12.15	59°	90°	10°	80°	60°
12.20	59°				
12.25	59°	10°	20°	50°	27°
12.30	58°				
12.35	58°	60°	80°	110°	83°
12.40	59°				
12.45	60°	10°	90°	60°	53°
12.50	59°				
12.55	60°	70°	0°	90°	53°
13.00	58°				

During the U.C.S/Bath University trial it was found that, in choppy seas, there was a tendency for the shallow Braystoke to twist around the deeper Braystoke cable. A modification to the meter system was incorporated into trials 10 and 11 (at positions D and E) in order to overcome this adverse effect.

This involved the use of a 2 metre long, 20 kg weight as the downward force for both meters (see figure 2.3). A polypropylene rope between the meters passes through two eyes in the weight. This serves two purposes. Firstly, it means that a two to one pulley effect is obtained allowing two people to raise and lower the apparatus, each person experiencing a pull equal to half the weight (10 Kg). Secondly, it ensures both meters are separated and cannot easily foul with each other.

Trials 14 and 15, at positions P and Q on the Skerries Bank, were performed in such shallow water (less than 10 metres) that it was decided to use only one meter located at half-depth to obtain the tidal current speed. The depth of the meter was adjusted from flood to ebb to maintain the Braystoke at half-depth. This was deemed necessary due to the exaggerated effect of the tide in determining the depth of water in such a shallow region.

Whenever possible, the positions visited were fixed using 'Decca Navigator' to an estimated accuracy, for the bay, of 25 metres. Sextant angles were used to locate a position on the other trials with an error estimated to be of the order of 50 metres.

Wind measurements were taken using a hand-held three cup anemometer, to measure the wind speed, and a wind stocking plus hand-held compass to measure the wind direction.

The experimental procedures used, whilst working off a boat, are ideally suited to short trials of less than about 13 hour duration, two people being required to obtain the data in this case.

In order to investigate the effects of tidal range upon the tidal current cycles, it was considered necessary to collect many cycles of tidal current data at one position. (This interrelationship between tidal range and the tidal current parameters is raised at the end of Chapter 3 and investigated in Chapter 4).

Two types of automatic anchored tidal current monitoring systems were used in an effort to secure these many cycles of data. These systems will now be described.

2.3 The Anchored Systems

The U.C.S. system is of the conventional design and is sketched in Figure 2.4. The sub-surface float provides sufficient upward force to keep the sensors approximately vertically above one another. Readings of tidal current speed and direction, from each sensor, are sampled at preset time intervals and magnetically recorded for process later by a computer.

This system was never used by the writer, although it's results were made available by U.C.S. and all but one of the positions where it was anchored were chosen after consultation with the University.

The system used by the writer was, of necessity, of an unconventional design.

This anchored current speed monitoring system was designed and constructed by the writer with some help from the University workshop.

It was intended to be used to gather tidal current speed records between a spring and neap tide, (about seven days) to allow an appreciation of the relationship between tidal range and tidal current speed to be achieved. Due to the events listed in Chapter 2.4, this was never realised, the results from the U.C.S. tidal current monitoring system at position 0 being utilised instead (see Chapter 4).

Positions N and P were the main locations where it was intended to anchor this system. As some 25% of the southern region of Start Bay consists of water between 4 and 10 metres deep (see Figure 2.5) it was decided that there was a real need for a system designed to record many cycles of data in such shallow water - a depth not really suited to a conventional anchored system (see Figure 2.4) as the subsurface float of such a system must be located at a comparable depth below the surface by marine law. Nevertheless, the Skerries Bank, comprising water depths between 4 and 10 metres, is probably the most interesting region in Start Bay.

For an investigation of the relationship between tidal range and tidal current speeds, it was deemed advisable to obtain the most accurate current speed cycles possible. Working in such shallow water poses no real problems provided a calm sea-state prevails. Unfortunately, the writer's experience of the weather in Start Bay is that it is best to anticipate the worst, for this was found to be usually the case. In other words, it was felt very unlikely that a calm sea-state would prevail for a seven day trial, so choppy seas had to be expected. Unfortunately, in choppy seas, where waves exist, physical effects impress themselves upon the recorded tidal current speed when operating from a boat in such shallow water.

The design of the anchored tidal current monitoring system revolved around the deemed necessity to remove the influence of as many of these physical effects as possible. (The main physical effects, which it is considered may have an adverse effect on tidal stream recording in shallow areas, are listed in Appendix 1, together with an account of how the unconventional design of this system minimised their effects upon the recorded data. This is demonstrated by reference to results collected at position N).

The entire marine half of the system is shown in Figure 2.6. Two empty 45 gallon oil drums provide sufficient buoyancy for the subsurface apparatus. One oil drum is anchored to the sea-bed via rope, heavy chain (to aid anchorage) and a heavy efficient anchor. The other oil drum, floating

on its end, is some six metres away, connected to the anchored oil drum by a length of polypropylene rope. This drum contains all the electronics and power supplies, access to them being possible via an inspection cover in the upper end of the drum. Three cables, from the three Braystokes used, enter this drum through sealed inlets in this cover. A 2½ metre whip aerial extends vertically upwards from it being supported by an insulated tripod structure (not shown).

Suspended beneath this drum is a 3½ metre long, 2½ cm diameter hollow steel rod, galvanised to overcome the corrosive effects of sea water. Some 2½ metres from the surface, another polypropylene rope (B) connects this rod to the anchored oil drum which provides a fixed reference position at sea level. Clamped onto this rod, so as to be at depths of 1½ and 3 metres below the surface, are two Braystoke current meters. They possess no fins. By being rigidly fastened to face the anchored oil drum they rely on the streaming of the apparatus to ensure that they face into the average tidal current direction. Suspended beneath the rod is the 2 metre weight described in Chapter 2.2. It is located at 6 metres from the surface, being suspended by two polypropylene ropes of equal length, and is modified to take a Braystoke at its front end. This Braystoke relies on the fins of the weight to be aligned with the current.

The tidal current speeds recorded by the three Braystokes are transmitted to a receiving station on the shore by radio telemetry. A block diagram of this radio telemetry link is shown in Figure 2.7. Briefly, the Braystoke pulses obtained by the closure of the reed switch in each instrument are divided by 50, so one pulse is obtained for every 50 revolutions of the Braystoke impeller. These signals are then fed into a summing amplifier whose voltage output is representative of the combinations of pulses present. This voltage is then converted to a square-wave frequency which is used to switch on and off a radio transmitter.

The received signal is demodulated and the frequency converted to a d.c. voltage. This is fed into voltage sensing circuits and through a decoder to give the correct output to operate the electromagnetic counters. Braystoke 1 operates counter 1 and so on.

The automatic operation of a solenoid for 0.45 seconds every 10 minutes activates a cine camera, via a cable release. This secures about eight photographs of these counters together with the face of a clock to give the time of recording. (The receiving apparatus is shown in Figure 2.8).

By using a radio telemetry link, a constant check on the operation of the whole system or just one Braystoke can readily be made. It may be seen that most of the complex and expensive equipment is based on the shore, whilst only the simple electronics is subjected to the sometimes merciless sea. The system is fully automatic and is designed to be anchored for eight days, to record the tidal current speed at three depths, during the period between a spring and neap tide.

2.4 Anchored System Trials

To check the operation of this unconventional anchored system, a position was chosen in Start Bay where low magnitude tidal currents were believed to exist. Accordingly, the system was first anchored in June 1972 at position M (see Figure 2.1).

Apart from the 6 metre depth Braystoke being damaged when the system was laid, everything worked well even during a force 6 south-westerly gale which lasted for a day. As, however, the weather forecasts were for unsettled weather, it was decided to remove the system from the sea. This trial was intended only as a test of the system, but 41 hours of valuable data were collected. Directions were obtained by sighting along the line of the drums from a convenient position on the shore using a hand-held compass.

In August 1972 at attempt to anchor the system on the Skerries Bank had to be abandoned because of abnormally bad weather for the time of year. However, the system was anchored again in October 1972 at position N (see Figure 2.1). With characteristic swiftness for the area, an unexpected force 9 to 10 gale matured after about 12 hours. This caused heavy swell characterised by eight foot waves. The system continued to function perfectly, however, giving excellent results from all three Braystokes. Unfortunately, the folly of pinning the eye-bolts to the ends of the metal rod rather than welding them became only too clear when, in waves estimated to be about 15 foot high, one of these eye-bolts parted company with the metal rod, the pin fastening it to the rod having sheared off. This resulted in the buoyancy drum containing all the electronics tilting over, immersing the radio aerial in the sea.

Although no longer transmitting signals, the system remained anchored on position for five days until, in the presence of 20 foot waves, it parted company with its anchor and drifted ashore onto Hallsands Beach. Here it was quickly rescued by the local fishermen, to whom a great debt is owed. Little real damage, however, was incurred by this experience and within a few weeks the system was once again ready to be anchored in Start Bay.

Unfortunately, this intention was never realised, because the Ministry of Agriculture, Fisheries and Food's local representative finally decided to object to the use of metal oil drums as floats, and requested that the system was not used again. This request was reluctantly complied with and terminated this anchored system's life in Start Bay.

It was indeed fortunate that U.C.S. laid their 'subsurface' anchored system in Start Bay on three occasions during this work, achieving a slightly better outcome than the writer. The first U.C.S. anchored system trial took place in May 1971, the position being agreed after consultation with the University. After some three weeks in the sea, this system was recovered only to discover that the tape-recorder had not recorded the data from the sensors.

The second laying of this system initiated better results. In June 1972 the system was laid at position 0.½ (Unfortunately the writer had no say in the choosing of this location which, as will become apparent in later Chapters, was not the best location lying as it does on the 'submarine cliff' off the eastern margin of the Skerries Bank). Speed and direction readings were recorded every 8 minutes for 71 tidal cycles (about six weeks). Upon investigation of the readings, it was found that one speed sensor had worked nearly continuously throughout the trial and readings from four direction sensors were intermittantly available. The offer of these results was gratefully accepted. They form the basis of the investigations detailed in Chapter 4.

A third laying of the U.C.S. system in May 1973 led to another failure at a position 'inside' the Skerries Bank, decided upon by the writer. Why the system failed to work is not altogether clear.

The experimental procedures used in the obtaining of tidal current speed and direction data at the nine locations in the southern region of Start Bay having been described, the following Chapter describes how vertical integration brings this data into a more convenient form.

CHAPTER 3 DATA PROCESSING

In the previous chapter the accumulation of tidal stream data from nine locations in the southern region of Start Bay was described. This raw data is in a very inconvenient form. At one position, the value of tidal current speed is known only at 15 feet below the surface; at two positions it is known only at half the water depth and at three more positions it is known only at 1/3rd and 2/3rds the depth of water. A similar problem exists with the raw tidal current direction data.

The following sections describe how vertical integration (depth averaging) allows this data to be brought into a more convenient form.

Because of their importance in the following chapter, the vertical integration of the position 0 results is treated separately, being performed in section 3.2.

3.1 Vertical Integration

This process enables all the tidal current speed and direction values in each time increment, during a recorded tidal cycle, to be reduced to a single vertically integrated value for each parameter; a process adopted by Acton (1972).

By arithmetically averaging the mean values of tidal current speed recorded 6 feet from the surface, at half depth and at 6 feet from the bottom, his vertically integrated tidal current speed was obtained. However, due to the change in experimental procedure adopted for this work, this method of obtaining the vertically integrated tidal current speed can no longer be employed.

Van Veen (1936) asserts that, in the Dover Straits, the tidal current speed s_z at depth h_z is given by the relationship

$$s_z = k(h-h_z)^{0.2}$$

where h denotes the total depth of water.

The vertically integrated tidal current speed $\bar{s}$ is thus given by

$$\bar{s} = \frac{1}{h}\int_0^h s_z \, dz$$

$$= \frac{k}{h}\int_0^h (h - h_z)^{0.2} \, dz$$

or $$\bar{s} = \frac{k h^{0.2}}{1.2}$$

But as $s_z = k(h - h_z)$, then

$$k = \frac{s_z}{(h - h_z)^{0.2}}$$

Hence $$\bar{s} = \frac{1}{1.2}\left(\frac{h}{h - h_z}\right)^{0.2} s_z \qquad 3.1.1$$

In an attempt to discover if this relationship holds true for the Start Bay region, one of the writer's colleagues, Mrs C M Dyer, analysed the U.C.S. results (obtained by cycling of a Dentan meter), at positions D', H, J, K and L for both the flood and the ebb. These yielded results for the power in equation 3.1.1 of between 0.1 and 0.35. The errors associated with these values were, however, of a comparable order to the value itself. This made any conclusion concerning the validity of Van Veen's formula in Start Bay impossible until more data is collected. However, apart from position N, it is found that at every position visited the tidal current speed displays a tendency to increase in magnitude with increasing height above the sea bed, in general agreement with Van Veen's law. It is, therefore, assumed, for the purpose of vertical integration, that $\bar{s}$ in the southern region of Start Bay is given by equation 3.1.1.

This allows the parameter $\bar{s}$ to be calculated throughout a tidal cycle at all the positions visited in this region. Table 3.1 gives the method of achieving this at these positions: h denotes the total depth of water present.

Table 3.1 Methods of obtaining $\bar{s}$.

Trial No.	Position	Depths at which speed readings are available.	Depth of recorded s_z used in equation 3.1.1
Admiralty	A	15 feet	15 feet
4, 6	D	6, $h/2$, $h-6$ feet	$h/2$ feet
10	D	$h/3$, $2h/3$ feet	$h/3$, $2h/3$, $\bar{s}$ calculated for both cases and averaged
U.C.S.	D'	Meter Cycled	$h/2$ feet
9	J	$h/3$, $2h/3$ feet	$h/3$, $2h/3$, $\bar{s}$ calculated for both cases and averaged
U.C.S.	K	Meter cycled	$h/2$ feet
13	N	5, 10, 20 feet	20 feet
U.C.S.	O	$h/2$ feet	$h/2$ feet
14	P	$h/2$ feet	$h/2$ feet
15	Q	$h/2$ feet	$h/2$ feet

Just as the tidal current speed results vary in format from position to position, so do the tidal current direction results. At the majority of positions the drogue apparatus, for measuring this direction, was used. However, at positions D' and K, tidal current direction results were obtained at height increments as the Dentan meter used was cycled from the sea-bed to the surface. For these two positions, all direction readings taken so close to the ship, so as to be in water which was considered likely to be affected by its presence, are ignored. The arithmetic mean of the remaining tidal

current direction readings, obtained during each cycle of the Dentain, is taken as the vertically integrated tidal current direction $\bar{\theta}$ for the time increment in question.

It was rarely found that any individual direction reading during a cycle of the Dentan meter varied by more than $\pm 5^{o}$ from the defined $\bar{\theta}$ value. This finding seems to suggest that, to a good approximation, there exists constant tidal current direction with depth. Indeed, the only results contrary to this view are found at position 0, where a variation of tidal current direction with height appears present on the ebb. It is felt, however, that this is due to the large topographical variations in the vicinity of this position, it being unfortunately located on the steep eastern margin of the Skerries Bank. Certainly at all the other positions visited no evidence of a serious variation (greater than $\pm 5^{o}$) of tidal current direction with depth was found, As a consequence, the drogue apparatus, described in Chapter 2.2 is assumed to yield the value of $\bar{\theta}$ directly.

The position 0 results will now be considered.

3.2 Position 0 results

Two typical examples of the computer print-out for position 0 are given in Figures 3.1A and 3.1B. Figure 3.1A shows a sample taken from the ebb half-cycle; Figure 3.1B one from the flood half-cycle. Reference to Table 3.2 will be made to explain these readings.

Table 3.2 Example of data print-out from position 0

33D 23H 52M 0S					
Sensor 1	Sensor 2	Sensor 3	Sensor 4	Sensor 5	Sensor 6
232.50	358.75	192.50	358.75	187.50	358.75
222.50	358.75	187.50	358.75	192.50	358.75
242.50	358.75	187.50	357.50	187.50	167.50
0.13	0.	0.13	0.	0.13	186.94

The time elapsed, referred to the start of the trial, is given first - in days (D), hours (H), minutes (M) and seconds (S). During the following 8 minutes each of the 6 sensors transmit 4 readings to the tape recorder.

Considering sensor 1 as an example, the 4 readings are 232.50, 222.50, 242.50 and 0.13. The first 3 readings are instantaneous tidal current direction obtained from the compass incorporated in the sensor. They are transmitted 2, 4 and 6 minutes respectively after the quoted time. The fourth reading, transmitted 8 minutes after the quoted time, represents the tidal current speed. As 'integrating' speed sensors were used, the number of impeller revolutions being counted over the 8 minutes, these values are time-averaged. They require dividing by 200 to obtain the tidal current speed in meters per second.

Sensors 2, 3, 4, 5 and 6 behave exactly the same as sensor 1, transmitting 3 direction and a speed reading 2, 4, 6 and 8 minutes respectively after the quoted time.

It should be pointed out that a direction reading of 358.75 or a speed reading of 0.13 or 0. corresponds to the sensor in question failing to function. As can be seen, sensors 1, 3, 4, 5 and 6 give intermittant direction readings; sensor 2 being unfortunately broken when the system was laid.

The method employed for obtaining the vertically integrated tidal current direction $\bar{\theta}$ required averaging the direction readings, in every 8 minutes interval, for each sensor, and then forming the arithmetic mean of these values. This ensured that each sensor had equal influence on the value of $\bar{\theta}$. Furthermore, $\bar{\theta}$ was only calculated when readings of direction were available from all 4 sensors, 3,4, 5 and 6, due to the apparent change in direction with height on the ebb. The readings from sensor 1 were ignored because of their inconsistency.

As an example of this method, referring to figure 3.1a, the only obtainable value of $\bar{\theta}$ is for the 8 minute interval initiated at 34D 0H 24M 0S as this is the only case where sensors 3 to 6 all give direction readings. These yield

average directions of 190.8°, 197.5°, 192.5° and 165.0° for sensors 3 to 6 respectively. The value of $\bar{\theta}$, obtained by averaging these values, is thus 186°, its associated time being 4 minutes after the initiation of the set of readings (34D,0H 28M 0S).

The definition for $\bar{\theta}$ is felt to be inaccurate, in the absolute sense - at least for the ebb - as no direction results are available in the upper half of the sea. Due to the position being so close to the Skerries Bank, it is difficult to even estimate these directions with any degree of confidence, the water in this upper half of the sea having apparently flowed off the bank itself (see Figure 7.3). The relative values of $\bar{\theta}$ at position 0 do, however, allow a comparison of the direction cycles. (This is discussed further in Chapter 4).

Using Van Veen's formula (3.1.1) the vertically integrated tidal current speed $\bar{s}$ is obtained from the output of sensor 6, the only sensor to have consistently given speed data throughout the trial. It was located at approximately half-depth.

It is now possible to present the vertically integrated cycles of tidal current speed and direction eminating from all the positions where data is available in southern Start Bay. This will, however, be deferred until the end of the next chapter for the reasons that will now be given.

Figure 3.2 shows two of the 71 tidal speed cycles recorded at positions 0. The values of the tidal current speed have been vertically integrated using Van Veen's relationship (equations 3.1.1) as described previously in this chapter.

For these (and all other tidal current speed cycles presented later) the ebb flow is taken as positive; the flood negative. (This is a convention adopted by, for example, Dronkers and Schonfield, 1955). The cycles have been referred to the time of low water at Dartmouth, this time being obtained from records produced by a bubble tide gauge (as described by Redfield, 1962) sited at Sand Quay, Dartmouth.

The quoted tidal range Z, prevailing when these cycles were recorded, is also obtained from the tide gauge records. It is defined as the difference between the water elevations at high and low water. For the flood half-cycle, the tidal range is the difference between the water elevations of the high water occurring during this half-cycle and the following low water. For the ebb half-cycle it is taken as the range of water elevation between the preceding high water and the low water occuring during the ebb half-cycle.

The two tidal speed cycles presented in figure 3.2 represent the results obtained near the extremities of an average tidal range scale in Start Bay. One cycle was collected during an average spring tide (tidal range of 4 metres), the other when an average neap tide prevailed (tidal range of 2 metres). Two major differences between these cycles are apparent. Although the general shape of both cycles is the same, the magnitude of the maximum flood and ebb speeds varies and the 'position' of the cycle on the time axis is different.

These two presented cycles suggest that changes in the tidal range affect not only the magnitude of the tidal current speed, but also - in some way - the associated time scale. Here then is the reason why the cycles of the vertically integrated tidal current speed and direction, accumulated at all data positions in southern Start Bay, have not yet been presented. In order to model, by whatever means chosen, the tidal streams in this region it is first necessary to possess all data in a compatable form. It is necessary not only to vertically integrate all the data but also to refer it to a reference tidal range. In order to achieve this, as accurately as possible, the interrelationships between tidal range and the prevailing tidal current vector at position 0 are now investigated.

CHAPTER 4 INTER-RELATIONSHIPS BETWEEN TIDAL RANGE AND TIDAL CURRENT PARAMETERS

In this chapter the 71 tidal current speed and direction cycles obtained by the U.C.S. anchored current monitoring system at position 0 are analysed. The availability of so many cycles of data from one position, spanning the tidal range scale, enables any inter-relationships between tidal range and the vertically integrated tidal current parameters to be investigated.

The effects upon the vertically integrated tidal current speed $\bar{s}$ caused by changes in the prevailing tidal range are considered first.

4.1 Tidal Current Speeds

Figure 3.2, presented and explained in the last chapter, shows two typical vertically integrated tidal current speed cycles from position 0. Despite being at different extremes of the tidal range scale, these two cycles do exhibit certain similarities. These similarities will be called 'events'.

An 'event' is defined, for this work, as a marked characteristic of a tidal cycle brought about by some change in the pertinent physical situation. For example, referring to figure 3.2, both the spring and neap tidal range referred flood half-cycles exhibit a sharp maximum flood speed. This is followed by a decline in the magnitude of the tidal current speed until a second 'peak' presents itself. These are both considered 'events', their formation being attributed to a change in the physical situation prevailing at the time. Indeed for both cycles displayed in figure 3.2 there are considered to be five main events (arrowed): the two already mentioned plus the three transitions where $\bar{s}$ is effectively zero, the current flow changing from ebb to flood or vice versa.

The occurence of the two flood current speed 'peaks' in both of the cycles shown in figure 3.2, is suggestive that these events are reproducable from cycle to cycle. To discover the truth of this, ten tidal current speed cycles, referred to tidal ranges varying from 1.6 metres to 4.3 metres, are plotted in figure 4.1. For ease of comparison they have been drawn using constant vertical displacements, the tidal current speed cycles being normalised by dividing each cycle by the maximum flood tidal current speed. These cycles appear to display the reproducibility of the two above mentioned flood half-cycle events. The two events are certainly present on all the cycles characterised by a tidal range in excess of 2.5 metres. Below this tidal range the two events still prevail, but the 'second' speed 'peak' increases in magnitude, relative to the first, exceeding it in the 1.6 metre tidal range cycle.

(This phenomena, existing only at neap tides, of the presence of two approximately equal magnitude flood current speed 'peaks' is well known to the fishermen of Hallsands. They lay crab pots along the outer edge of the Skerries Bank, the floats marking them being submerged when the currents run fast. Personal correspondance with Mr J Trout, a Hallsands fisherman, led to him relating the experience, only present at neap tides, of the crab pot floats surfacing (after the first peak) only to disappear again about half an hour later (second peak)).

Statistical analysis of the 71 tidal speed cycles, obtained at position O, shows that the five events attributed to the current speed cycles at this location exhibit a linear variation in time with tidal range. This is shown by the broken lines in figure 4.1. This fact forms the basis of the method used in section 4.3 to transform the independent variable (the time). However, before considering this it is considered wise, by way of an introduction, to consider the relationship between the tidal range and the maximum tidal current speed. The consideration of this, in the following section, leads to a scaling of the dependent variable (the speed).

4.2 Scaling of the dependent variable

The suggested procedure for tidal stream analysis given by "The Admiralty manual of hydrographic surveying, volume 2" (Hydrographer 1969, page 109) involves a linear correction to the tidal current speed for changes in tidal range.

"... the rates are assumed to be directly proportional to the range of the tide at the standard port concerned".

Armed with the 71 cycles of data collected at position O, it was decided to obtain a more precise relationship for the southern region of Start Bay.

A very general relation between speed and range, which includes the linear hypothesis as a special case, is

$$\bar{s}(max) = \alpha Z^{m} + \beta \qquad 4.2.1$$

where $\bar{s}$ (max) denotes the maximum ebb or flood vertically integrated value of tidal current speed per half-cycle. It is assumed to vary as the mth power of the tidal range Z, α and β being constants. If, however, the tidal range Z be put equal to zero then as no hydrostatic potentials would exist, it seems reasonable to expect $\bar{s}$ to be zero. β may therefore be put equal to zero without any loss of generality.

In order to compute the precise values of α and m, equation 4.2.1 was put into its logarithmic form: viz

$$\log (\bar{s}(max)) = m \log (Z) + \log (\alpha) \qquad 4.2.2$$

a linear equation. The values of the slope m and intercept log (α) were calculated using the method of least squares (see for example Moroney 1951, page 284) using all 71 values of $\bar{s}$ (max) for both the ebb and flood.

Results give the relationship between the maximum vertically integrated ebb tidal current speed $\bar{s}\ (max)_e$ and tidal range Z to be given by the empirical equation:

$$\bar{s}\ (max)_e = 0.46\ Z^{0.55} \qquad 4.2.3$$

Figure 4.2 shows the plot of log $(\bar{s}(max)_e)$ against log (Z) the computed best straight line fit being shown. The correlation coefficient for this straight line is 0.90, Student's t test showing it to be a highly significant fit to the data.

For the flood the relation between the maximum vertically integrated tidal current speed $\bar{s}\ (max)_f$ and tidal range is found to be

$$\bar{s}\ (max)_f = 0.57\ Z^{0.75} \qquad 4.2.4$$

The best straight line fit to the data is shown in figure 4.3, the logarithm of $\bar{s}\ (max)_f$ being plotted against the logarithm of Z. This linear fit to the data exhibits a correlation coefficient of 0.81 and, when tested by Student's t test, is also found to be a highly significant fit. (The correlation coefficient is detailed in, for instance, Moroney 1951, page 286; Student's t test being discussed in the same reference on page 311).

A very interesting feature resulting from a comparison of equations 4.2.3 and 4.2.4 is the apparent difference in the value of the power of Z between the flood and ebb cases. This difference was investigated and shown to be significant by statistically computing the likely error in the values of the power. Equations 4.2.3 and 4.2.4 then become

$$\bar{s}(max)_e \propto Z^{0.55 \pm 0.03}$$
$$\bar{s}(max)_f \propto Z^{0.75 \pm 0.04} \qquad 4.2.5$$

(These equations are in general agreement with the results of a theoretical study on the relationship between tide and current performed in Appendix 2, where the power of Z is predicted to lie between 0.5 and 1.0. The difference between the powers of Z in the flood and ebb cases, is discussed in detail in this Appendix).

Equations 4.2.5 are very important to the art of tidal current speed mapping when available data has been collected at different tidal ranges. They allow the maximum flood and ebb tidal current speeds to be scaled to any desired reference tidal range. This will now be demonstrated by reference to data collected at positions O and D. (These are, unfortunately, the only two data positions in the southern region of Start Bay where tidal speed data

has been collected for more than one tidal range).

Figure 4.4A refers to data collected at position 0. Here a tidal speed cycle collected during a 2.8 metre tidal range is scaled, using equations 4.2.5, to refer to a tidal range of 4 metres (broken curve). This prediction is compared to tidal speed data actually collected during a 4 metre tidal range (circles). A comparison of these two cycles will show that the use of equations 4.2.5 results in an excellent prediction of the maximum flood and ebb vertically integrated tidal current speeds.

A harsher test of the equations is shown in figure 4.5A which refers to data collected at position D, a substantial distance from position 0. A tidal speed cycle collected during a tidal range of 3.6 metres is scaled (by use of equations 4.2.5) to refer to a tidal range of 2.7 metres. Actual data collected during a 2.7 metre tidal range is also presented. Once again the agreement in the maximum value of the flood and ebb vertically integrated current speeds, between the predicted and actual tidal speed cycles, is excellent.

However, although equations 4.2.5 allow a scaling of the dependent variable, there still exists an outstanding difficulty associated with tidal range scaling. This may clearly be seen in both figures 4.4A and 4.5A, where it appears that the time-scale of the tidal current speed cycle is influenced by tidal range. In the cases considered, the result of this is a likely error of prediction of order 0.5 m/s at position 0 and of order 0.1 m/s at position D. In the next section, which follows immediately, this difficulty is overcome.

4.3 Transformation of the independent variable

Apart from influencing the magnitude of the tidal current speeds, changes in tidal range also distort the 'shape' of the tidal current speed cycles. It is proposed that this distortion is the effect resulting from the tidal cycle possessing a time-scale which is dependent on tidal range.

Furthermore, as the durations of the half-cycles vary linearly with tidal range (see Section 4.1) it will be assumed that this tidal range dependence on the time-scale is linear in nature.

Using this assumption a new time-scale for the flood half-cycle, which is independent of tidal range, will now be evoked. Δf is defined by the transforamtion

$$\Delta f = \frac{t - t_1}{t_2 - t_1} \qquad 4.3,1a$$

where t_1 denotes the time of occurance, with respect to low water, of the ebb to flood transition ($\bar{s} = 0$), t_2 the flood to ebb transition ($\bar{s} = 0$) and t an event occurring during the flood half-cycle. Δf, which will be termed the flood phase index, has a value of zero for the start of the flood half-cycle ($t = t_1$) and unity at the flood to ebb transition ($t = t_2$).

Similarly, the ebb phase index Δe is defined by the transformation

$$\Delta e = \frac{t - t_2}{t_3 - t_2} \qquad 4.3.1b$$

where t_3 denotes the time of occurance, with respect to low water, of the end of the ebb half-cycle ($\bar{s} = 0$).

Both phase indices are dimensionless numbers ranging in value from 0 to 1. Further, if the assumption of a linear dependence of the tidal speed cycle time-scale with tidal range is correct, then the defined values of phase index Δ for particular events should be totally independent of tidal range. As a check upon this at position 0, the value of Δf for the maximum flood speed, chosen for it's sharpness, has been obtained for the 71 available tidal speed cycles. It is found that the mean value of Δf for this event is 0.35, the associated standard deviation being 0.01. By calculation of the correlation coefficient it is found that the value of Δf is independent of tidal range for this event. Similarly, for the event of the second

current speed peak on the flood (see figure 3.2) statistical analysis shows Δf to be 0.59. It has a standard deviation of 0.03 and is also found to be independent of tidal range by calculation of the correlation coefficient. Thus, the assumption that the time-scale is linearly affected by tidal range appears handsomely substantiated. In turn, this leads to the validity of the use of the transormations 4.3.1 to overcome these tidal range effects at position 0. Can, however, these transformations be applied to the entire southern region of Start Bay to overcome the adverse time-scaling effects of tidal range variations?

The only results available to throw light on this are at positions D and D' just off Torcross. These positions are so close together that, if taken as one, five tidal cycles of data are available for analysis. The tidal range values for these cycles vary from 1.71 metres to 3.60 metres. (At all other positions visited in the southern region of Start Bay, no more than two cycles of data, at virtually the same tidal range, have been collected). Once again the value of the flood phase index Δf corresponding to the maximum flood speed is computed. It is found that Δf has a mean value of 0.41 for this event and an associated standard deviation of 0.01. The correlation coefficient, when calculated, once again shows this value of Δf to be unaffected by changes in the tidal range. Thus, the use of the transformations 4.3.1 to overcome the effects of tidal range unpon the time-scale of the speed cycle just off Torcross, appears substantiated.

Based upon these results, it will be assumed that the values of Δf and Δe are independent of tidal range at every position in the southern region of Start Bay. In order to use the transformations 4.3.1 to overcome tidal range effects it is first necessary to obtain the expressions for t_1, t_2 and t_3.

Statistical analysis of the results from position 0 yield the empirical relationships

$$t_1 = -0.31\ Z - 8.07 \text{ hours}$$
$$t_2 = -1.01\ Z - 0.01 \text{ hours} \qquad 4.3.2$$
$$t_3 = -0.41\ Z - 4.67 \text{ hours}$$

Student's t test shows these linear equations to give a highly significant fit to the data. Rewriting equations 4.3.2 for the general case they become

$$t_1 = -0.31\ Z + p$$
$$t_2 = -1.01\ Z + q \qquad 4.3.3$$
$$t_3 = -0.41\ Z + r$$

These equations assume that the tidal range dependence on the values of t_1, t_2 and t_3 are the same throughout the region. The constants p, q and r have characteristic values for each position. (The physical significance of these constants is presented in Appendix 3.3 and will not be commented on here). At position 0 their values are (standard deviations given) -8.07 ± 0.10 hours; -0.01 ± 0.15 hours, and 4.52 ± 0.15 hours respectively. At the grouped positions D and D' their values are (once again standard deviations given) -7.92 ± 0.06 hours; -0.95 ± 0.07 hours, and 4.67 ± 0.13 hours respectively.

Thus, substituting equations 4.3.3 into the transformations 4.3.1 the effect of tidal range upon the time of occurrance (with reference to low water) of an event during a tidal speed cycle may be predicted. If the event occurs during the flood half-cycle then

$$t = t_1 + \Delta f\,(t_2 - t_1) \text{ hours}$$

or $$t = -0.31Z + p + \Delta f\,(-0.70Z + q - p) \text{ hours} \qquad 4.3.4a$$

is the appropriate relationship to use. However, if the event occurs during the ebb half-cycle then

$$t = -1.01Z + q + \Delta e(0.60Z + r - q) \text{ hours} \qquad 4.3.4b$$

is the appropriate relationship to use.

The utilisation of equations 4.2.5 (to scale the dependent variable) and 4.3.4 (to transform the independent variable) appears to overcome the problems associated with the tidal range scaling of tidal current speed cycles in the southern region of Start Bay. This will now be demonstrated by returning to figures 4.4 and 4.5.

Figure 4.4B shows that, at position O, the use of equations 4.2.5 and 4.3.4 results in a more accurate scaling than use of equations 4.2.5 alone. (The continuous curve represents the cycle obtained utilising both equations 4.2.5 and 4.3.4, and the broken curve, representing the predicted cycle using only equations 4.2.5, has been omitted for clarity).

At position D also, the use of equations 4.2.5 and 4.3.4 results in a much better agreement between the actual and predicted tidal current speed cycles. This is shown in figure 4.5B, where the same notation used in figure 4.4B is adopted. Positions O and D are the only positions (as previously mentioned) in the southern region of Start Bay where tidal cycles have been obtained for various tidal ranges. However, there exists one further position in Start Bay, outside the southern region, where tidal cycles at various tidal ranges are available. This is position E.

To judge the utility of the transformations they have been subjected to a particularly harsh test by being applied to this position.

Figure 4.6A shows a tidal speed cycle collected during a prevailing 2.7 metre tidal range. It is scaled by use of equations 4.2.5 only to refer to a tidal range of 3.6 metes (broken curve). Sea-trial data collected at this tidal range of 3.6 metres is also presented. When equations 4.3.4 are also used the agreement is considerably improved (continuous curve in figure 4.6B) The agreement between these two cycles is very good considering that position E is a particularly harsh test of equations 4.2.5 and 4.3.4 lying, as it does, nearly 10 km northwestward of position O.

In summary, it appears that equations 4.2.5 and 4.3.4 possess the ability to allow a tidal speed cycle to be scaled to any desired tidal range

with a considerable degree of success.

The interrelationships between tidal range and tidal current speed having been discussed, attention is now turned to the effects of tidal range upon the cycles of vertically integrated tidal current direction.

4.4 Tidal current directions

The direction results from position 0 are very inconsistent, as shown in figures 3.1 Further, the transitions of the direction from ebb to flood is sometimes clockwise, sometimes anti-clockwise in nature. However, certain relationships between the direction cycles and tidal range may be obtained.

Figure 4.7 shows how the vertically integrated direction cycles vary with tidal range Z. These cycles are the average of all the cycles obtained at the specified tidal ranges. The ebb to flood transition has been shown as varying clockwise although this did not always happen. This figure once again highlights the tidal range influence on the duration of the flood and ebb half-cycles.

Figure 4.8 shows that the variation of the vertically integrated tidal current direction at low and high waters with tidal range is extremely small. (The analysis of over a hundred tidal amplitude cycles, obtained from the tide gauge at Dartmouth, shows that on average high water occurs six hours before low water, this time difference being independent of tidal range).

The mean flood (high water) direction is found to be 10^{o} with a standard deviation of $\pm 1^{o}$; whereas the ebb (low water) exhibits less consistency having a mean value of 186^{o} with a standard deviation of $\pm 3\frac{1}{2}^{o}$. This increased scatter in the ebb values of $\bar{\theta}$ is probably due to the highly turbulent nature of the water flowing off the shallow Skerries Bank into the deeper Channel. There is not, however, any significant variation in the value of $\bar{\theta}$ with tidal range, either at low water or high water. (The correlation coefficients at low water and high water are 0.04 and 0.02 respectively Student's t test shows these values to be not significant).

Therefore a variation in tidal range appears to affect the shape of the tidal direction cycles but has little effect on the value of the dependent $\bar{\theta}$ variable. A transformation of the independent variable appears all that is necessary to correct for tidal range effects.

Figure 4.9A shows two direction cycles recorded at position 0, one for a tidal range of 2 metres (broken curve), the other 4 metres (circles). There are large errors localised to the transitional regions. Use, upon the 2 metre tidal range cycle, of the transformations 4.3.3 results in a very good prediction of the 4 metre tidal range direction cycle, as shown by the continuous curve in figure 4.9B. It should, however, be noted that, as previously stated, not all the current direction transitions from ebb to flood follow a clockwise rotation.

Indeed, figure 4.12 displaying the tidal current parameters at position D', shows this uncertainty over the directional transition from ebb to flood. The first ebb to flood transition is anti-clockwise in nature, whereas the second, some 12.4 hours later, displays a clockwise rotation. There seems no such uncertainty over the directional transitions from flood to ebb, however, the rotational sense of these direction transitions appearing stable. (This is probably due to the influence upon the flood current directions of the eddy, described in Chapter 7 and Appendix 3.3).

Therefore, a transformation of the independent variable appears all that is necessary to adjust a tidal direction cycle so that it is referred to any new tidal range. However, the rotation of the current direction from ebb to flood may well be in the wrong sense.

Equations 4.2.5 and 4.3.4, when used, therefore allow cycles of the vertically integrated vectorial parameters of the tidal current at a position to be adjusted to refer to any chosen tidal range.

The sea-trial results will now be presented, the effects of tidal range having been investigated.

Figures 4.10 to 4.18 inclusive show one cycle of tidal stream data from each of the nine positions visited in southern Start Bay. (Figures 4.19 to 4.21 inclusive show one cycle of data collected at positions, visited by the writer in the course of the work, but which lie outside the region of immediate interest). The values of tidal current speed and direction are vertically integrated using equation 3.1.1. Also, use is made of equations 4.2.5 and 4.3.4 to refer all these cycles to a chosen reference tidal range of 4 metres. This is approximately the average maximum spring tidal range experienced in Start Bay.

(The cycles shown in figures 4.19 to 4.21 inclusive, are not referred to the chosen standard tidal range because it is believed likely that equations 4.2.5 may break down in northern Start Bay, although they work very well at position E (section 4.3). This feeling is a direct result of the work presented in the following chapter and Appendix 2).

It must be emphasised that the presentation of this data differs radically from that of Acton in that the concept of a preincipal axis has not been evoked. (The concept of a principal axis is detailed by Acton, 1972, chapter 3.4). Although the ebb flow appears to 'lock' to a constant direction, the flood, in general, exhibits no such constant directional flow. The flood $\bar{\theta}$ values vary with time as may be seen by reference to figure 4.14 for instance. Adopting the principal axis notation would mask this variation in $\bar{\theta}$ on the flood and this would, it is felt, be detrimental to this work as this $\bar{\theta}$ variation is an important factor in this region and will be referred to in forthcoming chapters.

Hence, although the use of a principal axis notation may be perfectly acceptable in the central region of Start Bay, it will be shown to be an unwise concept to adopt in the southern region. Because of this, cycles of both $\bar{s}$ and $\bar{\theta}$ are presented for each sea-trial location. The values of $\bar{\theta}$ are referred to true north.

The data presented in figures 4.10 to 4.18 is in a totally compatible

form for a tidal range of 4 metres. Hence, if the value of $\bar{s}$ is required at (say) low water for all the data positions in southern Start Bay, (as it will be when the tidal streams in this region are modelled and the results statistically compared to the sea-trial data) the values can be read directly off the presented curves.

Provided a modelling method is available, this compatibility of results enables the tidal streams, referred to any time during a tidal cycle, to be obtained.

The decision as to which modelling technqiue to employ, in this particular region, is taken in Chapter 6. As a necessary preliminary, however, in the following chapter the hydrodynamic equations are applied to southern Start Bay in order to ascertain the principle hydrodynamic forces at work in this region.

CHAPTER 5 THE HYDRODYNAMIC EQUATIONS

In this chapter the hydrodynamic equations of motion and continuity are introduced. Throughout emphasis is placed on assessing the order of magnitude of the various terms in these equations in order to discover if any terms may reasonably be neglected compared to others.

By using a space-averaging technique, many terms are found to be negligible, resulting in the hydrodynamic equations of motion and continuity being reduced in complexity. The resulting approximate equations, which describe the water flow in the southern region of Start Bay, are shown to be drastically different from those normally used.

This chapter commences by introducing the continuity equation.

5.1 The Continuity Equation

This equation simply expresses the fact that water is virtually incompressible. A derivation of the equation is given by Proudman (1953) who includes a term to account for any rainfall. This correction for rainfall is very small for the work described in this thesis and is neglected. The continuity equation is thus given by

$$\frac{\partial(hu)}{\partial x} + \frac{\partial(hv)}{\partial y} + \frac{\partial \zeta}{\partial t} = 0 \qquad 5.1.1$$

where u and v are the vertically integrated values of the tidal current speed components in the horizontally perpendicular x and y directions. The 'bars' over these letters have, for convenience, been omitted but are nevertheless implied.

The first term represents the excess amount of water flowing into or out of a volume in the sea in the x direction; the second term, the excess amount of water flowing into or out of a volume in the sea in the y direction. The third term denotes the rise or fall in sea level, ζ representing the level of the sea above some fiduciary level. These three terms must, when

added, be equal to zero if the water in the sea is incompressible.

Besides the continuity equation, classical hydrodyamics supplies two more equations relating u, v and ζ . These are the equations of motion.

5.2 The Equations of Motion

The two basic equations of motion, in their vertically integrated form, are given by Proudman (1955). Allowing for a change of notation, these equations are

$$\frac{\partial u}{\partial t} - Cv = -g\frac{\partial \zeta}{\partial x} - \frac{1}{\rho}\frac{\partial P_a}{\partial x} + \frac{1}{\rho h}(X_s - X_b) \qquad 5.2.1a$$

$$\frac{\partial v}{\partial t} + Cu = -g\frac{\partial \zeta}{\partial y} - \frac{1}{\rho}\frac{\partial P_a}{\partial y} + \frac{1}{\rho h}(Y_s - Y_b) \qquad 5.2.1b$$

where u and v are once again the vertically integrated velocity components in the x and y directions, the 'bars' over them having been omitted for convenience. ρ is the water density, and the other symbols are discussed below.

The righthand sides of the equations contain the terms causing the current to flow. These, for the x direction, are the pressure gradient terms $-g\frac{\partial \zeta}{\partial x}$ and $-\frac{1}{\rho}\frac{\partial P_a}{\partial x}$ and the body force per unit mass terms Xs and Xb. The term $-g\frac{\partial \zeta}{\partial x}$ represents the pressure gradient caused by the slope of the sea and $-\frac{1}{\rho}\frac{\partial P_a}{\partial x}$ the atmosphere pressure gradient caused by a variation with x of the atmospheric pressure Pa. The two important body forces are those of wind (Xs, Ys) and bottom friction (Xb, Yb). At the surface, wind will produce a shearing force tending to drive the water in the direction of the wind; at the bottom, the water is slowed by the drag resistance of the stationary bottom tending to oppose the current.

These forces upon the right hand side are balanced upon the left by the corresponding mass accelerations. These are the direct acceleration terms

such as $\frac{\partial u}{\partial t}$ and the geostrophic accelcration arising as a consequence of the movement taking place upon a rotating globe (Coriolis effect). Here C is the Coriolis coefficient equal to $2\Omega \sin \phi$: Ω being the angular frequency of rotation of the Earth and ϕ the angle of latitude.

Equations 5.1.1 and 5.2.1 are the hydrodynamic equations which are supposed to describe the tidal flow in southern Start Bay. However, this region possesses an eddy during some or all of the flood half-cycle, as may be seen by reference to figure 5.1. (Here 'tidal range corrected' values of $\bar{\theta}$ at high water, from all data positions in Start Bay, are plotted as arrows).

Such an eddy, which is known to exist by the local fishermen, would not be expected to arise in the solution of the equations 5.1.1 and 5.2.1 because they are linear in u and v.

The continuity equation 5.1.1 is exact but equations 5.2.1 are, in fact, first order approximations.

In his investigations, Proudman neglected the second order advection terms, such as $u\frac{\partial u}{\partial x}$, present in the Euler equations of classical hydrodynamics - see for instance Lamb (1945), page 4. In the work he is discussing, it is felt that Proudman is perfectly justified in doing this. Indeed, the argument is commonly given, when dealing with the open sea, that the advection terms will be neglected because the tidal current vector does not change rapidly with space. In the open sea one does not, however, usually encounter a region exhibiting such radical changes in topography as exists in the southern region of Start Bay. The tidal current vector - it is believed as a result of these changes in topography - exhibits considerable variation throughout this region. In the present investigation, the second order advection terms will therefore be included in the equations of motion (5.2.1).

Because these advection terms are non-linear, exact vertical integration is complicated. Since, however, the purpose of the analysis performed in

this chapter is to assess the order of magnitude of the various terms, an approximate expression for the vertically integrated advection terms will suffice. Using Proudman's approximate physical model of the flow velocity being independant of depth,(Proudman, 1953, page 303) the vertically integrated advection terms can be approximated, for the x direction, by

$$u\frac{\partial u}{\partial x} + v\frac{\partial u}{\partial y}$$

and for the y direction by

$$u\frac{\partial v}{\partial x} + v\frac{\partial v}{\partial y}$$

With this done, equations 5.2.1 become

$$\frac{\partial u}{\partial t} + u\frac{\partial u}{\partial x} + v\frac{\partial u}{\partial y} - Cv = -g\frac{\partial \zeta}{\partial x} - \frac{1}{\rho}\frac{\partial P_a}{\partial x} + \frac{1}{\rho h}(X_s - X_b) \qquad 5.2.2a$$

$$\frac{\partial v}{\partial t} + u\frac{\partial v}{\partial x} + v\frac{\partial v}{\partial y} + Cu = -g\frac{\partial \zeta}{\partial y} - \frac{1}{\rho}\frac{\partial P_a}{\partial y} + \frac{1}{\rho h}(Y_s - Y_b) \qquad 5.2.2b$$

These equations are in a rather general form, but they may be simplified by applying them to specially chosen conditions as described by Acton (1972).

In Chapter 2.3 of his thesis, by considering the results of Neumann and Pierson (1966) and Ekman's results (Neumann, 1968), Acton concludes that in Start Bay, for wind speeds of less than 10 m.p.h., the effects of wind drag and atmospheric pressure gradient are negligible.

Apart from half a tidal cycle recorded at position N, wind speeds prevailing during the sea-trials detailed in Chapter 2 were less than 10 m.p.h. Accordingly equations 5.2.2 become

$$\frac{\partial u}{\partial t} + u\frac{\partial u}{\partial x} + v\frac{\partial u}{\partial y} - Cv = -g\frac{\partial \zeta}{\partial x} - \frac{1}{\rho h}(Xb) \qquad 5.2.3a$$

$$\frac{\partial v}{\partial t} + u\frac{\partial v}{\partial x} + v\frac{\partial v}{\partial y} + Cu = -g\frac{\partial \zeta}{\partial y} - \frac{1}{\rho h}(Yb) \qquad 5.2.3b$$

Acton's 'calm weather approximation' having been employed.

These equations can be made more explicit by using the 'hydraulic approximation' for the friction terms detailed again by Acton, in his Chapter 2.4. Here an estimation of these friction terms is obtained by studying the parameters of the Darcy formula (see for instance Barna, 1964, Chapters 4 and 5) which relates the steady speed of water flow to the gradient down which it flows.

By considering a limited region of the sea as corresponding to a wide channel and denoting the hydraulic radius by the depth of water, Acton argues that the Darcy formula may be used to obtain Xb and Yb. The necessary proviso to be satisfied is that the vectorial parameters of the tidal currents should not change greatly over distances an order of magnitude greater than the depth h. In the southern region of Start Bay, the average depth is about 20 metres, so the condition to employ the hydraulic approximation for the friction terms is that the tidal current vector shall not vary greatly over distances of order 200 metres.

It is felt that, considering the region as a whole, this condition is satisfied, although in certain areas one may be approaching the limit of it's validity. As, however, in section 5.3 interest is centred on the 'space-averaged' equations of motion, the use of this hydraulic approximation to the friction terms in equations 5.2.3 is considered justified and will be employed.

The friction term in equation 5.2.3a is thence given by

$$\frac{1}{\rho h}(Xb) = \frac{f\sqrt{u^2+v^2}.u}{8h}$$

where f is the hydraulic friction term given by Barna (1964), table 4.4. Similarly, for the y direction, Yb is given by

$$\frac{1}{\rho h}(Yb) = \frac{f\sqrt{u^2+v^2}.v}{8h}$$

Substitution of these relationships into equations 5.2.3 yield the final form of the approximate vertically integrated euqtions of motion; thus

$$\frac{\partial u}{\partial t} + u\frac{\partial u}{\partial x} + v\frac{\partial u}{\partial y} - Cv + \frac{f|s|u}{8h} = -g\frac{\partial \zeta}{\partial x} \qquad 5.2.4a$$

$$\frac{\partial v}{\partial t} + u\frac{\partial v}{\partial x} + v\frac{\partial v}{\partial y} + Cu + \frac{f|s|v}{8h} = -g\frac{\partial \zeta}{\partial y} \qquad 5.2.5b$$

where the 'bars' signifying vertically integrated values are implied and use has been made of the relationship

$\sqrt{u^2+v^2} = s$, the vertically integrated tidal current speed.

Thus classical hydrodynamics has supplied three differential equations (5.1.1 and 5.2.4) which give a mathematical account of the flow at every position in the southern region of Start Bay. These equations are difficult to solve mathematically due to the presence, in the equations of motion, of the second order advection terms.

It is, however, possible - using knowledge gained from the sea-trials - to approximate these three equations into a simpler form. The method to be presented involves obtaining the space-averaged equations of motion and continuity, and is discussed in detail in the following sections.

5.3 The Space-averaged Equations of Motion

Before deducing the space-averaged equations of motion, it is perhaps useful to briefly discuss the reasons behind the use of this process.

Equations 5.2.4 describe rather accurately the flow at any position in the southern region of Start Bay. However, it is difficult to appreciate what terms are really influencing the current most in this region. By the process of space-averaging an order of magnitude for the terms on the left-hand side of equations 5.2.4 can be obtained, and it will be shown that some of these terms can be neglected when compared to the others.

For instance, if the friction and advection terms are found dominant by space-averaging, then it may be concluded that, considering the southern region of Start Bay as a whole, the water flow is affected most by these terms. The space-averaged equations would then be equations 5.2.4 suitably adjusted by the omission of the direct acceleration and Coriolis terms. These simpler approximate equations will, in general, be easier to solve than the original set.

The process used is based on the process of Normalization (see for instance Li and Lam, 1964, page 172) which reduces the number of parameters involved in the solution of equations by the use of a linear dimension L and a speed S.

We define S as the space averaged, depth-averaged speed and L the typical distance over which the tidal current speed s changes by S. Using the substitutions

$$\begin{aligned} s &= Ss' \\ u &= Su' \\ v &= Sv' \\ x &= Lx' \\ y &= Ly' \end{aligned} \qquad 5.3.1$$

in equation 5.2.4a, results in this becoming

$$S\frac{\partial u'}{\partial t} + \frac{S^2}{L}u'\frac{\partial u'}{\partial x'} + \frac{S^2}{L}v'\frac{\partial u'}{\partial y'} - CSv' + \frac{fS^2|s'|u'}{8h} = -\frac{g}{L}\frac{\partial \zeta}{\partial x'}$$

Approximating $\frac{\partial u'}{\partial t}$ by $j\omega u'$, where ω is the angular frequency of the tidal cycle, and dividing by $\frac{S^2}{L}$ results in this equation becoming

$$j\left(\frac{\omega L}{S}\right)u' + u'\frac{\partial u'}{\partial x'} + v'\frac{\partial u'}{\partial y'} - \left(\frac{CL}{S}\right)v' + \left(\frac{fL}{8h}\right)|s'|u' \approx -\frac{g}{S^2}\frac{\partial \zeta}{\partial x'} \qquad 5.3.2$$

(It is perhaps interesting to note that the dimensionless terms bracketed may be expressed differently:

$\frac{\omega L}{S} = \frac{2\pi}{St}$ where St is the Strouhal number

$\frac{CL}{S} = \frac{1}{R_o}$ where R_o is the Rossby number

and

$\frac{fL}{8h}$ is a dimensionless friction number

It should, however, be noted that these are space-averaged values.

Now, because L is defined as the typical distance over which Δs equals S, it follows that $(\partial u'/\partial x')$ and $(\partial u'/\partial y')$ are of order unity when space averaged. Using this fact and dividing by u', equation 5.3.2 becomes

$$j\frac{\omega L}{S} + 1 + \frac{v'}{u'} - \frac{CL}{S}\frac{v'}{u'} + \frac{fL|s'|}{8h} \approx -\frac{g}{S^2u'}\frac{\partial \zeta}{\partial x'}$$

However, when averaged over space, the ratio v'/u' can be made of order unity by a suitable choice of axes. Also, as S is the space-average of all the tidal current speed s values and s' is s/S then, when space-averaged, s' will equal unity.

Hence one obtains

$$j\frac{\omega L}{S} + 1 + 1 - \frac{CL}{S} + \frac{fL}{8h} \approx \text{Hydrostatic term} \qquad 5.3.3$$

This equation allows the order of magnitude of the terms comprising the equations of motion to be deduced. These terms are, working from left to right, the direct acceleration term $j\frac{\omega L}{S}$, the advection terms 1 + 1, the Coriolis term CL/S and the friction term fL/8h.

Now, in the southern region of Start Bay, the results from chapter 2 allow an estimation of S and L to be made. The value of S is taken as 0.5 m/s for low and high water, L as 1 km, the Coriolis coefficient C as 1.11×10^{-4} sec^{-1}, and the angular frequency of a tidal cycle ω as 1.41×10^{-4} sec^{-1}. Knowledge concerning the value of f is, unfortunately, still very imperfect. The value of f adopted to allow an estimate of the order of magnitude of the friction terms in equation 5.3.3 is 0.04, in agreement with the value adopted by Acton (1972) who, on page 69 of his thesis, says

> "The value of f used here" .... "was 0.04, representing a mean between the likely limits of 0.02 and 0.08, suggested by the friction charts (Barna 1964, page 55)".

Hence, the order of the terms in equation 5.3.3, for the southern region of Start Bay, is given by

$$j0.28 + 1 + 1 - 0.22 + 0.25 \sim \text{Hydrostatic term}$$

where h, the space-averaged depth, is taken as of order 20 metres.

Thus, in the southern region of Start Bay it appears reasonable to simplify by neglecting all except the advection terms on the left hand side of the equations of motion. Hence

$$u\frac{\partial u}{\partial x} + v\frac{\partial u}{\partial y} = -g\frac{\partial \zeta}{\partial x} \qquad 5.3.4a$$

and $$u\frac{\partial v}{\partial x} + v\frac{\partial v}{\partial y} = -g\frac{\partial \zeta}{\partial y} \qquad 5.3.4b$$

are considered to approximately describe the flow in this region.

The same process is now applied, out of interest, to the northern part of Start Bay. Here the experimental data suggests S = 0.5 m/s., L ≈15 km. and h ≈ 25 metres and equation 5.3.3 becomes

$$j4{\cdot}2 + 1 + 1 - 3{\cdot}3 + 3{\cdot}0 \approx \text{Hydrostatic term}$$

Thus, in the northern part of the bay it appears reasonable to neglect the advection terms and retain the direct acceleration, Coriolis and friction terms. This is the usual practice in oceanographic calculations.

This space-averaging process is now applied to the continuity equation.

5.4 The space-averaged continuity equation

The continuity equation, given in section 5.1 is

$$\frac{\partial(hu)}{\partial x} + \frac{\partial(hv)}{\partial y} + \frac{\partial \zeta}{\partial t} = 0 \qquad 5.4.1$$

As in the last section, the substitutions 5.3.1 are employed together with the additional relationship that h equals Hh' where H is the typical change in depth over distance L. This converts equation 5.4.1 to

$$\frac{HS}{L}\frac{\partial(h'u')}{\partial x'} + \frac{HS}{L}\frac{\partial(h'v')}{\partial y'} + j\omega\zeta = 0 \qquad 5.4.5$$

where, approximating, $\partial\zeta/\partial t$ has been put equal to $j\omega\zeta$.

As in the last section, the definition of L allowed $\partial u'/\partial x'$ and $\partial v'/\partial y'$ to be put of order unity, the additional definition of H as the

typical depth change over distance L allows $\partial(h'u')/\partial x'$ and $\partial(h'v')/\partial y'$ to be put of order unity when space averaged. Using this fact and dividing by $\frac{HS}{L}$, equation 5.4.2 becomes

$$1 + 1 + j\frac{\omega L}{HS}.\zeta \qquad 5.4.3$$

Now for the southern region of Start Bay H is of order 10 metres and ζ, for a spring tide, 4 metres. Hence, for the order of magnitude of the terms in the continuity equation one obtains

$$1 + 1 + 0{\cdot}12$$

Thus, for the southern region of Start Bay the space-averaged approximation of the continuity equation becomes

$$\frac{\partial(hu)}{\partial x} + \frac{\partial(hv)}{\partial y} = 0$$

the term $\partial\zeta/\partial t$ having been neglected. It may again be noted that if the northern region of Start Bay is considered, putting L = 15 km and H = 20 metres it is found that no term in the continuity equation may be omitted.

5.5 The Approximate Equations

The work of the preceding section suggests that the motion of water in the southern part of Start Bay may be approximately represented by the space-averaged hydrodynamic equations

$$u\frac{\partial u}{\partial x} + v\frac{\partial u}{\partial y} = -g\frac{\partial \zeta}{\partial x}$$

$$u\frac{\partial v}{\partial x} + v\frac{\partial v}{\partial y} = -g\frac{\partial \zeta}{\partial y} \qquad 5.4.4$$

$$\frac{\partial(hu)}{\partial x} + \frac{\partial(hv)}{\partial y} = 0$$

By comparison, the approximate hydrodynamic equations describing the tidal flow in the northern part of Start Bay are

$$\frac{\partial u}{\partial t} - Cv + \frac{f|s|u}{8h} = -g\frac{\partial S}{\partial x}$$

$$\frac{\partial v}{\partial t} + Cu + \frac{f|s|v}{8h} = -g\frac{\partial S}{\partial y} \qquad 5.4.5$$

$$\frac{\partial(hu)}{\partial x} + \frac{\partial(hv)}{\partial y} + \frac{\partial S}{\partial t} = 0$$

Comparison of these two sets of equations highlights the variation in tidal flow across Start Bay. In the northern part the differential equations that describe the flow are like those with 'open sea' conditions, and the advection terms may be sensibly neglected. Some 15 km to the south the situation radically changes. Here the 'second order' advection terms, negligible in the northern region, dominate the equations of motion and the effect of tidal rise and fall ($\partial S/\partial t$) appears to have little effect. (Appendix 3.3 provides further evidence of the radical differences that exist between northern and southern Start Bay).

These equations (5.4.4 and 5.4.5) are not necessarily correct at every position. Because they are space-averaged, they represent the approximate hydrodynamic equations describing the tidal flow over the region taken as a whole. Hence, for example, although bottom friction appears negligible in equations 5.4.4, it may play a significant part in influencing the tidal streams in discrete parts of this region. The shallow Skerries Bank, with it's numerous sand-wave structures (Robinson, 1961), is such a region.

The tidal stream configuration in northern Start Bay is readily soluble using mathematical modelling techniques. However, as the southern region has second order advection terms describing the tidal stream configuration, the question of whether mathematical modelling is still a viable proposition must be raised. Accordingly, the best modelling procedure to adopt for this region is considered next.

CHAPTER 6 SOLUTION OF THE HYDRODYNAMIC EQUATIONS

Space-averaging has suggested that, unlike the normal case typified in the northern part, southern Start Bay is something of an 'oddity' The approximating equations appear to be quite different in their mathematical structure from those describing 'open sea' conditions. In particular, the second order non-linear advection terms are too large to be neglected or even to be regarded as pertibations. This chapter considers some alternative techniques for the solution of theseunusual equations.

6.1 Mathematical Modelling

Numerical modelling appears to be the main technique used in investigating tidal currents in the sea (see, for instance, Dronkers and Schonfield, (1955), Heaps (1969) or Acton (1972)).

One modelling technique involves programming a computer to solve the relevant hydrodynamic equations. With this done, various hypothetical boundary conditions may be fed into the computer; hypothetical tidal stream maps resulting. By, say, statistical comparison with sea-trial data collected at data positions, these maps may be deduced as statistically significant or statistically non-significant as a representation of the tidal streams in the area under consideration.

Two problems exist if this technique is considered for use in modelling the tidal streams of southern Start Bay. Firstly, devising a computer algorithm to solve the non-linear hydrodynamic equations (5.4.4) is difficult. The presence of the second order advection terms in the equations of motion makes this so.

Secondly, assuming a satisfactory algorithm to be available, the choice of possible and plausible boundary conditions is countless. To hit upon the right combination of boundary conditions may take a considerable length of time. This problem - of suitable boundary conditions - is relatively trivial in the solution of linear differential equations because the principle

of superposition can be employed. It is the lack of a superposition principle for the non-linear equations which stimulated the search for alternatives to mathematical modelling.

Another mathematical modelling technique involves interpolating between data positions at which the tidal current vector is known. By a suitable choice of interpolating function, the tidal stream vector existing between data positions may be deduced. However, this relies heavily on knowing what interpolating function to use.

In the northern part of Start Bay, a relatively flat sea-bottom exists. There, therefore, exist few physical obstructions to the flow of water, the tidal current vector varying little with space. Consequently, a linear interpolating function may suffice. In southern Start Bay, however, the topography of the sea-bed is quite different. The flat bed of the northern region is replaced by an uneven topography which the Skerries Bank dominates. Considerable variation of water depth and tidal current vector, with space, prevail. It seems unreasonable to expect linear interpolation to work in such a region unless numerous data positions are available, which is not the case. Hence, one is forced to use a non-linear interpolation function: but what function? Acton (1972) suggests that the degree of this function (that is the number of maxima and minima it possesses) between two positions, should be the same as the degree of the equation describing the depth changes. However, the existence of an eddy complicates this picture. Consider figure 6.1. This is really a reproduction of part of figure 7.6. An eddy exists to the north of Start point. It may be seen that the topographically inferred interpolation function bears no relationship to the tidal current vector variation along the line XY. The presence of an eddy, such as the one which exists in southern Start Bay during the flood half-cycle, therefore upsets numerical interpolation. Further, the sea-trial locations were not chosen to lie along straight lines as this method

demands. Hence, such mathematical modelling in this particular region must be considered undesirable.

It was these difficulties with mathematical models which led the author to consider hydraulic modelling. The usual objections to such models is their size and cost. The next section shows that small, low cost, hydraulic models have a special application to the present problem.

6.2 Hydraulic Modelling

Noda (1972, page 511) states of hydraulic scale models

"Scale models of hydraulic phenomena are, in essence, a means of replacing the analytic integration of the differential equations governing the process including very complicated initial and boundary conditions. But before reliable information can be derived from scale models, the physical laws which cause the process must be understood so that the relative magnitude of the forces involved remain the same".

The relative magnitudes of the hydrodynamic forces operating in the sea and in a hydraulic model are given by equations 5.3.3 and 5.4.3. These equations are

$$j\frac{\omega L}{S} + 1 + 1 - \frac{CL}{S} + \frac{fL}{8h} \sim \text{Hydrostatic term} \qquad 5.3.3$$

and

$$1 + 1 + j\frac{\omega L}{HS}.\zeta \sim 0 \qquad 5.4.3$$

Noda's criteria to employ a hydraulic model to duplicate the tidal stream configuration in part of the sea, dictates that the relative magnitudes of the hydrodynamic forces, both in nature and in the model, remain the same.

For southern Start Bay, these criteria are that the algebraic terms in the above equations be neglectable compared to the 'unity advection terms'.

The Coriolis effect upon the water flow in a small model is well known to be minute and will, as usual, be taken as zero. Hence $\frac{CL}{S}$ may be neglected compared to unity for any scale model. Further, if a constant water flow is employed through the model, then $j\frac{\omega L}{S}$ and $j\frac{\omega L}{HS}.S$ become zero as, these conditions correspond to $\omega = 0$.

Finally, consider the model to exhibit a horizontal scale of 1:25,000 and an exaggerated vertical scale of, say 1:1440. In this case h becomes 0.014 metres when space-averaged. Assuming a space-averaged water speed of 0.04 metres per second leads to the space-averaged Reynolds number Re being about 500. Now, under laminar flow conditions, the friction factor f is given by (see, for instance, Barna, 1964, page 57)

$$f = \frac{64}{Re}$$

For this as yet hypothetical model, f is thence found to be of value about 0.13. Hence $\frac{fL}{8h}$ becomes of order 0.3L where L is the typical distance over which the tidal current speed s changes by the space-averaged tidal current speed S (see Chapter 5.3). Now the value of L in the model is difficult to ascertain until water actually starts to flow. Accordingly, the writer constructed a crude representation of Start Bay in a stream near his home. With a flow-rate through this model of about 0.04 metres per second, it soon became apparent that L in the region of interest would certainly not exceed 0.1 metres and would probably be less than half this value. Taking 0.1 metres to be the value of L, the value of $\frac{fL}{8h}$ becomes of order 0.03; very much less than unity. (If the model genuinely reproduces the tidal streams in southern Start Bay, L would be of order 0.04 metres and the friction term in equation 5.3.3 would become of order 10^{-2}; very small compared to unity).

So, for this model, equations 5.3.3 and 5.4.3 become

$0 + 1 + 1 - 0 + 0.03 \sim$ Hydrostatic term

and $1 + 1 + 0 \sim 0$

Thus, the approximate hydrodynamic equations describing the flow in this scale model representation of southern Start Bay are identical to those describing the flow in nature, viz.

$$u\frac{\partial u}{\partial x} + v\frac{\partial u}{\partial y} = -g\frac{\partial \zeta}{\partial x}$$

$$u\frac{\partial v}{\partial x} + v\frac{\partial v}{\partial y} = -g\frac{\partial \zeta}{\partial y}$$

$$\frac{\partial (hu)}{\partial x} + \frac{\partial (hv)}{\partial y} = 0$$

Although the whole of this section is semiquantitative, it served to suggest that it is a plausible hypothesis that a simple small-scale hydraulic model of Start Bay, incorporating a vertical scale exaggeration and replacing the highly turbulent nature of the sea ($Re \sim 10^8$) by a constant lamina flow ($Re \sim 500$), will allow the tidal streams in the southern region to be modelled.

It was decided to put this hypothesis to the test by constructing such a model. The proof of the utility of the model in no way rests upon the work of this and the last chapter but upon the comparisons between it's predictions and real sea data.

A description of this model and it's predictive use is now presented.

CHAPTER 7 THE HYDRAULIC MODEL

7.1 Introduction

In the last chapter it was concluded that the space-averaged approximate hydrodynamic equations describing the tidal flow in southern Start Bay (5.4.4) are especially suited to solution by hydraulic modelling.

The first serious attempt to use hydraulic modelling to investigate tidal flow, appears to be that performed by Professor Osborne Reynolds in 1885 (Reynolds, 1887). His model represented a stretch of the river Mersey between Liverpool narrows and Runcorn. Using a bed of sand Reynolds found that, by simulating some 2000 tides, the sand was shaped by the action of the model currents so as to agree closely with the configuration in nature.

Since these initial trials of Reynolds, tidal modelling utilizing hydraulic scale models has become an accepted possibility although such models are mainly confined to solving for the tidal flows experienced in river estuaries and ports. (Examples of such modelling are Gibson (1933) on the probable effects of a proposed tidal barrage to develop hydro-electric power from the very high tides in the Severn estuary; Elsden (1939) on an investigation of the outer approach channels to the port of Rangoon or, more recently, a British Transport Docks Board Report (1970) on an investigation of the tides in the Humber).

These hydraulic models are invariably very large in size, require ingeneously designed tide-generating equipment and are both expensive to build and operate. Fortunately, southern Start Bay is not as demanding of a model as most tidal regions; a fact which was displayed in Chapter 6 and will be considered further when the description of the model used is given in the next section.

7.2 Description of the Hydraulic Model

The model is shown in figure 7.1. A constant flow of water enters the model via the rubber tube shown on the right hand side of the photograph. This flow is subjected to a 180° turn, passing through an angular piece of 'dexion' in doing so. By then being subjected to passage through three more pieces of 'dexion' and a triple row of closely spaced 'dexion' bolts stood on end, this constant flow of water is made more uniform in approach to the coastal outline.

The physical model of the Start Bay region comprises a polystyrene outline of the entire bay mounted on a base of perspex. This is coupled with the most accurate scaled representation of the submarine topography that it was possible for the writer to practically make. The polystyrene outline, weighted to overcome it's buoyancy, was carefully constructed to a horizontal scale of 1:25,000. It differs from a scaled down version of the situation in nature only in respect of the sealing off of the Dart estuary. (The comparatively trivial quantity of water entering or leaving this estuary was considered unlikely to have any significant effect on the water flow in the southern part of the bay).

The submarine topography exhibited a vertical scale of 1:1,440, being exaggerated compared to the horizontal scale (1:25,000) to satisfy the second criteria given in Chapter 6. The modelling of this submarine topography was performed using clay moulded to be level with the extreme tops of pieces of copper wire vertically mounted in a perspex base. The lengths of these pieces of wire were scaled to correspond to 50 metres minus the datum depth of water, obtained from the hydrographic chart of the area (Hydrographer, 1972b). They are located on the intersections of a ½ km. (in nature) grid. Using this method, it is estimated that the submarine topography, corresponding to less than 50 metres depth, was everywhere modelled to be accuracy equivalent to about ± 2 metres. Depths greater than 50 metres lie well out in the English Channel and were not modelled being represented everywhere by a

constant depth equivalent to 50 metres.

Furthermore, the submarine topography and coastal outline in the model were rotatable to allow for ease of setting up of the desired flow. The required depth of water in the model is preset by the height of the weir shown in the bottom right of figure 1. This enabled the water level to be adjusted to refer to either low or high water.

A camera mounted vertically over the model allowed time-lapse photographs of a float traversing the region of interest to be secured. Illumination for this was supplied by a strobe. The float being virtually neutrally buoyant, extending from the surface down to a real-life depth of 5 metres, ensured clearance over the shallow Skerries Bank region. The relative speed of this float is assumed representative of the relative vertically integrated tidal current speed in Start Bay once a representative flow pattern has been obtained. (The obtaining of this flow pattern is detailed in the next section).

A grid, located just above the surface of the water and corresponding to one minute intervals of latitude and longitude, provided a reference for determining the float positions.

The flow used for all the modelling runs exhibited a space-averaged water speed of about 0.04 m/s. and associated Reynolds number of about 500. The use of this model to solve equations 5.4.4 for the ebb flow in southern Start Bay is now detailed.

7.3 Modelling the ebb flow pattern

For the success of the hydraulic model, equations 5.4.4 dictate that the advection terms must be dominant. Another criteria is that a constant flow be used. These conditions are best satisfied by a fast constant flow. Accordingly, it was decided to model the tidal streams at low and high water when it is generally true that the water speed is close to a maximum

The hydraulic model was first used to interpolate the current directions

between data positions. To achieve this, the flow into the model was first adjusted until the water flow directions at the points corresponding to data positions A, D, J and K, in southern Start Bay, bore close agreement with the tidal current directions recorded on sea-trials.

The tidal current direction at low water at position H, in the extreme northeastern corner of Start Bay is 212^{o} (figure 4.20). As a starting point, therefore, the incident direction of the model water flow, relative to the coastal outline, was varied from 205^{o} to 225^{o} in 5^{o} intervals. This was achieved by slightly rotating the coastal outline, in the model, relative to the undirectional and uniform water flow. For each of the five incident water flow directions, the model flow pattern was obtained by the following method.

The 35 mm camera, mounted vertically over the model, and an electronic strobe - operating at a constant frequency of about two flashes/second - were used to obtain time-lapse photographs of a float traversing the region of interest. To ensure that this float attained equilibrium with the water flow before passing into this region, it was carefully placed into the water some 10 cm upstream from the boundary of the region representing southern Start Bay. Just before it (the float) passed into this modelled region, the camera shutter was opened and remained so until the float passed out of the region of interest. By this means, a time-lapse photograph of the track was obtained; the motion of the float being frozen everytime the strobe activated. (A float track obtained in such a fashion is shown in figure 7.2).

Using the grid as reference and projecting the developed negative onto a screen, these float positions were transferred onto a chart of Start Bay. The pathline of the float through the model resulted from the smooth joining of these points. However, as a constant water flow was used in the model this pathline also represents the water flow streamline. So, by performing this float tracking technique some 60 times from different initial positions,

a picture of the model flow pattern (for incident flow directions of 205^{o}, 210^{o}, 215^{o}, 220^{o} and 225^{o}) resulted. Deductions of the model-predicted current directions at the positions corresponding to the sea-trial positions A, D, J and K, for each of the five cases, were then made. These values, for each incident direction of model water flow upon the coastal outline, were compared to the sea-trial tidal stream directions obtained from figures 4.10 to 4.18. For the ebb, the use of the constant and uniform flow of water - incident upon the coastal outline at a direction of 215^{o} (see figure 7.1) was found to yield results which were in agreement with those from nature at the above mentioned four positions to $\pm 2^{o}$. This model flow pattern is shown in figure 7.3.

To test whether this figure represents the real situation throughout the southern part of the bay, it was then used to predict the flow directions at the five other data points not used in the initial adjustments. Table 7.1 gives a comparison between the predicted low water current directions from the model and those observed in nature. (The sea-trial results used in setting up the flow are not included in this table).

Table 7.1 Comparison between observed and model predicted $\bar{\theta}$ results at low water

Trial	Position	Current direction $\bar{\theta}$		
		Observed values(s)	Mean observed value	Model predicted value
U.C.S. U.C.S.	D' D'	208^{o} 198^{o}	203^{o}	201^{o}
13 13	N N	172^{o} 172^{o}	172^{o}	172^{o}
U.C.S.	O	186^{o}	186^{o}	190^{o}
14	P	180^{o}	180^{o}	180^{o}
15	Q	188^{o}	188^{o}	190^{o}

The first column gives the identifying number of the sea-trial; the second the position visited and the third column gives the tidal current direction recorded. The mean value of the tidal current directions recorded at a position is given in column 4 and compared to the model prediction givin in the last column.

This table shows the excellent agreement achieved, between the hydraulic model predictions of the tidal current direction at the five listed sea-trial positions, and that observed in nature. Statistical analysis suggests that figure 7.3 is representative of nature to an accuracy of about $\pm 3^{o}$. Hence, figure 7.3 enables a deduction of the vertically integrated tidal current direction at low water (referred to a tidal range of 4 metres) at any position within the presented area, to be made.

During this modelling of the ebb flow pattern, an interesting 'phenomena' was seen to exist just south of Start Point. In order to check that the float was behaving satisfactorily, potassium permanganate crystals were sprinkled into the water. After settling on the bottom, these crystals began to dissolve. Under the influence of the model currents, the potassium permanganate tracers given off by the crystals showed up a slowly rotating clockwise eddy. This lay just south of Start Point.

The continuation of the model flow pattern outside the southern region of Start Bay, to highlight the existence of this eddy, is also shown in figure 7.3. These flow lines are represented by broken lines. It must be emphasised that the flow pattern in this region is only sketched and should not be used to deduce $\bar{\theta}$. Lying outside the region of interest, this apparent eddy will largely be ignored although it is mentioned briefly in Appendix 3.3.

The modelling of the ebb tidal current speeds is now considered.

7.4 Modelling the ebb flow tidal current speeds :

The strobe operated at a constant frequency throughout a trial. Hence, the speed of water flow in the model is represented by the relative movement of the float between strobe activations. From the photographic observations of float movement, the distance between float positions were measured along the pathline. By performing this technique for the 60 or so float tracks, used to obtain the flow pattern shown in figure 7.3, a contour map of the model 'speeds' was obtained.

These model 'speeds' do not, however, correspond in absolute terms to the observed sea-trial speeds. What is preserved, in the modelling, is the ratio of the speeds at any two points. Hence, if X denotes some arbitrary position, then

$$\frac{\text{Model speed at X}}{\text{Model speed at 0}} = \frac{\text{Real speed at X}}{\text{Real speed at 0}}$$

Rearranging this relationship yields

$$\text{(Model predicted) real speed at X} = \text{Real speed at 0} \frac{\text{Model speed at X}}{\text{Model speed at 0}}$$

From the contour map of the model speeds, the ratio of the model speed at X to that corresponding to position 0 in nature was computed. Next, by using the mean value of tidal current speed at low water, collected at sea at position 0 during prevailing tidal ranges of 4 metres, the model prediction for the real speed elsewhere in southern Start Bay was computed. Figure 7.4 shows the contour map of these model predicted speeds.

Table 7.2 gives the comparison between model predicted and sea-trial recorded tidal current speeds. The prediction of $\bar{s}$ at position N is given as less than 0.4 m/s because the float, on passing so close to the coastal outline, exhibited an overwhelming attraction to it, veering onto a collision course.

As was the case with the model predicted flow pattern (figure 7.3), the model prediction of the tidal current speed contours gives very good agreement

Table 7.2 Comparison between observed and model predicted $\bar{s}$ values at low water

Trial No	Position	Current speed $\bar{s}$		
		Observed value(s)	Mean observed value	Model predicted value
Admiralty	A	0.94 m/s	0.94 m/s	1.06 m/s
4	D	0.46 m/s		
6	D	0.55 m/s	0.52 m/s	0.56 m/s
10	D	0.56 m/s		
U.C.S.	D'	0.54 m/s	0.55 m/s	0.59 m/s
U.C.S.	D'	0.56 m/s		
9	J	0.76 m/s	0.76 m/s	0.75 m/s
U.C.S.	K	0.90 m/s	0.92 m/s	0.94 m/s
U.C.S.	K	0.93 m/s		
13	N	0.35 m/s	0.35 m/s	0.40 m/s
13	N	0.35 m/s		
U.C.S.	O	0.92 m/s		
U.C.S.	O	0.94 m/s		
U.C.S.	O	0.96 m/s	0.97 m/s	Reference Speed
U.C.S.	O	0.98 m/s		
U.C.S.	O	1.03 m/s		
14	P	0.67 m/s	0.67 m/s	0.76 m/s
15	Q	0.75 m/s	0.75 m/s	0.68 m/s

with nature. Statistical analysis, performed upon the comparisons listed in table 7.2, suggests that figure 7.4 is representative of nature to $\pm$ 0.08 m/s.

It is interesting to ponder awhile on table 7.2. The agreement between the model predictions and real life are very good but three positions are worth commenting on.

The largest discrepancy between the sea-trial speed data and that predicted by the model arises for position A. Here an error of 0.12 m/s exists. In most cases this might be considered an acceptable error but, compared to the accuracy of prediction of the speeds at the other positions, it seems that something is amiss.

This data position was surveyed by the Admiralty in 1951. Returning to

Chapter 2.1, it will be seen that the curves presented in figure 4.10 (which yield the sea-trial value of $\bar{s}$) rely on data collected by a pole logship. The effective depth of these readings is 15 feet beneath the surface. A datum depth of 138 feet exists at this position (Hydrographer, 1953) so the data collected may well be considered data collected in the 'surface region'. Certainly a depth of 15 feet is nowhere near half-depth (about 69 feet), the depth at or about which the data from the other positions in southern Start Bay was collected.

It is a well-known fact (see, for instance, Muir Wood, 1969; page 23) that on an imaginary journey from the sea-bed to the surface, one will experience increasing tidal current speed with height until the surface region is approached. Here, due to air (wind) resitance and the distribution of currents within waves, the tidal current speed decreases in value. This was practically observed at position J where the surface speed was found to be approximately three-quarters of the speed at 1/3rd depth. (This information was obtained by Mr D Daniels as part of a B.Sc project in 1971).

Van Veen's formula (3.1.1), which states that the tidal current speed continuously increases from sea-bed to sea surface, therefore breaks down in this surface region. In Chapter 3, where Van Veen's formula is employed to calculate $\bar{s}$, no mention of this implied limitation to the use of equation 3.1.1 is mentioned. However, provided the value of s_z, used in equation 3.1.1, lies in the region away from this disturbance, where Van Veen's formula may be expected to reasonably apply, the correction necessary for this adverse effect is considered negligible.

But, if the value of s_z substituted into equation 3.1.1 lies - or is influenced by - the surface region, then the value of $\bar{s}$ may well be expected to be lower than the true value. The discrepancy in table 7.2, for position A, may be due to this effect.

The second comparison of interest in table 7.2 is for position P, located on the shallow Skerries Bank. The predicted speed is 0.09 m/s greater than the observed speed in nature. This part of the Skerries is

saturated with sand-waves of five to ten feet amplitude. In such a situation, it seems likely that bottom friction will impart its effect on the tidal stream tending to slow them down. However, as stated in Chapter 5.4, equations 5.4.4 neglect this bottom friction effect, it being found small in order compared to the advection terms. But in certain areas bottom friction may not be negligible and it is in these areas that the model may predict a larger value of tidal current speed than is present in nature. Position P appears to lie in such an area.

To a certain extent, position Q contradicts this, the value of $\bar{a}$ predicted by the model being 0.07 m/s lower than that found in real life. This position is also located on the shallow Skerries Bank in a region of smaller amplitude sand-waves. Figure 7.4 suggests that, as one moves northeastwards away from Start Point, (the vicinity of the already mentioned eddy) the degree of variation of tidal current speed with space decreases. Consequently, perhaps equations 5.4.4 are starting to break down when position Q is reached and this may help to explain this discrepancy.

Summarizing, it appears that figures 7.3 and 7.4 predict the tidal streams in southern Start Bay, to an apparent accuracy of $\pm 3^{o}$ in direction and $\pm$ 0.08 m/s in magnitude.

Encouraged by this modelling success, attention was then turned to the techniques of modelling the flood flow, where the time of high water (six hours prior to low water) was, for the reasons given in section 7.1, chosen as representative.

7.5 Modelling the flood flow

For the ebb, the use of a constant and uniform flow of water, incident upon the coastal outline at a direction of 215^{o}, was found to yield results which were in very good agreement with those from nature. By comparison, the setting-up of the flood flow proved far more difficult.

It was noted that, at a position 3.3 nautical miles south of Start Point (Hydrographer, 1948, position Q5) the tidal current direction during the flood varies from 60^{o} to 65^{o}. Accordingly, to model the flood flow, a uniform flow of water incident upon the coastal outline at directions of 50^{o}, 55^{o}, 60^{o}, 65^{o} and 70^{o} were tried in order to obtain a realistic flow pattern, by getting good agreement between the model flow directions and the sea-trial directional data corresponding to positions A, D, J and K. The agreement reached in each case was poor, an error of 10^{o} to 20^{o} being common. In each case, however, an eddy was generated north of Start Point, the size and shape of this eddy being dependant on the angle of water attack upon the modelled coastal outline.

Incident angles of water flow as 'small' as 350^{o} and as 'large' as 90^{o} gave no better agreement. Indeed, in many cases the agreement was much worse. The eddy was, in each case, still generated.

After many unsuccessful attempts to obtain a realistic flow pattern, the use of 'deflectors' was tried. These 'deflectors', pieces of metal placed at an angle to the flow, were all located outside the region of interest. Their function was to attempt to make the directions at the sea-trial positions come right. This also failed to improve the situation.

Finally, the closest agreement between the model and real-life current directions at high water was achieved. Two separate flows were employed. One was uniform and incident upon the model at a direction of 300^{o}; the other localised to just south of Start Point at an incident direction of 90^{o}. This arrangement is diagrammatically shown in figure 7.5. By adjusting the speeds of these two flows, relative to each other, an agreement of $\pm 8^{o}$ between the model and the real-life directions recorded at positions A, D, J and K resulted. The corresponding flow pattern is shown in figure 7.6.

Table 7.3 gives the comparison between the model prediction for the unused sea-trial positions and the real data collected at sea, as a test of the correspondence.

Table 7.3 Comparison between observed and model predicted $\bar{\theta}$ values at high water

Trial No	Position	Current direction $\bar{\theta}$		
		Observed values(s)	Mean observed value	Model predicted value
U.C.S.	D'	359^{o}		
U.C.S.	D'	345^{o}	352^{o}	358^{o}
U.C.S.	D'	351^{o}		
13	N	175^{o}		
13	N	176^{o}	176^{o}	176^{o}
U.C.S.	O	10^{o}	10^{o}	26^{o}
14	P	357^{o}	357^{o}	360^{o}
15	Q	359^{o}	359^{o}	356^{o}

A statistical analysis performed on the comparisons given in this table suggests that figure 7.6 is representative of nature to about $\pm 9^{o}$. This, although not as accurate as the ebb case, is still a fairly good agreement. Indeed, many of the latest current monitoring instruments, which automatically record current direction as well as current speed, are subject to direction inaccuracies of this order.

The model predicted current speed contour map representing the current speeds at high water, being referred to a tidal range of 4 metres, was obtained in the same manner as for the ebb case. This contour map is shown in figure 7.7. Inside the eddy, the current speeds were so slow (being everywhere less than 0.4 m/s) compared to the rest of the region, that they have not been included in this figure.

The comparisons between the predictions of figure 7.7 and nature are given in tabular form in Table 7.4.

Statistical analysis shows that figure 7.7 is representative of nature to an apparent accuracy of $\pm$ 0.24 m/s.

As in the ebb case, it is interesting to ponder awhile on Table 7.4. By far the greatest contributions to the statistical inaccuracy of prediction

Table 7.4 Comparison between observed and model predicted $\bar{s}$ values at high water

		Current speed $\bar{s}$		
Trial No	Position	Observed value(s)	Mean observed value	Mean predicted value
Admiralty	A	1.03 m/s	1.03 m/s	1.41 m/s
4	D	0.39 m/s		
6	D	0.24 m/s	0.27 m/s	0.20 m/s
10	D	0.18 m/s		
U.C.S.	D'	0.19 m/s		
U.C.S.	D'	0.24 m/s	0.24 m/s	0.22 m/s
U.C.S.	D'	0.29 m/s		
9	J	1.36 m/s	1.37 m/s	1.41 m/s
9	J	1.38 m/s		
U.C.S.	K	0.23 m/s	0.19 m/s	0.58 m/s
U.C.S.	K	0.15 m/s		
13	N	0.45 m/s	0.44 m/s	0.4 m/s
13	N	0.42 m/s		
U.C.S.	O	1.06 m/s		
U.C.S.	O	1.07 m/s		
U.C.S.	O	1.10 m/s	1.10 m/s	Reference Speed
U.C.S.	O	1.13 m/s		
U.C.S.	O	1.14 m/s		
14	P	0.66 m/s	0.66 m/s	0.60 m/s
15	Q	0.63 m/s	0.63 m/s	0.70 m/s

given above, occurs for positions A and K. A possible reason for position A giving a lower sea-trial current speed than predicted, is discussed in section 7.4. Position K, however, gave a good agreement between nature and model prediction when the ebb was modelled. In Table 7.4 an error of 0.39 m/s exists. This comparison is a very interesting one. Figure 7.7 shows position K to be situated in the fast channeled flow along the leading 'edge' of the eddy (see Appendix 3.2). Suppose that, due to the relative inaccuracy of setting up the flood flow pattern in the model, compared to the ebb flow pattern, the eddy is slightly larger at high water than shown in figure 7.7. Position K would then be 'within' this eddy and experience relatively slow tidal current speeds, possibly as low as the 0.19 m/s. recorded.

The conclusion would seem to be that this flood flow modelling gives an indication of the situation in nature but the corresponding statistical accuracies of $\pm 9^{o}$ in direction and $\pm$ 0.24 m/s in speed are not as good as for the ebb flow.

(A discussion of the tidal stream maps presented in figures 7.3, 7.4, 7.6 and 7.7 is given in Appendix 3. Appendix 3.3 concentrates upon the eddy occuring during the flood half-cycle).

So the intention of this work, the procuring of tidal stream maps of southern Start Bay, has been completed. It remains to summarise the results gained during this work and draw conclusions from them. This follows immediately.

CHAPTER 8 CONCLUSIONS

8.1 Summary of results and conclusions

Tidal current speed and direction data for semi-diurnal cycles have been collected at eight positions in Start Bay, of which four lie in the southern region. The use of intergrating current meters is preferred to direct reading meters as the subjective element in the deducing of the tidal current speed is removed. Secondly, the drogue apparatus - described in Chapter 2 - has proved itself far superior to relying on the tidal current direction readings emanating from a compass-carrying current meter. Finally, although set-backs have to be expected, the use of automatic anchored current monitoring systems - such as the two described in Chapter 2.3 - provide the best way of accumulating many cycles of data at one position.

Tidal cycles of raw data, collected at different tidal ranges, are shown to be incomparable in Chapter 3. Accordingly, empirical formulae have been deduced from many cycles of data collected at one position to allow all the recorded tidal cycles to be corrected to refer to a standard tidal range. Unlike previous correction methods, the formulae are used to scale both the dependant and the independant variables. The empiracal equations which transform the variables appear to work well wherever their validity can be tested. Accordingly, it is concluded that these equations are useful for correcting data, collected at different tidal ranges, throughout the whole of Start Bay.

A study of the order of magnitude of the various terms in the equations of motion and continuity has been made, and a case established for believing that, in the southern part of the bay, a predominately inertial flow exists at high and low water. The process of space-averaging is concluded to be a very useful tool in understanding which forces dominate the flow.

It has been shown that, for the region of interest, numerical modelling has special difficulties but small-scale hydraulic modelling should give a good correspondence with the real situation.

A hydraulic model of Start Bay has been constructed and used to achieve the ultimate intention of this work: the procuring of tidal current stream maps. The predictions are shown to accord well with nature, particularly for the ebb flow, forcing the conclusion that hydraulic modelling is a viable proposition in inertial flow regions.

The model showed that an eddy develops during a flood tide. The importance of the prediction of this eddy in the model is that it shows that such an eddy can be produced by no other cause than an inertial effect alone. It is concluded that, although other causes (such as concentration gradients associated with fresh water from the river Dart or the general nature of the prevailing winds) cannot be excluded, the model has shown that an inertial eddy is to be expected during every flood tide. This will be true even in prolonged calm weather, which seems to accord well with the practical observations.

Using data taken around the Skerries Bank to set up the model, the tidal vectors over the Skerries have been inferred. These model predictions have been checked by, what is believed to be, the first practical measurements of the tidal streams over this bank. The real data and the model predictions agree so well that only relatively slow currents are concluded to exist over this sand bank despite the traditional view of very fast currents. This conclusion accords well with Acton's (1972) belief of slow tidal currents over this bank.

To summarize, the work presented here shows firstly that, with careful corrections, it is possible to obtain mutually consistant results from observations made at different periods in the tidal cycle. Secondly, it demonstrated the value of the technique of space-averaging as a guide to the best approach to the solution of the oceanographic equations. Thirdly, it demonstrates that small-scale hydraulic modelling can provide surprisingly

accurate solutions in just those situations in which numerical modelling is least appropriate.

8.2 Suggestions for future work

It is hoped that the procedure adopted in this thesis, for modelling tidal streams in inertial regions of coastal bays, will prove useful in itself.

The southern region of Start Bay is by no means the only marine region where inertial flow is likely to prevail. For example, the region in the vicinity of the Shambles (see figure App. 3.6) east of Portland Bill and Lynmouth Bay (see figure 8.1), a region more nearly topographically analagous to Start Bay, may well exhibit similar tidal stream configurations. Eddies exist in both bays: in Portland Bay an eddy exists during the flood tide whilst in Lynmouth Bay an eddy exists during the ebb tide. It would be of interest to discover if the tidal streams in these regions could be modelled using the techniques described in this thesis. Further, it would be of interest to discover whether relatively low magnitude tidal streams prevail over the shallow Shambles bank and Sand Ridge as well as over the Skerries bank.

The effects of variations of the prevailing tidal range upon the vectorial parameters of tidal streams is an exciting field of research. On the theoretical side, it may be possible to deduce these effects by a study of the hydrodynamic equations. Practically - and using Start Bay as an example - the collecting of many cycles of tidal stream data throughout the bay by employing automatic anchored current monitoring systems, such as those described in Chapter 2.3, would allow the effects of tidal range variation upon the tidal streams in an inertially dominant (southern) region and an inertially negligible (northern) region to be deduced. This investigation alone may throw some light on the question of how and why the time-scale is affected by tidal range.

In the last section, it was concluded that an inertial eddy is to be expected in southern Start Bay during every flood tide. It was, however, accepted that the eddy may be affected by the prevailing winds and concentration gradients, if any, existing because fresh water may eminate from Salcombe harbour or the Dart estuary. Investigations of the effects of wind upon tidal streams and the variation of salinity throughout the bay, would allow an estimation of the importance of these processes in determining the tidal stream configuration.

Finally, an investigation of the sand-wave structures on the Skerries bank would be a fascinating line of research. Apart from trying to answer the question of whether these sand-waves move, this is a region where maybe it would be possible to determine when they moved. Echo sounder or side scan sonar operated along a defined line, crossing these sand-waves, could possibly give an answer to this question. One of the main conclusions of this work is that only relatively slow tidal currents prevail over this bank. Accordingly, and because of the shallow nature of this region, waves may be the main influence in forming these waves of sand. Investigations of particular sand-waves during a calm period when compared to records obtained immediately after a gale may prove or disprove this suggestion.

APPENDICES 1 - 3

APPENDIX 1 THE ANCHORED SYSTEM DESIGN

In this appendix, the five physical effects which are considered to influence the accuracy of recording tidal stream data in shallow water are listed. Explanation is then given of how the design of the writer's anchored system overcame these effects by minimising them or eliminating them altogether. The success of the design in achieving this is demonstrated by reference to the results obtained, using this system, at position N.

Appendix 1.1 Problems associated with recording tidal current data in shallow water

It is felt that there exist five main physical effects which influence the operation of a current meter in recording tidal current speeds in shallow water. The first three of these may easily be made to exhibit negligible effect on the tidal current speed readings. The last two eminate from the presence of waves. They were considered likely, under rough conditions, to lead to large enough errors to make the prevention of their effects desirable in the design of the anchored system. In fact, it is felt that the design of this anchored system (given in Chapter 2.3) overcomes all five of the physical effects that will now be listed.

a. 'Turbulence'. The turbulent nature of the sea causes the tidal current speed to fluctuate with time. This is probably prevented from having any significant effect on the recorded tidal current speed if 'integrating' current meters are employed and the readings are averaged over a time long enough to smooth out these turbulent fluctuations.

b. 'Streaming'. Meters placed at depths of, say, 1/3rd. and 2/3rds the total depth of water, at slack water, will not remain at these depths throughout a tidal cycle. As the tidal current speed increases, so will the drag on the meters (which is proportional to the square of the tidal current speed) the result being that these meters will stream with the current. This means that for much of the tidal cycle the meters will be closer to the surface than planned. Their exact depth is difficult to

calculate. However, provided the meters are not located at a depth where the tidal current speed varies significantly over the anticipated limits of a meter's depth, due to streaming, then this is not considered a serious problem.

c. 'Ship effects'. The current streamlines are affected by the presence of a boat, or indeed any foreign body, tending to diverge around it. This leads, close to the boat, to a region of abnormally high tidal current speed. This effect is, therefore, only important close to the surface although the depth to which the presence of a boat affects the tidal current speeds is felt uncertain. So, in shallow water, it may have an effect on the recorded tidal current speed if the meter is located too close to the boat or surface buoy.

d. 'Vertical wobble'. This is probably the worst physical effect upon the correct operation of a current meter in choppy sea-state conditions when relatively slow currents prevail. In anything but a dead calm sea condition any boat will pitch and roll to a certain extent due to the passage of the waves. The meters, being fastened to the boat via their suspension cables, will, therefore, undergo vertical oscillations, the amplitude of these oscillations being dependent on the stability of the chosen boat and the prevailing sea-state. Because most current meters possess horizontal fins, this vertical movement causes the meter to tilt upwards as it is subjected to a pull from the surface and to tilt downwards when it is allowed to fall under gravity. If this vertical movement is excessive, then the meter starts to record the speed of it's own vertical movement rather than the tidal current speed. This could, it is true, be prevented by only performing trials when the sea is calm but to limit oneself in this way would, it is felt, be inviting the obtaining of little or no results.

e. 'Horizontal wobble'. This is undoubtably mainly caused by waves when they run at an angle to the current, although turbulence may exhibit itself in this phenomena. The visual effect is that the meter wobbles (or

oscillates), in the horizontal plane, about the mean tidal current direction. This observed motion is usually nearly an oscillatory wobble lending evidence to its cause being mainly due to surface waves. As discussed at length by, for example, Defant (1960, Chapter 2), surface waves will impart to each individual water particle an elliptic-harmonic orbit. It is believed this is the reason for the horizontal wobbling of the meter about the mean current direction. The meter possessing vertical fins and a fast time constant, will tend to follow the elliptic-harmonic orbits of the water particle. The tidal current speed recorded by the meter will, therefore, be the oscillatory component about the mean current direction rather than the component in the mean direction. This is, however, only an important effect close to the surface or in shallow water for the effect falls off hyperbolically with depth to 1% of its surface value at a depth of $\lambda/2$, λ being the wavelength of the waves (Defant, 1960, Table 1). When no waves are present, this effect has not been observed and is considered not to occur.

The five main physical effects which influence the operation of a current meter in shallow water have now been discussed. 'Streaming' is only serious if fast current speeds prevail. 'Ship effects' may be minimised by working off a small boat with little draft. However, if one satisfied the above two conditions, working in shallow water off a small boat in relatively slack currents, then 'vertical wobble' becomes a serious effect, for a small boat will pitch and roll violently in choppy seas. Overall, these effects are very difficult to overcome when working from a boat, the best arrangement seems to be the use of a small boat and terminate the trial if a choppy sea develops. This was the arrangement used for the sea-trials listed in Chapter 2.

The design of the anchored system revolved around the deemed necessity to remove as many of these physical effects as possible. The description of the anchored system is given in Chapter 2.3 and will not be duplicated here.

It will now be described how the design of this system is considered to overcome the physical effects previously listed. These physical effects will now be relisted:

a. 'Turbulence': The use of integrating Braystoke meters overcomes the effect of turbulence as time-averaging over a period of 10 minutes is employed. This averages out the turbulent fluctuationsin the tidal current speed.

b. 'Streaming': The effective triangle of forces formed by the metal rod and ropes A and B keeps the rod virtually vertical through a tidal cycle. The rod will not be vertical at every instant of time when surface waves are present. The count-rate obtained, however, will, it is believed, be virtually representative of the count-rate expected if this rod were vertical. As drum 1 rises with respect to drum 2, due to wave action, the rod will be pulled 'forward' causing a speed-up of the count-rate from the two meters located on the rod. But the rod will also drift 'backwards' when drum 1 falls to a lower elevation than drum 2, hence causing a slowing of the count-rate. Averaged over a long time interval (10 minutes), it is believed that these effects will cancel giving a count-rate as if the meters were always on a vertical rod. The weight will not stream appreciably due to the short lengths of rope connecting it to the rod and its low drag resistance. (Unfortunately, a rod long enough to accommodate all three meters was not used as it was thought unsafe and would probably lead to the collapse of the whole system. Later experience tends to lend evidence to the fact that this would be unlikely to happen). So the problem of streaming is reduced considerably if not virtually eleminated.

c. 'Ship effects': The meters sample the current speed before the water reaches the main apparatus; the whole apparatus having a greatly reduced effect on the currents than most boats. Slight effects may be present but these are deemed acceptable.

d. 'Vertical wobble': This system will rise and fall under the action of surface waves. However, the meters on the rod possess no fins and are held horizontal because they are perpendicularly mounted on an inherently vertical rod. Vertical motion will, therefore, not affect them. (When subjected to vertical oscillations in a tank of water, a horizontally held Braystoke produced no counts, the impeller being motionless). Also, the meter on the weight will not be affected as it is suspended from a single point and has too long a time constant to react to typical wave induced vertical motion (laboratory experiment). The system was, however, not envisaged to be anchored in really rough weather.

e. 'Horizontal wobble': This is felt eliminated as the meters are held into the average direction of the current. The rod arrangement streams along the average current direction, the two drums lying along this line. The meters (without fins) will, therefore, also lie in this direction as the system's time constant is very long. The weight also has a long time constant due to its length and mass ($\sim$20 Kg) so all three Braystokes are considered unable to react to the effects of horizontal wobble.

The results from position N give probably the best indication of the operation of this anchored system.

Appendix 1.2 Position N results

Two tidal cycles of speed data obtained at position N by this anchored system are shown in figures Appendix 1.1. The variation of wind speed with time, where known, is also shown.

Referring to figure Appendix 1.1A, the system was laid on a day when no wind was present and the sea-state was a flat calm. By (LW-4) hours the wind was starting to slightly increase although it was only force 1. (The wind forces are referred to the Beaufort Scale, see for example List 1968, page 119). This being about 23.00 hours, no further wind readings were taken until the following morning when at (LW-8) hours (figure Appendix 1.1B) the wind had risen to a force 3 northeasterly. This had caused a three to four foot swell. It is unfortunate that wind readings were not taken throughout the night for at (LW-3) hours (figure Appendix 1.1A) the shallowest Braystoke reading decreases in magnitude compared to the other meters. It seems likely that this is the effect of the wind influencing this meter. The wind does not, however, seem to have affected the 3 and 6 metre Braystokes. By 04.00 hours ((LW + 1) hour in figure Appendix 1.1A) the sea state was apparently still very calm. (This fact was related to the writer by a local inhabitant who, at this time, was walking his dog along Hallsands Beach). The speed cycles recorded during the first cycle were, therefore, obtained when the sea-state was very calm.

By comparison, the second set of speed cycles (shown in figure Appendix 1.1B) were recorded during a period when the sea state was choppy. On average, the waves were about four to five feet high. Once again the 1½ metre depth Braystoke reading seems affected by the wind. The 3 and 6 metre Braystoke readings do not, however. During this cycle the system was not only experiencing a stronger north-east wind but also considerable vertical motion due to the four to five foot waves. Recording so close to the surface,

this wave induced motion might well be expected to influence the readings from the meters used. (This would be a result of horizontal and vertical wobble described previously in this Appendix). However, a comparison between the 3 and 6 metre depth readings obtained in a flat calm (figure Appendix 1.1A) and a choppy sea (figure Appendix 1.1B) show no obvious difference. It is therefore felt a justifiable conclusion that waves do not affect the tidal current speed readings from this achored system. Further, the influence of the wind does not seem to have extended to 3 metres below the surface.

The effect of the wind upon the alignment of the anchored system was also found negligible. No apparent difference between the direction cycles throughout these two tidal cycles were found.

Based upon these results it is felt that this anchored system accurately records the tidal current speeds in shallow water, even when considerable swell is present, a common occurance. The problems which were considered to be associated with recording tidal current speeds in shallow water (section Appendix 1.1) are either of negligible order or have been eliminated. It is very unfortunate that this system had a limited life-time, but it is hoped that it may be utilised again the the near future.

Before ending this Appendix, it is considered of interest to point out that the tidal current speed results, shown in figures Appendix 1.1, display an increase in tidal current speed with depth. This is in direct contradiction to Van Veen's formula, used in Chapter 3.1 to obtain the vertically integrated value of the tidal current speeds. Indeed, in agreement with Van Veen, it was found that, at every other position visited in Start Bay, the tidal current speed decreased with depth. Why this particular position should exhibit such an ambiguity is felt uncertain. It is, however, another reason why this system should be re-employed if possible.

APPENDIX 2

Appendix 2.1 Correlation between tide and current

In Chapter 4.2 it was found that the correlation between the maximum flood speed and tidal range Z at position 0 is given by:

$$smax(f) = 0.57\ Z^{0.75}$$

with an error associated with the power of $\pm$ 0.04. For the maximum ebb speed the correlation yields

$$smax(e) = 0.46\ Z^{0.55}$$

with an error associated with the power of $\pm$ 0.03.

An interesting feature of these empirical equations is the difference in power between the flood (0.75) and ebb (0.55). These appear to be significantly different as the standard errors associated with them are considerably less than the difference between them. The theoretical prediction for this power will now be examined to see if it throws any light on this difference.

If it is considered that the tidal amplitude at Dartmouth is given by $Z_2 \cos(\omega t + \phi_2)$ and at Devonport by $Z_1 \cos(\omega t + \phi_1)$, where $Z_{1,2}$ are the tidal ranges and $\phi_{1,2}$ the associated phases at these places then, the slope of the sea between Dartmouth and Devonport will be assumed to be represented by $\partial\zeta/\partial\ell$ where

$$\frac{\partial \zeta}{\partial \ell} \propto Z_2 \cos(\omega t + \phi_2) - Z_1 \cos(\omega t + \phi_1)$$

As $\phi_{1,2}$ are likely to be small, then this equation becomes

$$\frac{\partial \zeta}{\partial \ell} \propto \cos\omega t(Z_2 - Z_1) + \sin\omega t(Z_1\phi_1 - Z_2\phi_2)$$

By putting $\phi_{1,2}$ equal to $\omega \phi_{1,2}$ where $\phi_{1,2}$ now represents the phase in seconds one obtains

$$\frac{\partial \zeta}{\partial \ell} \propto \left[(Z_2 - Z_1)^2 + \omega^2 (Z_1\phi_1 - Z_2\phi_2)^2 \right]^{\frac{1}{2}}$$

From the Admiralty tide tables (Hydrographer, 1972) it is seen that $Z_2 - Z_1 = -0.15$ metres at springs and -0.2 metres at neaps. However, as Z_1 and Z_2 are much greater than the difference between them, Z_1 is approximately equal to Z_2 so

$$\frac{\partial \zeta}{\partial \ell} \propto \left[(Z_2 - Z_1)^2 + Z_1^2 \omega^2 (\phi_1 - \phi_2)^2 \right]^{\frac{1}{2}} \qquad \text{Appendix 2.11}$$

Hence, by obtaining the values of Z_1, $(Z_2 - Z_1)$ and $(\phi_1 - \phi_2)$ from the Admiralty tide tables (Hydrographer 1972a) an indication of whether phase or amplitude dictates the tidal slope can be found, It is found that the phase term is always the larger and hence Appendix 2.1.1 may be approximated by

$\frac{\partial \zeta}{\partial \ell} \propto Z_1$, the tidal range at Dartmouth.

Now in Chapter 5.3, it is found that, when space-averaged, the advection terms are dominant on the left hand side of the equations of motion. Thus, in the x direction it is found that

$$u\frac{\partial u}{\partial x} + v\frac{\partial u}{\partial y} = -g\frac{\partial \zeta}{\partial x}$$

is the appropriate equation of motion. In this case it appears that the relationship between the sea slope and current speed s is given by

$$s \propto \frac{\partial \zeta}{\partial \ell}^{\frac{1}{2}}$$

Thus, one would expect the relation between maximum current speeds on both flood and ebb to follow the empirical law

$$Smax \propto Z_1^{0.5}$$

This is in good agreement with the ebb flow result but not the flood.

If the inertial terms were negligible in the equations of motion, then the current speed might well be expected to vary linearly with the slope of the sea. In this case

$$Smax \propto Z_1$$

would be appropriate, in agreement with the usual assumption (see for instance Acton, 1972 or Hydrographer, 1969).

Theory, therefore seems to predict that the power of Z should lie between 0.5 and 1.0 as it does for position 0. The reason for the flood flow at position 0 exhibiting a power as high as 0.75 is felt uncertain. It is known, however, that $\partial u/\partial t$ and $\partial v/\partial t$ at this position are high in value (see figure 4.16). Also, friction may play an important part, the position being so close to the shallow Skerries Bank and exhibiting very fast current speeds.

So, although these terms are found negligible when space-averaged, their localised value around position 0 may well be high, causing a correspondingly higher value of the power of Z.

This, if true, would cast some doubt on the assumption that the variation of the maximum current speeds with tidal range throughout the region is characterised by the variation at position 0. It is the reason why, as specified in Chapter 2.3, it was hoped to also obtain the relationship between tide and current at a position within the Skerries Bank. The achored system did not, unfortunately work. This is one of the suggestions for future work given in Chapter 8.2.

APPENDIX 3 Discussion of the tidal streams in Southern Start Bay

Robinson (1961), in his paper on the beach changes at Hallsands, shows a qualitative map of the tidal currents in southern Start Bay. This appears to be used to illustrate remarks made in the text about sediment movement. It contains no numerical data about the tidal current speeds or directions; however, there are remarks concerning the magnitudes of the tidal current speeds in certain areas.

By comparison, Acton (1972) produces maps of the flood and ebb tidal current directions and maximum speeds. These are obtained by a mathematical procedure employing the hydrodynamic equations and applying them to the central region of the bay. Here numerical data is available.

This appendix contains a discussion of the ebb and flood tidal stream maps, obtained in Chapter 7 using the hydraulic model. They are compared to the above mentioned results of Acton and Robinson.

Appendix 3.1 Discussion of the ebb flow pattern

The ebb flow pattern - shown in Figure 7.3 - and the vertically integrated tidal current speed contours - shown in Figure 7.4 - lead to the conclusion that, in the southern region of Start Bay, there are two main ebb flow channels. One tends to hug the western edge of the Skerries Bank, the other flowing along the eastern edge. These are diagrammatically shown in Figure Appendix 3.1. The main ebb channel lies along the eastern edge of the Skerries Bank. It appears, to the south of the region, to join with the minor ebb flow channel whose axis runs westward of the Skerries Bank, rejoining the main channel via the 'race'. (The race is the name given to the channel lying between the Skerries and Start Point - see Figure 2.4).

This twinned channel flow appears to be a direct result of the divergence of the tidal flow around the shallow Skerries Bank. The result of this divergence is a region over the Skerries of relatively slow currents (0.6 m/s to 0.8 m/s, on a spring tide). This highlights the channels of faster

current flow off the eastern and southern limits of the bank where, in the southern extremity of the region, the currents achieve speeds in excess of 1 m/s. on a spring tide.

It is interesting to compare this picture of the ebb flow in southern Start Bay with the views expressed by Robinson and Acton.

In his paper, Robinson,apparently influenced by the hydrography and the abundance of sand-waves 'facing' down channel over the Skerries Bank, deduces that the major ebb flow channel runs southwards across this shallow region. This is diagramatically shown in his figure 6 (reproduced in Figure Appendix 3.2), being described in a section entitled "Water movements" on page 67. In this section, Robinson states:

> "In the southern part of the bay" ... "the ebb stream is running southwards" ... "Measurements of the speed of the stream taken at a station"(probably the Admiralty position B, see figure 2.1)" within the Skerries indicate that the maximum at springs is less than 1.5 knots. "(0.75 m/s). It is likely, however, that the velocity is much greater over the Skerries Bank, a fact which led to difficulties in keeping R.V. Sarsia on station during the bottom sampling operations. Off the eastern margin of the Skerries, beyond the shelf edge, the streams run very strongly reaching" ... "2.2 knots on the ebb". (This fact is probably obtained from the Admiralty position A, see figure 2.1).

The current speed contour map, figure 7.5, gives results for the Skerries Bank in direct contradiction to the views expressed by Robinson of fast currents over this region. However, the difficulty of anchoring a boat on the Skerries was experienced by the writer during the collection of data at position P. It was found that a 15lb plough anchor plus 20 feet of heavy chain, was insufficient to hold the 20 foot long open fishing boat used. (The problem was finally resolved by the additional use of 56 lb weight).

The theory concerning the 'holding power' of anchors (see for instance Myers, et al (1969), page 4.70) suggest that, under favourable conditions, the anchor arrangement used at position P, should hold even the R.V. Sarsia! This anchorage problem was, however, judged not to be due to strong currents, a fact confirmed by the readings of the Braystoke current meter used (see Figure 4.17) and the time taken for orange peel to float the length of the boat. These two methods gave very good agreement provided the orange peel, used as a check that the Braystoke was working correctly, was thrown far enough away from the boat to be in water unaffected by it's presence.

It is felt that the difficulty of anchoring on this bank is primarily due to the heavy swell which is nearly always present. This causes the boat to 'snatch' at the anchor resulting in ineffective anchorage. (The sand waves over the Skerries may also be a direct result of this swell. Certainly on trial 14, at position P, the oscillatory nature of the current was observed, the count rate from the Braystoke current meter used rising and falling as the swell passed. When the components of current speed due to the tide and the swell added, the current speed rose to an estimated value of about 1 m/s., falling to about 0.4 m/s. when these two components opposed each other. Fortunately, the Braystoke meter used automatically smoothed out this variation as detailed in Chapter 2.2).

The main disagreement with Robinson's paper appears, therefore, to involve the magnitude of the tidal current speeds over the shallow Skerries bank. It is fortunate that a second reference, Acton (1972), is available to throw further light on this disagreement.

Summarising the results of his mathematical modelling of the central region of Start Bay, Acton says on page 74 of his thesis:

"The peak ebb and flood current magnitudes" ... "are predicted to be relatively low over the Skerries. The peak currents on the bank vary from about 0.55 m/s at the northern tip down to about 0.3 m/s in the central region".

Concerning the magnitude of the tidal current speeds over the Skerries Bank, it appears, in general, that the independent mapping procedures adopted by Acton and the writer both predict relatively low velocities.

This view of relatively slow currents over the Skerries seems to be supported by the very stability of the bank itself. A hydrographic survey, accurately conducted in 1853 (Hydrographer, 1853), when compared to the modern hydrographic chart of Start Bay (Hydrographer, 1953 or 1972b) shows that the Skerries bank has remained remarkably stable over the last hundred years or so. Personal correspondence with Dr J Hails from the Unit of Coastal Sedimentation located at Taunton (Hails, 1973) yielded the information that the Skerries consists of sand some 50 metres thick. It seems unbelievable that this sand bank could withstand the fast currents suggested in Robinson's paper and still remain stable in outline. This is, however, far more credible if there exist relatively slow currents over the Skerries as this and Dr Acton's thesis imply. Indeed, in discussing the stability of the Skerries, Robinson himself says (Robinson 1961, page 74):

"... the bank as a whole displayed a remarkable degree of stability considering that it is formed of sediment capable of transport by tidal streams of relatively low velocities".

To settle finally the question of whether fast or slow tidal streams prevail over the Skerries Bank, positions P and Q were visited by the writer. It is believed that the tidal stream measurements recorded at these positions are the only ones ever obtained on this shoal. Reference to Figures 4.17 and 4.18 will show that they contradict the traditional view of fast currents, but on the other hand are faster than the currents predicted by Acton.

The ebb flow having been discussed at length, it remains to discuss the flood flow results shown in Figures 7.6 and 7.7.

Appendix 3.2 Discussion of the flood flow

Just as from the ebb flow results from the hydraulic model it was concluded that there were two ebb flow channels, so on the flood there appear two flood flow channels. These channels are diagrammatically shown in Figure Appendix 3.3. The main flood flow channel runs northeastwards, off the eastern margin of the Skerries Bank; the minor flood channel being confined to the 'leading edge' of the eddy. This once again leads to a divergence of the water flow around the shallow Skerries Bank. As a result relatively slow tidal currents once again characterise this area.

A contour map of the peak flood speeds in the central region of Start Bay is given by Acton in his Figure 5.2 Comparison with Figure 7.8 of this thesis, although not representative of the maximum current speeds, yields general agreement. Like the writer, Acton predicts a fast flow off the eastern margin of the Skerries Bank which diminishes in magnitude upon approaching the shore.

The eddy is, however, undoubtably the most fascinating feature of the flood flow. It is unquestionably the reason for Robinson's assertion (Robinson 1961, page 67).

"In the southern part of the bay, for about 9 hours of the tidal cycle, the ebb stream is running southwards at a slight angle to the coast".

Indeed, just off Hallsands, the ebb does apparently last for about nine hours, about six hours true ebb flow, the other three hours being due to this eddy. This is highlighted in the results from positon N, shown in figure 4.15. Robinson, however, seemed unaware of the existence of this eddy, for nowhere in his paper can any reference to it be found. This eddy will now be discussed.

Appendix 3.3 The Start Bay eddy

In Chapter 7, Figure 7.6, the hydraulic model predicted as eddy occuring in southern Start Bay during the flood half-cycle. It is this eddy that is considered in this section.

(To be perfectly accurate, this is not the only eddy which exists in the Start Bay region. During the ebb half-cycle, an eddy exists, or is believed to exist, south of Start Point.

The evidence for the existence of this eddy is twofold. Firstly, when modelling the ebb flow at low water, an eddy was observed in this region in the small-scale model used (see Chapter 7.3). This eddy was mainly ignored lying, as it does, outside the region of immediate interest .

Secondly, the local fishermen know of the existence of this eddy. They state:

"About one hour before low water, whilst in the channel (English Channel) the tide is on the ebb, south of Start Point and near the coast it is on the flood".

Lying outside the considered region, this eddy is ignored although it's presence is acknowledged. The Start Bay eddy is defined as the eddy that exists northwards of Start Point during the flood half-cycle).

Equations 4.3.3., introduced in Chapter 4, describe how the time of occurance of events (referred to low water) vary according to the prevailing tidal range. For the general case, these equations are:

$$t_1 = -0.31 + p \qquad 4.3.3a$$

$$t_2 = -1.01 + q \qquad 4.3.3b$$

$$t_3 = -0.41 + r \qquad 4.3.3c$$

where Z denotes the prevailing tidal range in metres and the suffixed values t refer to the tidal speed (or direction) cycles such as those presented in Figures 4.10 and 4.21. t_1 denotes the time of occurance, in hours with respect to low water, of the initial ebb to flood flow transition, t_2 the

following flood to ebb transition and t_3 the ebb to flood transition which completes the presented tidal cycle. The constants p, q and r have characteristic values at every position. It is the values of these constants which enables one to deduce the behaviour of the Start Bay eddy.

At position D, equations 4.3.3 may be rewritten as:

$$t_{D_1} = -0.31Z + P_D$$

$$t_{D_2} = -1.01Z + q_D \qquad \text{Appendix 3.3.1}$$

$$t_{D_3} = -0.41Z + r_D$$

and at position 0 as

$$t_{0_1} = -0.31Z + p_0$$

$$t_{0_2} = -1.01Z + q_0 \qquad \text{Appendix 3.3.2}$$

$$t_{0_3} = -0.41Z + r_0$$

Provided the tidal range Z is the same for both cases (Chapter 4 allows this to be made so) then subtracting Appendix 3.3.2 from Appendix 3.3.1 yields:

$$t_{D_1} - t_{0_1} = p_D - p_0$$

$$t_{D_2} - t_{D_2} = q_D - q_0 \qquad \text{Appendix 3.3.3}$$

$$t_{D_3} - t_{D_3} = r_D - r_0$$

Here, then, is the physical significance of the constants p, q and r. The difference in the values of p between two positions gives the difference in the time of occurance of the ebb to flood transition; the difference in the values of q giving the variation in the time of occurance of the flood

transition and the difference between the values of r, once again gives the difference between the times of occurance of the ebb to flood transition. Both p and r referring to the same transition, it follows that

$$p_D - p_0 = r_D - r_0$$

The values of p, q and r for positions D and 0 are quoted in Chapter 4.3. Substituting these values into equations, Appendix 3.3.3 yields

$$t_D - t_0 = -7.92 + 8.07 = 0.15 \text{ hours}$$
$$t_D - t_0 = -0.95 + 0.01 = -0.94 \text{ hours} \qquad \text{Appendix 3.3.4}$$
$$t_D - t_0 = 4.67 - 4.52 = 0.15 \text{ hours}$$

It will be seen that, indeed, $p_D - p_0$ does equal $r_D - r_0$. Equations Appendix 3.3.4 therefore state that the ebb to flood transition occurs at position D 0.15 hours later than at position 0. Similarly, the flood to ebb transition occurs at position D 0.94 hours earlier than at position 0.

Here, then, is the key-hole through which to observe the Start Bay eddy. By deducing the values of p (or r) and q at every data position in Start Bay, the time sequence of the ebb to flood and flood to ebb transitions may be seen.

Figure Appendix 3.4 shows the values of p numerated in Start Bay, the decimal point in each case denoting the data position. Similarly, Figure Appendix 3.5 numerates the values of q.

Bearing the previous discussion about the physical significance of differences in the values of p and q in mind, the information these figures impart will now be detailed. Figure Appendix 3.4 will be considered first.

With the tidal flow down channel (on the ebb) and approaching the time of the ebb to flood transition, the southerly data positions feel the influence of the encroaching flood tide first. This, for the chosen tidal

range (4 metres), appears to occur about 8.3 hours before low water. As one works north-eastward across the bay, the values of p become successively lower magnitude negative numbers, position H in the top north-eastern corner having the lowest negative value, -7.3. So it appears that it takes 1 hour for all of Start Bay to succumb to the flood tide. In passing, it does appear that there may be a 'premature' flood stream directed northwards close in to the coast. The evidence for this comes from the values of p at positions N, (to some extent) D and M where these values are about 0.2 to 0.3 hours greater in negative value than the more easterly positions. It may, of course, be that the relationships derived in Chapter 4, which form the basis of this appendix, break down as the coast is neared.

This description, given above, is what one might expect to happen in a fairly 'well ordered' part of the sea.

To attempt to gain an an insight into the 'time history' of the eddy, it is Figure Appendix 3.5 that should be consulted. Here the flood to ebb transition is under observation. One might expect this transition to occur in the north of Start Bay first and then, with increasing time, extend southwards. With the exception of position M, to the north of the line of latitute $50^{o}18'$ this does appear to happen. However, south of this line the influence of the eddy appears to be felt.

In the north-eastern part of the bay, the flood of ebb transition occurs about 1.2 hours after low water. For 6 hours before this time, however, ebb flow has prevailed at position N for the value of q is -4.8 hours. As no other position possesses a value of q as low as this, then at and for some time after 4.8 hours before low water, position N is the only data position to experience the 'southward flow' within the eddy. Three hours after position N first experiences ebb flow, position K is affected (q = -1.8 hours). The eddy appears to have grown in size. Almost certainly, position P is now influenced by the 'northward flow' of the eddy'.

The eddy is, however, not only expanding eastwards for one hour before low water position D experiences the 'southwards flow' of the eddy. The continued expansion of this eddy leads to, in quick succession, positions P, O, Q and M experiencing ebb flow. It also appears that, close to this time, position A is influenced presumably by the rip stream coming out through the race. Positions P and J probably experience the 'northward flow' of the eddy at this time although they appear never to be subjected to the 'southward flow' within the eddy for their values of q continue the sequence started in the north of Start Bay.

So figures Appendix 3.4 and Appendix 3.5 appear to highlight the difference in the tidal flow across Start Bay. In the north of the bay a 'well-ordered' situation exists whilst in the south, particularly during the flood half-cycle, the influence of the second order advection terms may readily be seen. This is in agreement with the suggestive theory performed in Chapter 5.

The outstanding effect due to the dominance of the advection terms in southern Start Bay is the eddy. The apparent fact that it expands with time during the flood half-cycle is by no means a unique situation. In the "English Channel sailing directions" (Hydrographer, 1971b), on page 168 warning is given of the eddy off Portand Bill (see figure Appendix 3.6).

"East going stream - Eddy" ... "Soon after the stream begins an anti-clockwise eddy forms eastward of the Bill; from this time till the end of the east-going stream the eddy increases in size, and towards the end of the stream it fills the whole of the bay eastward of Portland...".

The Start Bay eddy does not appear to fill the whole of the bay but it certainly seems, during the later part of its existence, to circumnavigate the Skerries Bank.

REFERENCES

ACTON, J.R., (1972). Tidal stream cartography in shallow seas.
Ph.D Thesis. University of Bath. 1972

ACTON, J.R. and DYER, C.M. (1975).Mapping of Tidal Currents near the Skerries Bank.
Journal of the Geological Society, 131, 63-67

ALLEN, J., (1947). Scale models in hydraulic engineering.
London: Longmans, Green and Co., 415pp

BARNA, P.S., (1964). Fluid mechanics for engineers
London: Butterworth, 376pp

B.T.D.B. Report, (1970). British Transport Docks Board report on research 1969. Issued by B.T.D.B. Research Station, Southall, Middx.

DEFANT, A., (1960). Physical Oceanography, Volume 2
Oxford: Pergamon, 598pp

DRONKERS, J.J. and SCHONFELD, J.C., (1955). Tidal computation in shallow water
Proc. Amer. Soc. Civ. Eng., 81, Separate No. 714, 1

ELSDEN, O., (1939). Investigation of the outer approach-channels to the Port of Rangoon by means of a tidal model.
Jour. Inst. C.E., p.3

FREEMAN, J.R., (1929). Hydraulic Laboratory Practice.
Amer. Soc. Mech. Engs.

GIBSON, A.H., (1933a). Construction and operation of Severn Tidal model
H.M. Stationery Office, 63-78-82, 1933,2. Quoted in Allen (1947) p.182

GIBSON, A.H., (1933b). Severn model reports
H.M. Stationery Office, 63-78-2, 1933,24. Quoted in Allen (1947), p.192

HAILS, J.R., (1973). Private Communication

HANSFORD WORTH, R., (1904). Hallsands and Start Bay, Part 1. Trans. Devon Assoc., 36, 302-346

HANSFORD WORTH, R., (1909). Hallsands and Start Bay, Part 2. Trans. Devon Assoc., 41, 301-308

HANSFORD WORTH, R., (1923). Hallsands and Start Bay, Part 3. Trans. Devon Assoc., 55, 131-147

HANSON, W., (1956). Theorie zur Errechnung des Wasserstandes und der Stromungen in Randmeeren rebst Anwandungen. Tellus, 8, (3) Quoted in Acton (1972) p.5

HEAPS, N.S., (1969). A two dimensional numerical sea model Phil. Trans. Roy. Soc., A, 265, 93

HYDROGRAPHER, The (1853). Start Bay, Admiralty Chart No 1634 (fathoms and feet), Crown copyright 1853.

HYDROGRAPHER, The (1942). English and Bristol Channels, procket tidal stream atlas, Hydrographic Dept., Admiralty Crown copyright, 1961

HYDROGRAPHER, The (1948). Tidal streams - European Waters, Part II, second edition. Hydrographic Dept., Admiralty Crown copyright, 1948.

HYDROGRAPHER, The, (1953). Start Bay. Admiralty Chart No 1634 (fathoms and feet), Crown copyright, 1962

HYDROGRAPHER, The (1962). The Solent and adjacent waters, tidal stream atlas (NP 337). 16pp Hydrographer of the Navy; Crown Copyright, 1962

HYDROGRAPHER, The (1965). Approaches to Portland, tidal stream atlas (NP 257) 16pp Hydrographer of the Navy; Crown copyright, 1962

HYDROGRAPHER, The (1969). Admiralty Manual of Hydrographic Surveying, Volume 2, Chapter 2: Tides and Tidal Streams. (NP 1346 (2)) 119pp. Hydrographer of the Navy; Crown copyright, 1969.

HYDROGRAPHER, The, (1970). Admiralty Tide Tables, Volume 1, 1971. European Waters. Crown copyright, 1970.

HYDROGRAPHER, The, (1971a). Admiralty Tide Tables, Volume 1, 1972. European Waters, Crown copyright 1971.

HYDROGRAPHER, The, (1971b). Channel Pilot (NP27). 713pp
Hydrographer of the Navy, Crown copyright, 1971

HYDROGRAPHER, The (1972a). Admiralty Tide Tables, Volume 1, 1973.
European waters. Crown copyright, 1972

HYDROGRAPHER, The, (1972b). Start Bay, Admiralty Chart No 1634 (Metres)
Crown copyright, 1972

LAMB, H., (1945). Hydrodynamics
Dover, 738pp

LI, W.H. and LAM, S.H., (1964). Principles of Fluid Mechanics.
London: Addison-Wesley, 374pp

LIST, R.J., (1968). Smithsonian Meteorological Tables,
Washington: Smithsonian Institutional Press, 527pp

MORONEY, M.J., (1956). Facts from figures
London: Penguin, 463pp

MUIR WOOD, A.M., (1969). Coastal Hydraulics
Macmillan, 187pp

MYERS, J.J., HOLM, C.H. and McALLISTER, R.F., (1969). Handbook of Ocean and Underwater engineering
New York: McGraw-Hill, 1090pp

NEUMANN, G., (1968). Ocean Currents.
Amsterdam: Elsevier, 309pp

NEUMANN, G and PIERSON, W.J., (1966) Principles of physical oceanography
London: Prentice-Hall International, 506pp

NODA, E.K., (1972). Equilibrium beach profile scale-model relationship.
Proc. Amer. Soc. C.E., November 1972, p511

PENGELLY, W., (1869). On the submerged forest at Blackpool, near Dartmouth, South Devon.
Trans. Devon Assoc., 3, 127

PROUDMAN, J., (1953). Dynamical Oceanography
London: Methuen, 401pp

PROUDMAN, J., (1955). Note on the dynamics of storm surges.
Monthly Notices Ast. Soc., 7, 44

REDFIELD, A.C., (1962). A practical portable tide gauge.
Limnology and Oceanography, 7, 262

REYNOLDS, O., (1887). On certain laws relating to the regime of rivers and estuaries and on the possibility of experiments on a small scale.
Brit. Assoc. Report 1887

ROBINSON, A.H.W., (1961). The hydrography of Start Bay and its relationship to beach changes at Hallsands.
Geographical Journal, 127, 63

VAN VEEN, J., (1936). Onderzoekingen in de Hoofden. Measurements in the Straits of Dover and their relation to the Netherlands coast.
Quoted in Muir Wood (1969), p.23

LIST OF FIGURES

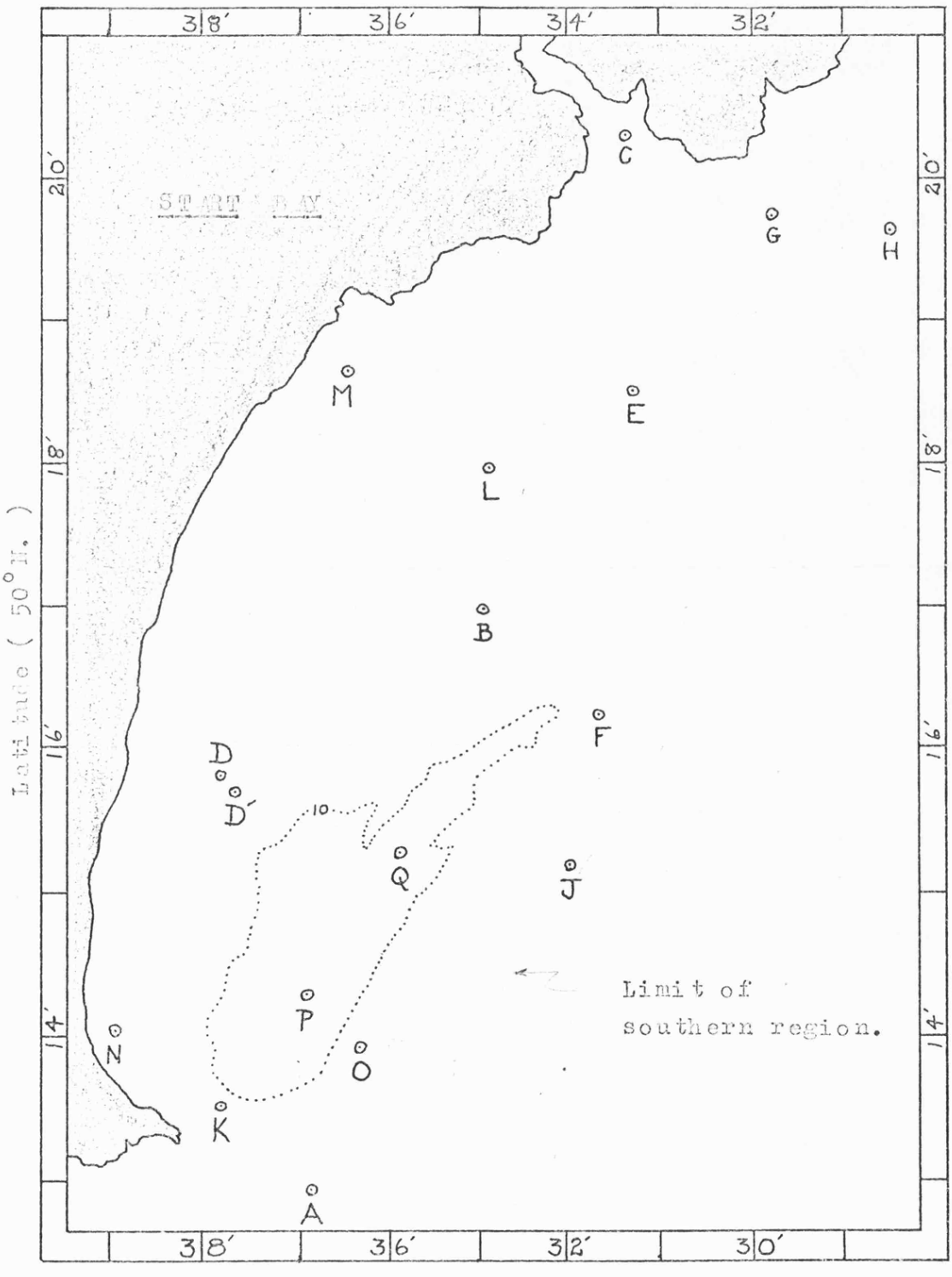

SEA TRIAL LOCATIONS.

FIGURE 2.1.

BRAYSTOKE ARRANGEMENT.

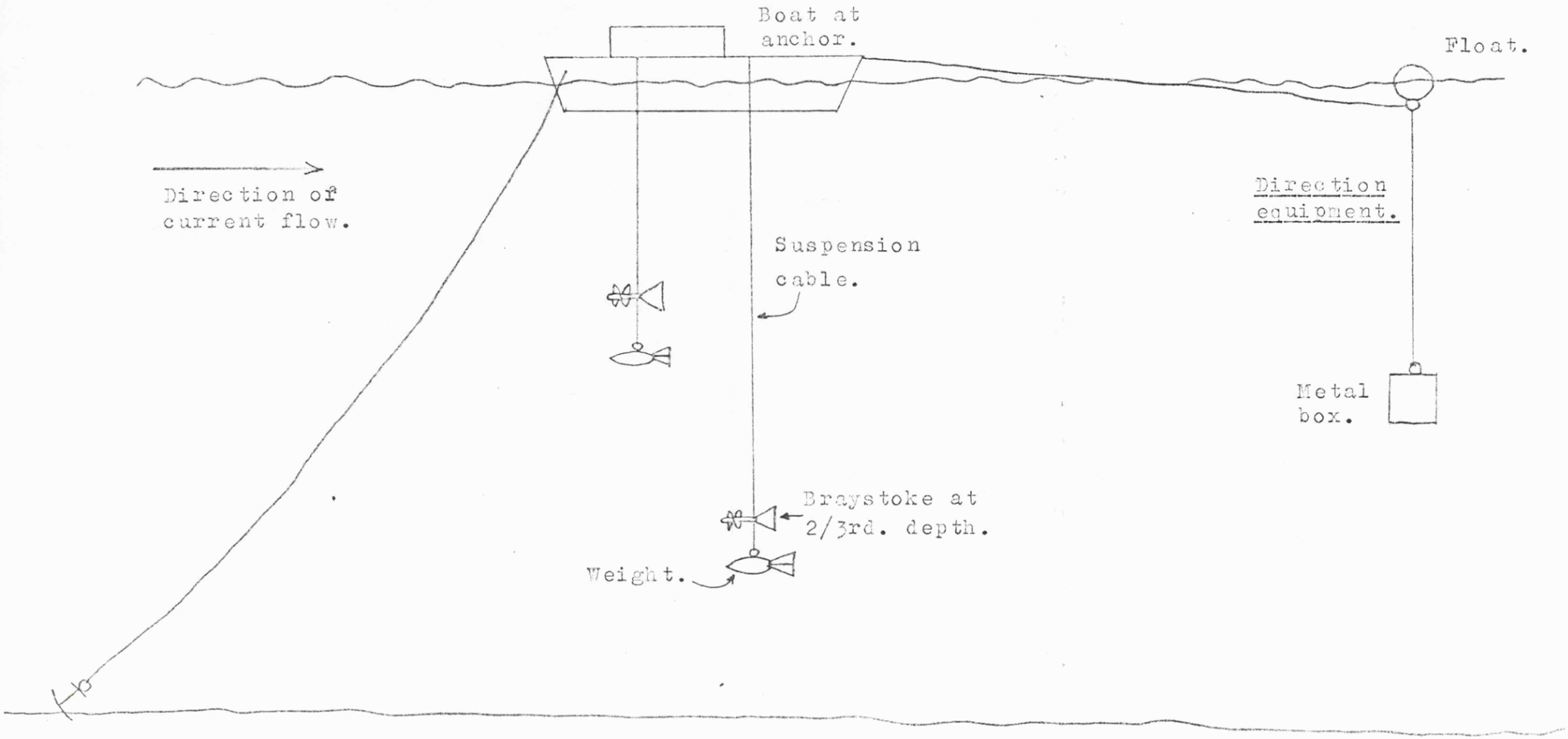

FIGURE 2·2.

MODIFIED BRAYSTOKE ARRANGEMENT.

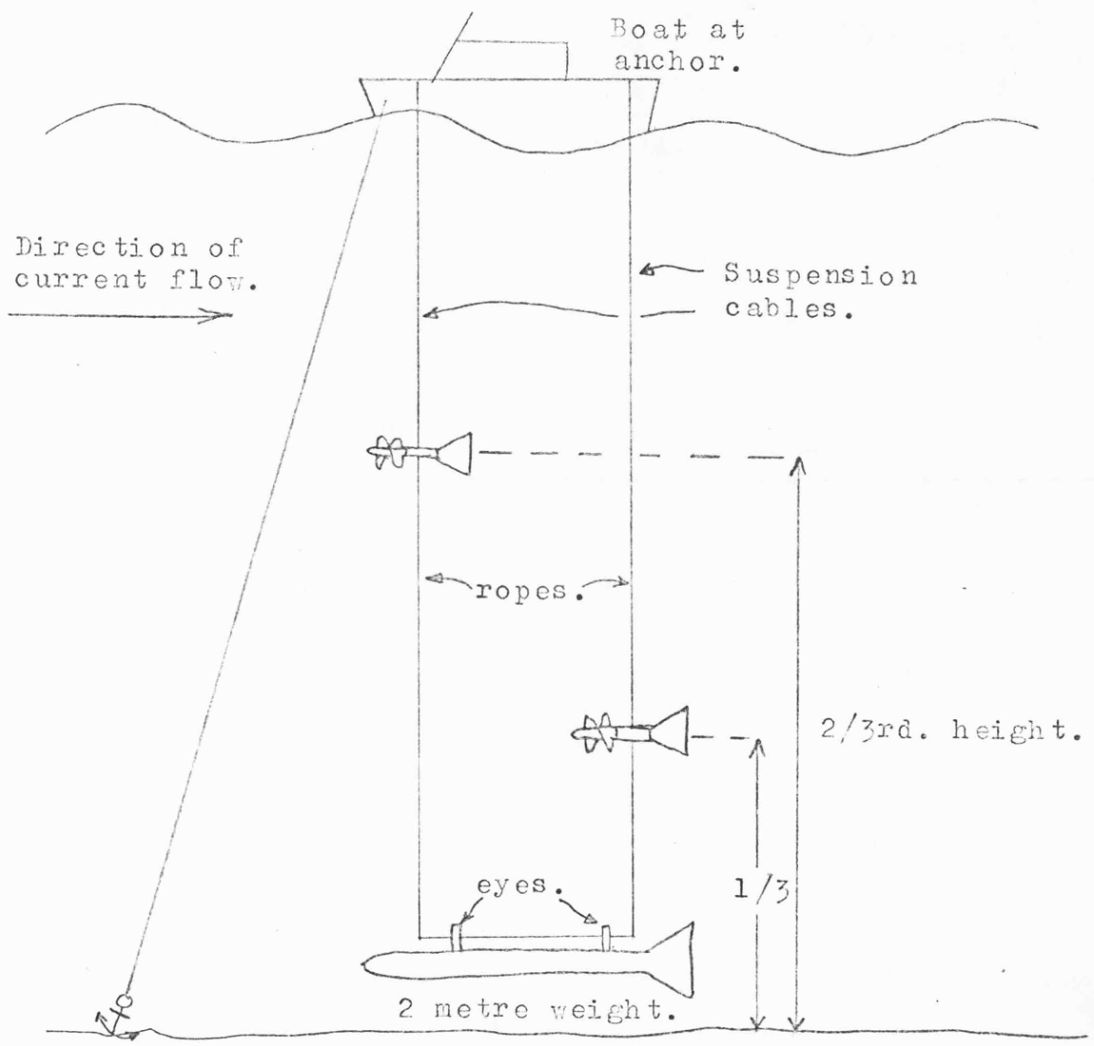

FIGURE 2·3.

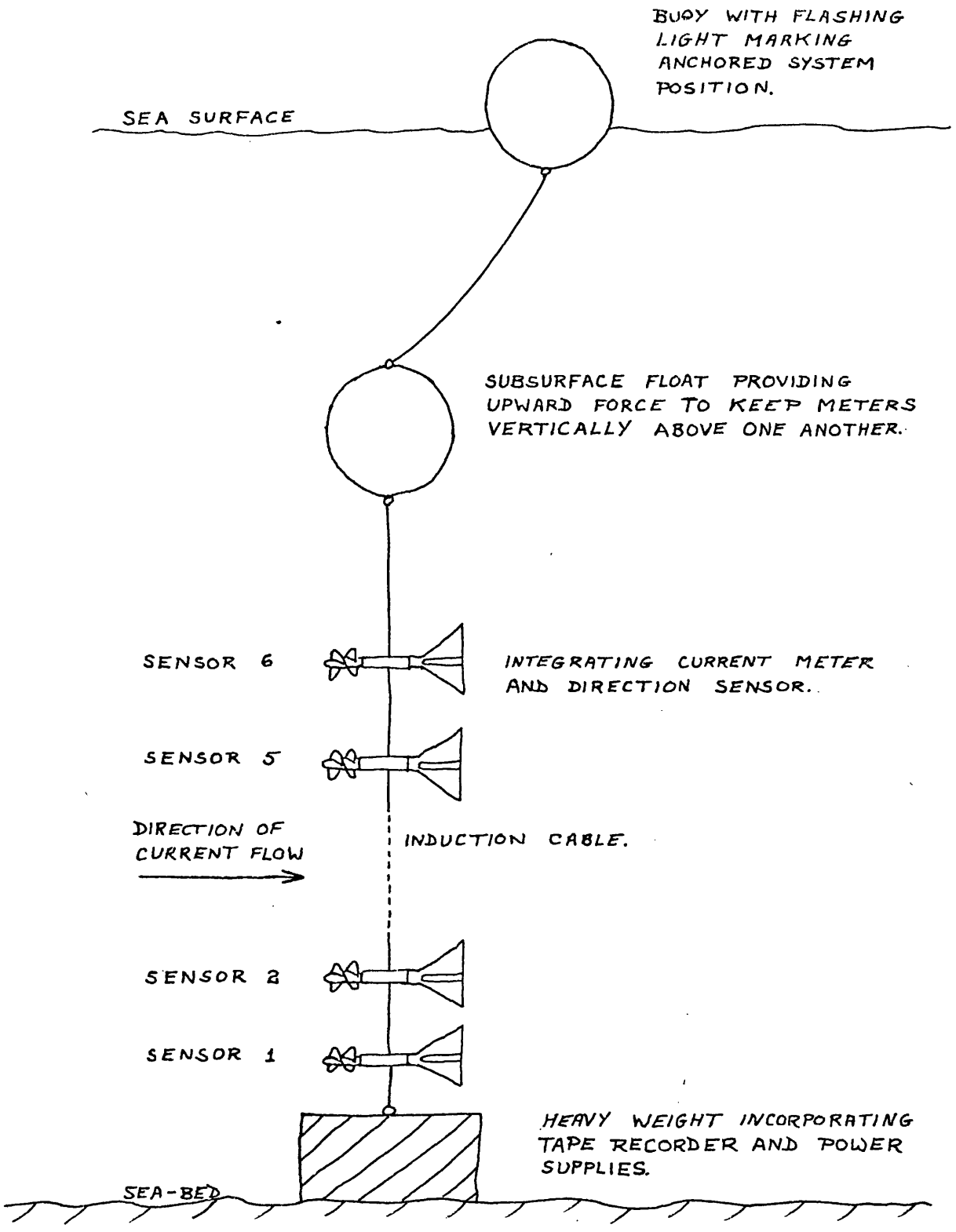

THE C.S.U. ANCHORED SYSTEM. (SKETCH)

FIGURE 2.4

10 METRE CONTOURS.

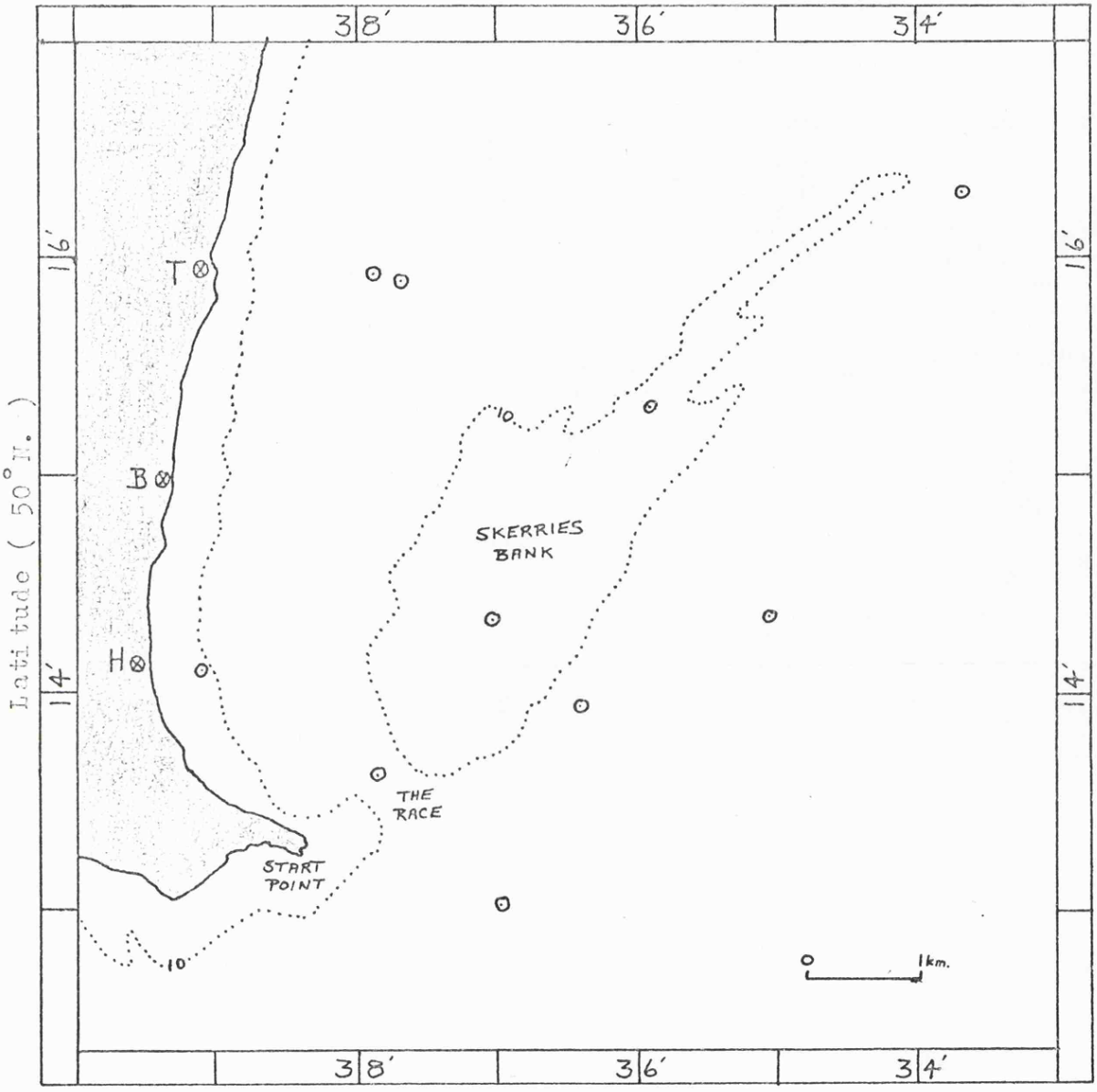

H.... Hallsands.

B....Beesands.

T....Torcross.

FIGURE 2.5.

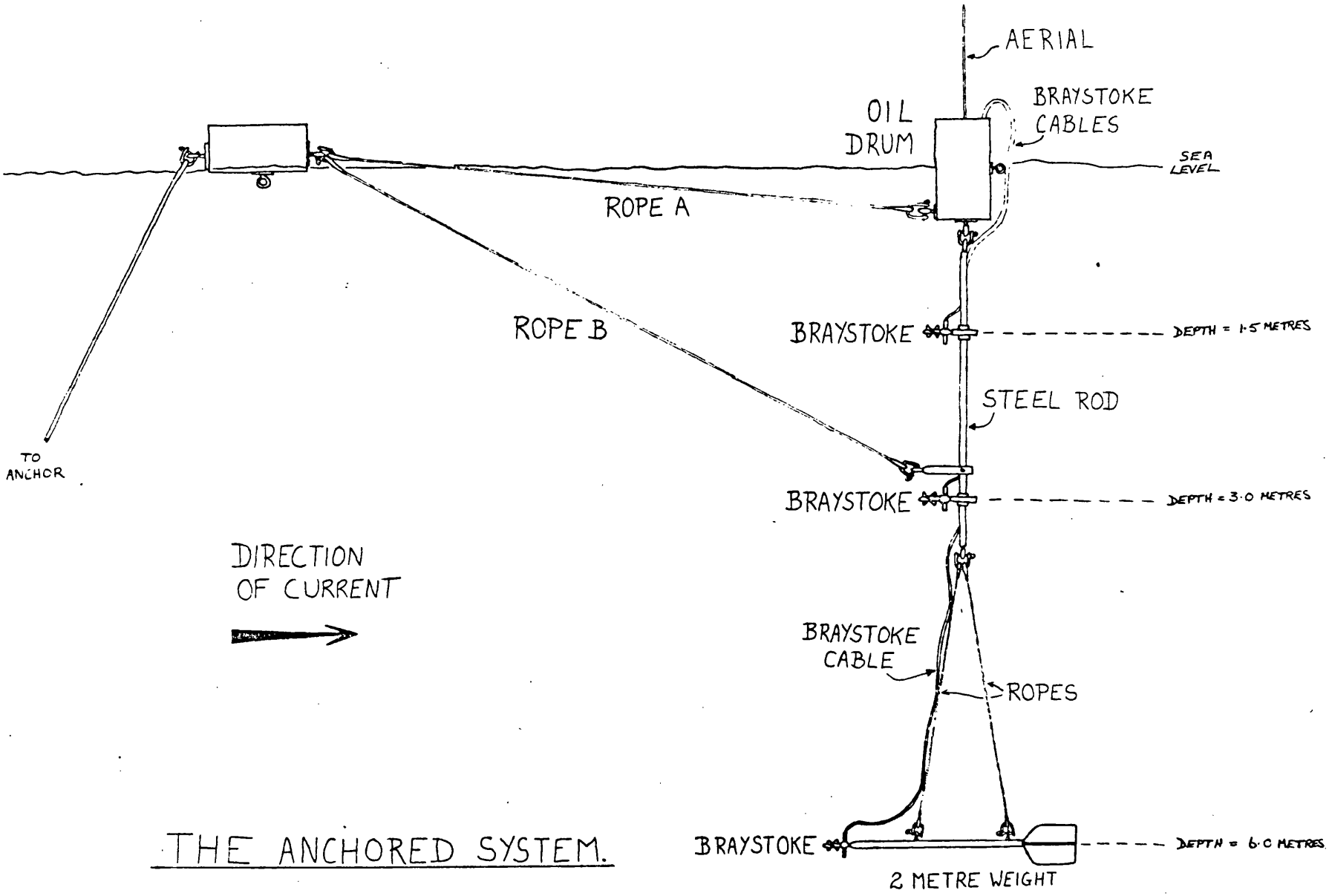

THE ANCHORED SYSTEM.

FIGURE 2·6

FIGURE 2·7

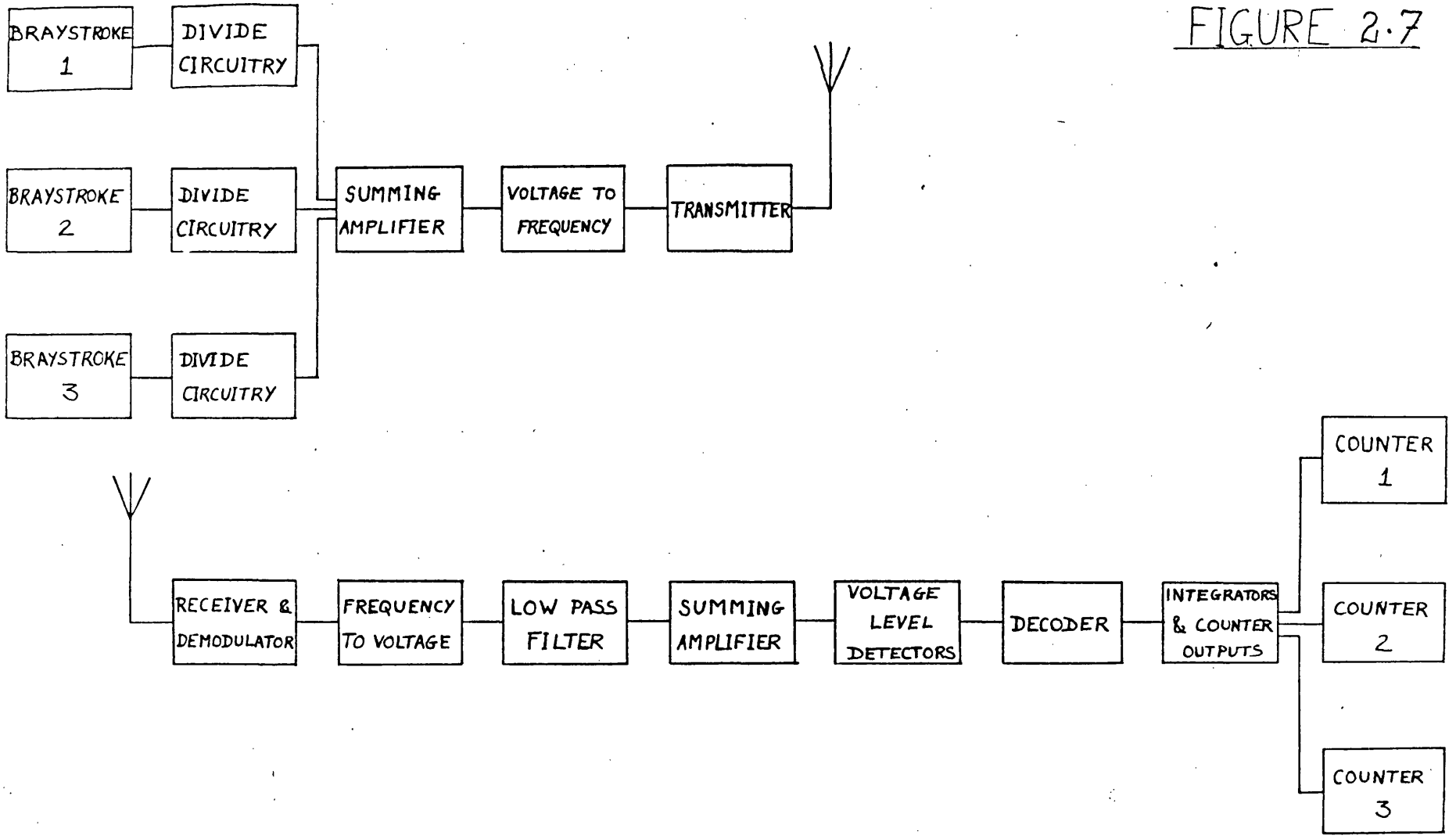

RADIO TELEMETRY SYSTEM [BLOCK DIAGRAM]

FIGURES 2.8 Radio receiving system

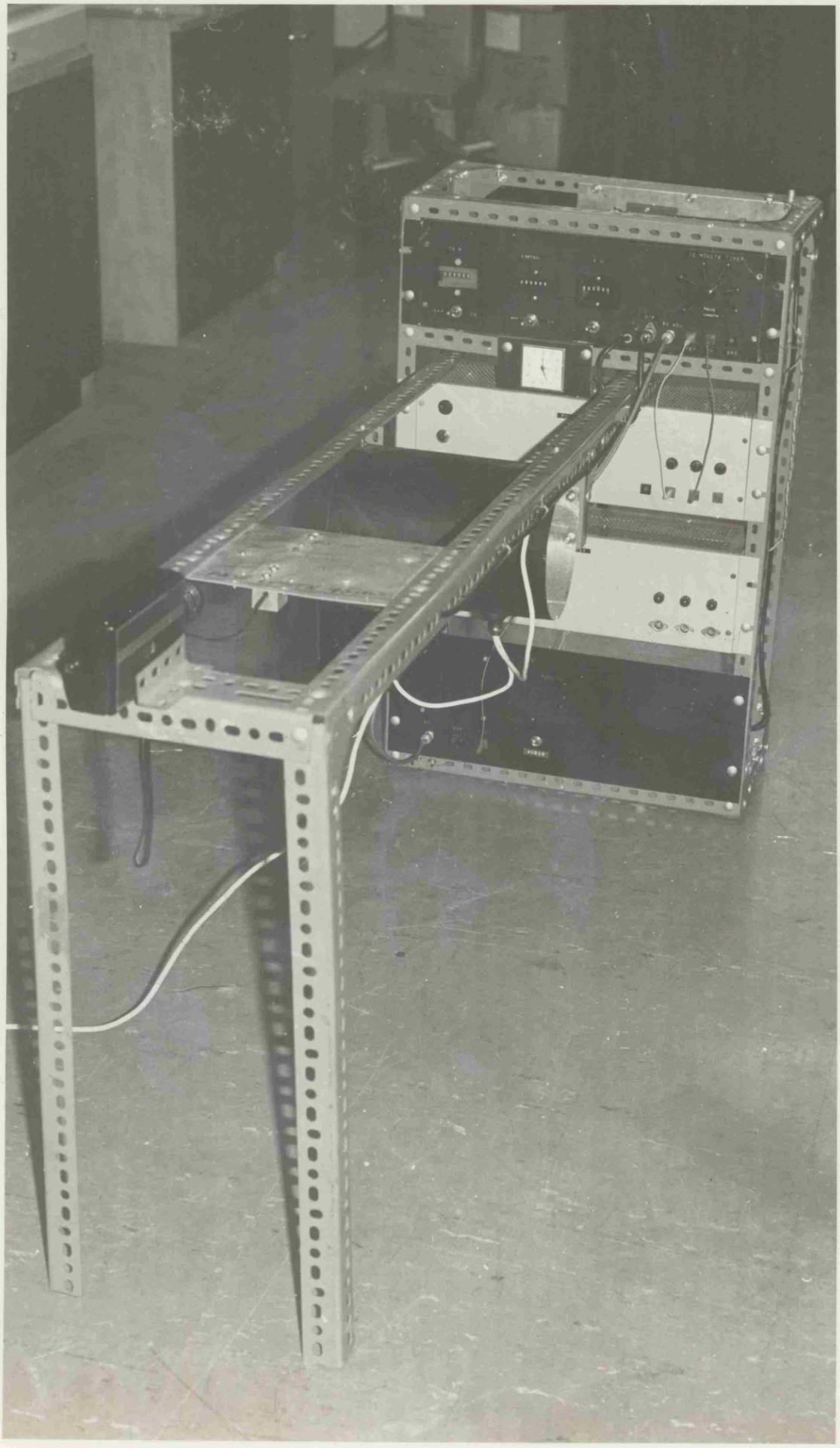

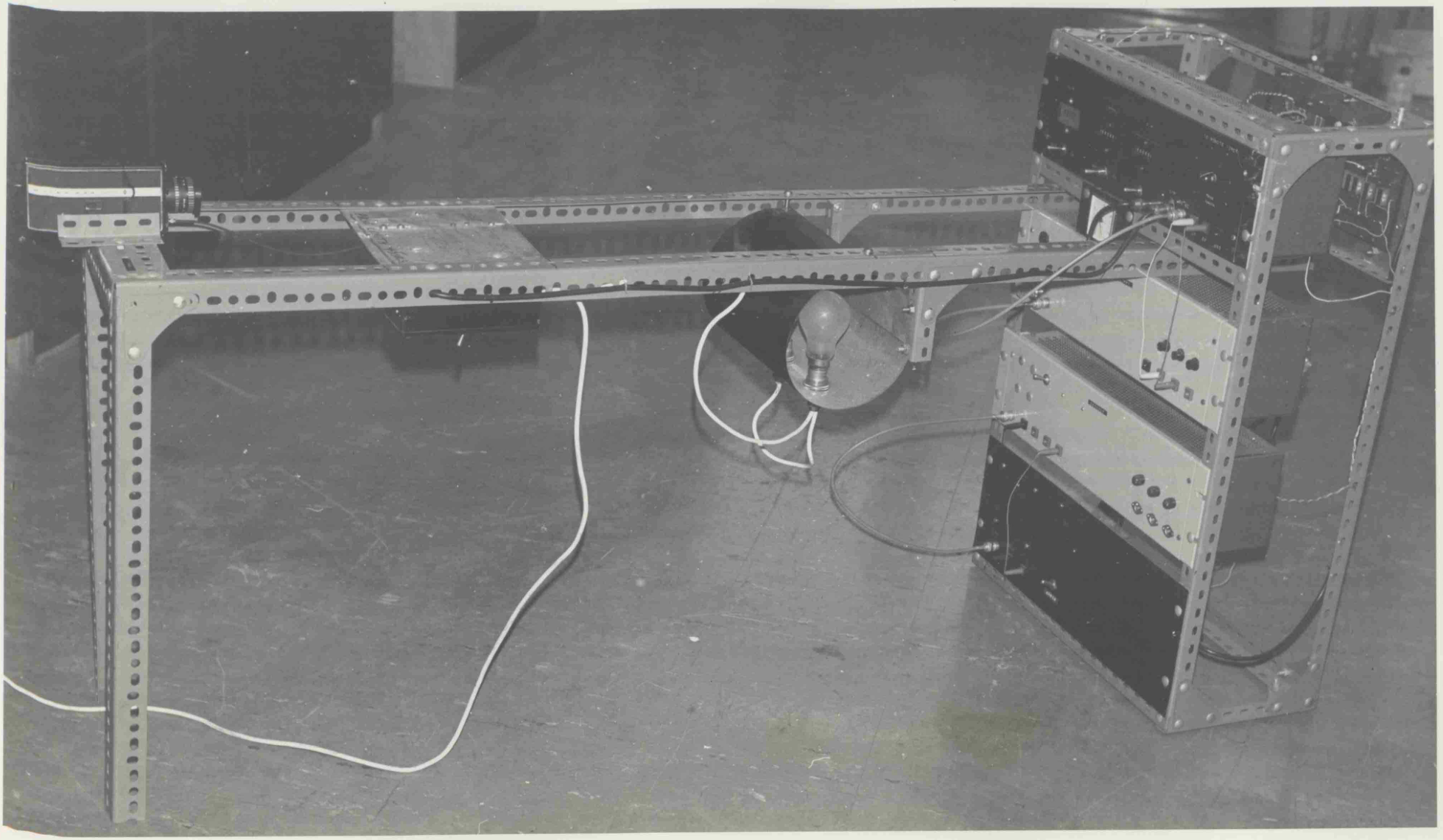

SPECIMEN OF COMPUTER PRINT-OUT FOR POSITION 0 - EBB.

2937120	33 D	23 H	52 M	0 S		
232.50	358.75	192.50	358.75	187.50	358.75	
232.50	358.75	187.50	358.75	192.50	358.75	
242.50	358.75	187.50	357.50	187.50	167.50	
0.13	0.	0.13	0.	0.13	186.94	
2937600	34 D	0 H	0 M	0 S		
217.50	358.75	197.50	358.75	187.50	358.75	
242.50	358.75	187.50	357.50	197.50	162.50	
242.50	358.75	182.50	358.75	192.50	358.75	
0.13	0.	0.13	338.20	0.13	184.15	
2938080	34 D	0 H	8 M	0 S		
222.50	358.75	197.50	358.75	182.50	358.75	
232.50	358.75	187.50	358.75	212.50	358.75	
217.50	358.75	192.50	358.75	192.50	358.75	(L.W.)
0.13	0.	0.13	0.	0.13	180.21	
2938560	34 D	0 H	16 M	0 S		
207.50	358.75	192.50	357.50	192.50	167.50	
247.50	358.75	182.50	358.75	182.50	358.75	
227.50	358.75	192.50	358.75	192.50	358.75	
0.13	0.	0.13	338.20	0.13	189.87	
2939040	34 D	0 H	24 M	0 S		
202.50	358.75	192.50	197.50	202.50	162.50	
222.50	358.75	192.50	358.75	187.50	358.75	
242.50	358.75	187.50	358.75	187.50	167.50	
0.13	0.	0.13	0.	0.13	180.34	
2939520	34 D	0 H	32 M	0 S		
227.50	358.75	187.50	357.50	187.50	162.50	
247.50	358.75	197.50	357.50	187.50	157.50	
227.50	358.75	197.50	357.50	197.50	167.50	
0.13	0.	0.13	195.07	0.13	187.20	
2940000	34 D	0 H	40 M	0 S		
247.50	358.75	192.50	358.75	182.50	358.75	
247.50	358.75	187.50	358.75	192.50	358.75	
222.50	358.75	182.50	358.75	187.50	358.75	
0.13	0.	0.13	0.	0.13	184.91	

FIGURE 3·1A

SPECIMEN OF COMPUTER PRINT-

OUT FOR POSITION 0 - FLOOD.

2916000		33 D	18 H	0 M	0 S			
12.50	358.75		12.50	358.75		7.50	358.75	
12.50	358.75		2.50	358.75		7.50	358.75	
12.50	358.75		12.50	358.75		7.50	358.75	
0.13	0.		0.13	17.53		0.13	239.14	
2916480		33 D	18 H	8 M	0 S			
12.50	358.75		7.50	358.75		7.50	358.75	
2.50	358.75		7.50	358.75		7.50	358.75	
12.50	358.75		17.50	358.75		12.50	358.75	
0.13	0.		0.13	0.		0.13	222.38	
2916960		33 D	18 H	16 M	0 S			
12.50	358.75		12.50	358.75		12.50	358.75	
12.50	358.75		12.50	358.75		12.50	358.75	
12.50	358.75		12.50	358.75		7.50	358.75	
0.13	0.		0.13	0.		0.13	219.84	
2917440		33 D	18 H	24 M	0 S			
12.50	358.75		7.50	358.75		7.50	358.75	
12.50	358.75		7.50	358.75		7.50	358.75	
12.50	358.75		7.50	358.75		12.50	358.75	(H.W.)
0.13	0.		0.13	0.		0.13	199.52	
2917920		33 D	18 H	32 M	0 S			
12.50	358.75		7.50	358.75		12.50	358.75	
12.50	358.75		12.50	358.75		12.50	358.75	
12.50	358.75		7.50	358.75		7.50	359.75	
0.13	0.		0.13	17.53		0.13	177.29	
2918400		33 D	18 H	40 M	0 S			
12.50	358.75		7.50	358.75		7.50	358.75	
12.50	358.75		7.50	358.75		12.50	358.75	
12.50	358.75		7.50	358.75		12.50	358.75	
0.13	0.		0.13	0.		0.13	164.85	
2918880		33 D	18 H	48 M	0 S			
7.50	358.75		7.50	358.75		7.50	358.75	
12.50	358.75		7.50	358.75		7.50	358.75	
12.50	358.75		7.50	358.75		7.50	358.75	
0.13	0.		0.13	0.		0.13	161.93	

FIGURE 3·13.

POSITION 0.

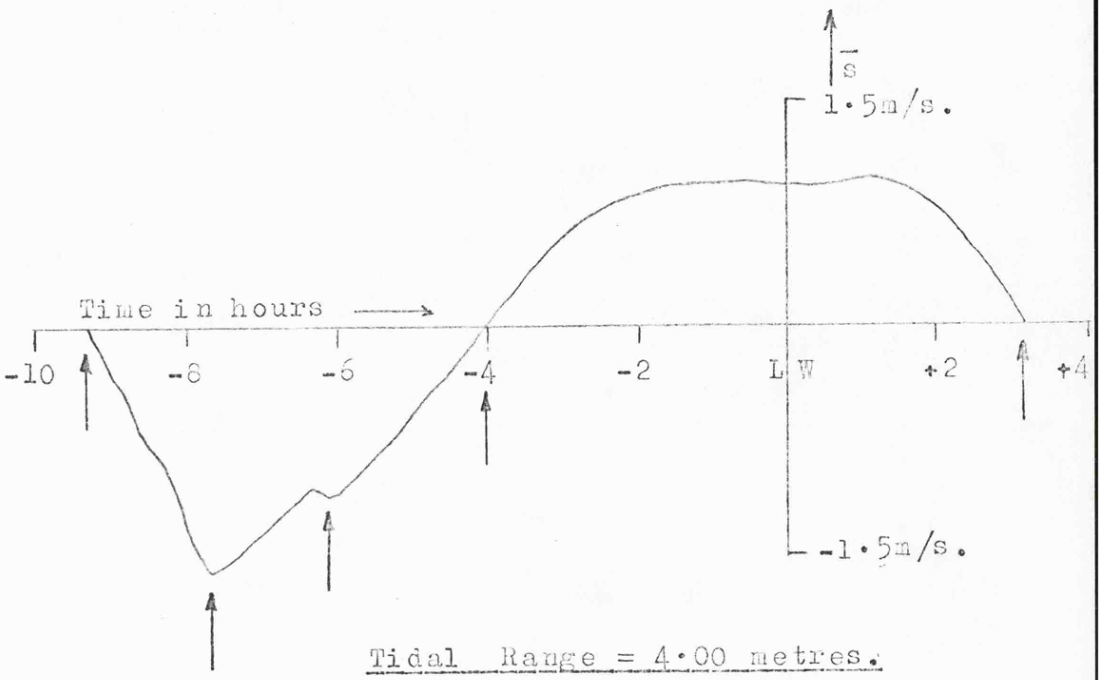

Tidal Range = 4·00 metres.

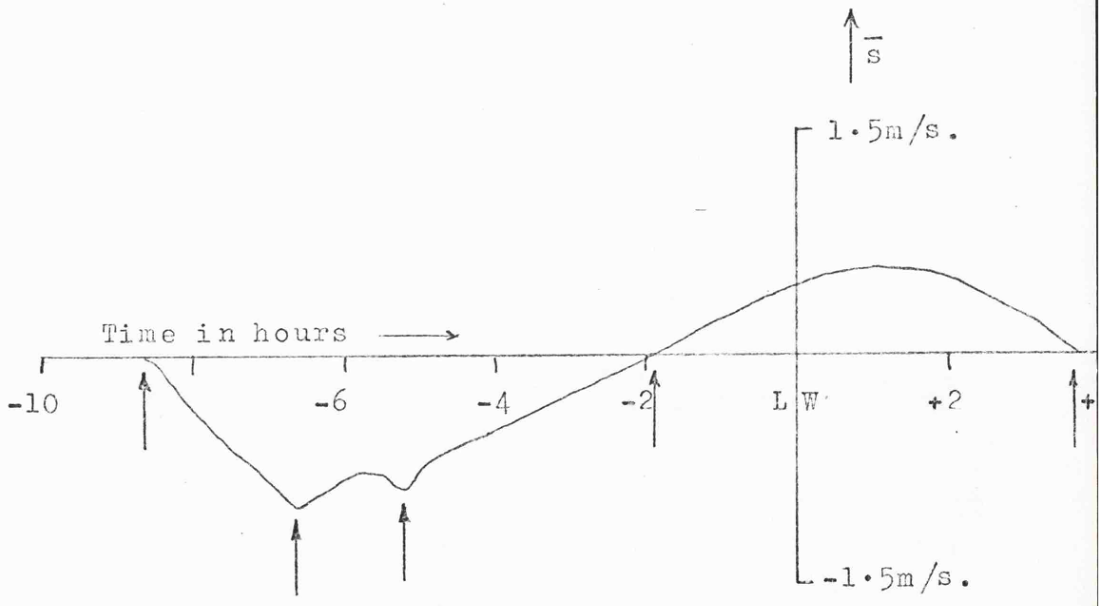

Tidal Range = 2·00 metres.

SPRING & NEAP TIDE SPEED CYCLES.

FIGURE 3·2.

VARIATION OF NORMALISED CURRENT SPEED CYCLES WITH TIDAL RANGE.

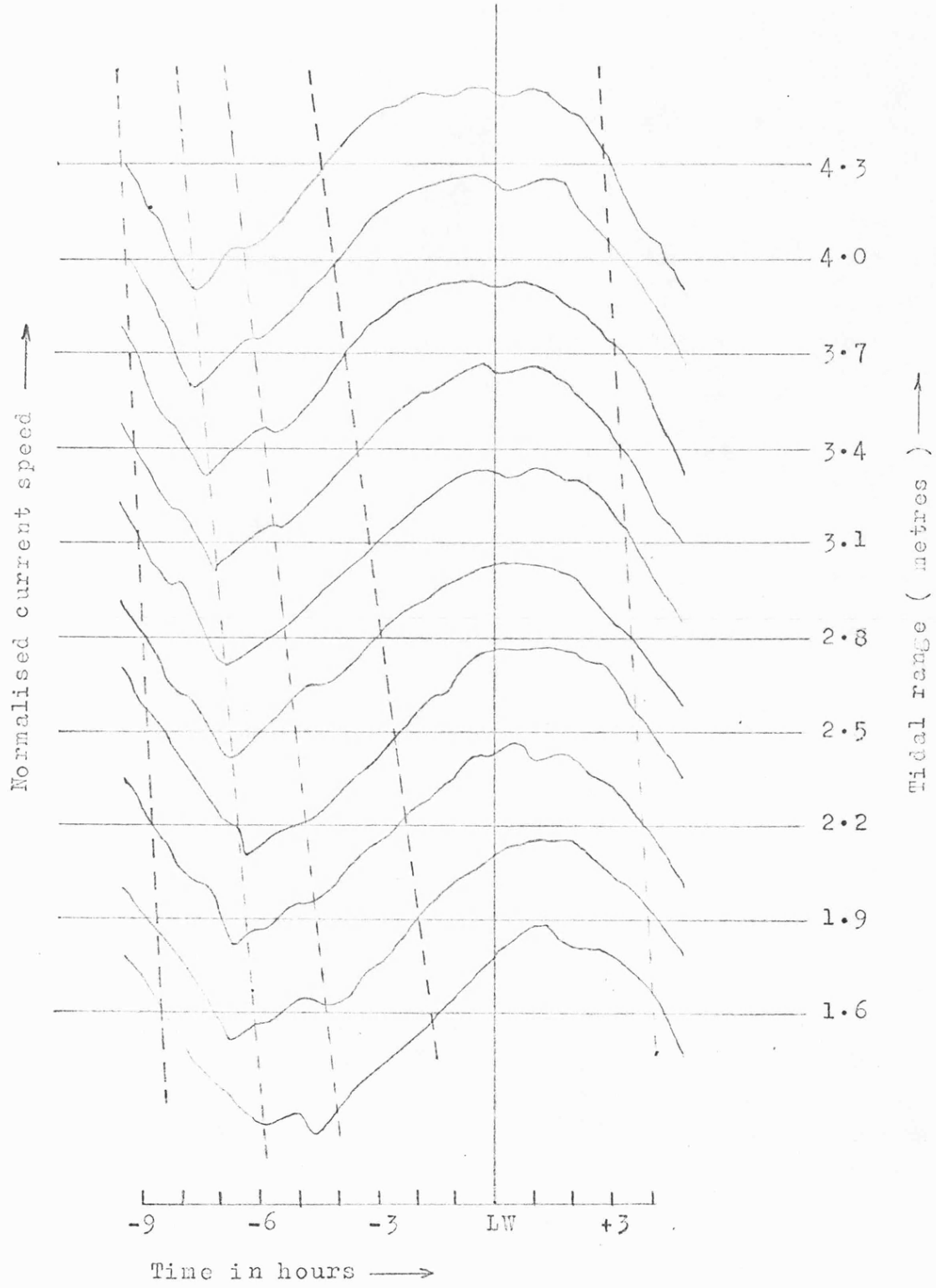

FIGURE 4·1.

EBB FLOW.

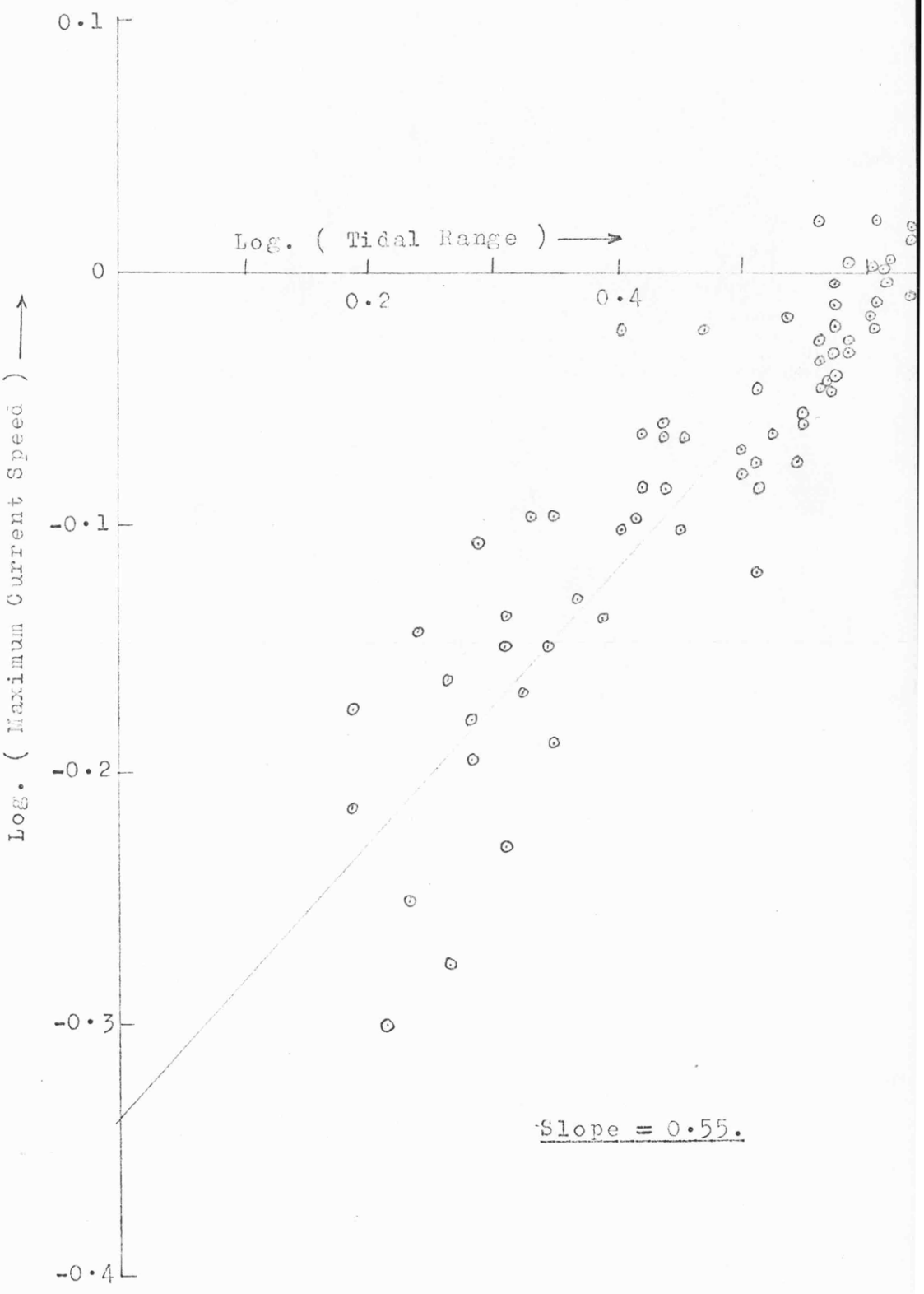

FIGURE 4·2.

FLOOD FLOW.

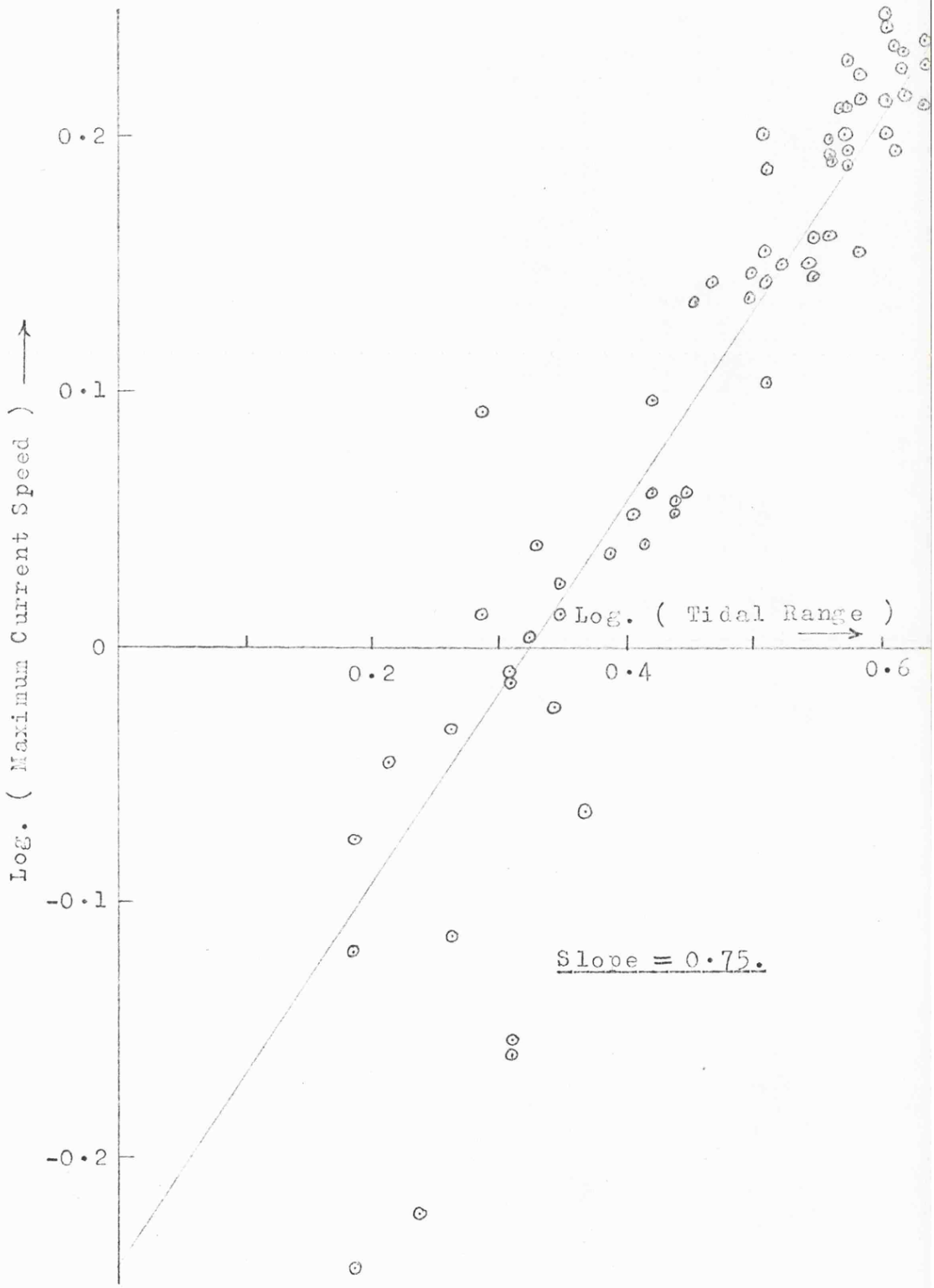

FIGURE 4·3.

POSITION O.

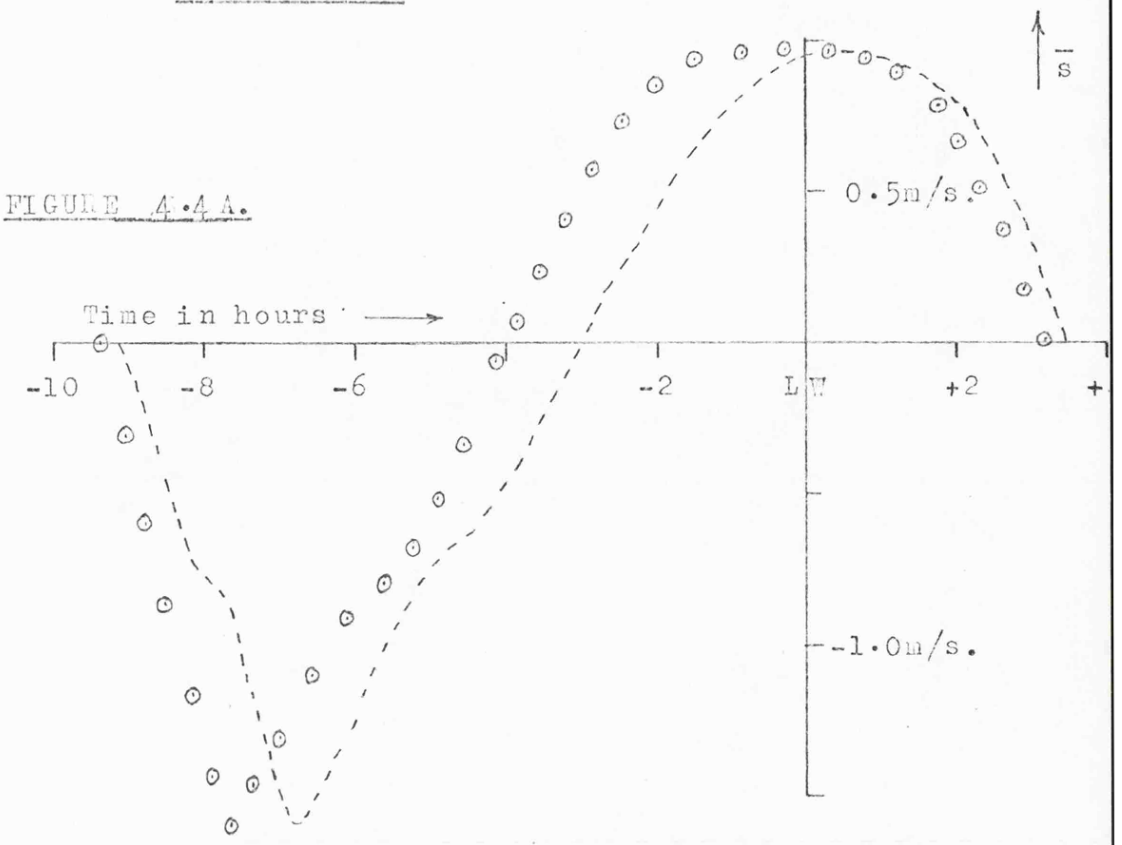

FIGURE 4·4 A.

Tidal Range = 4·00 metres.

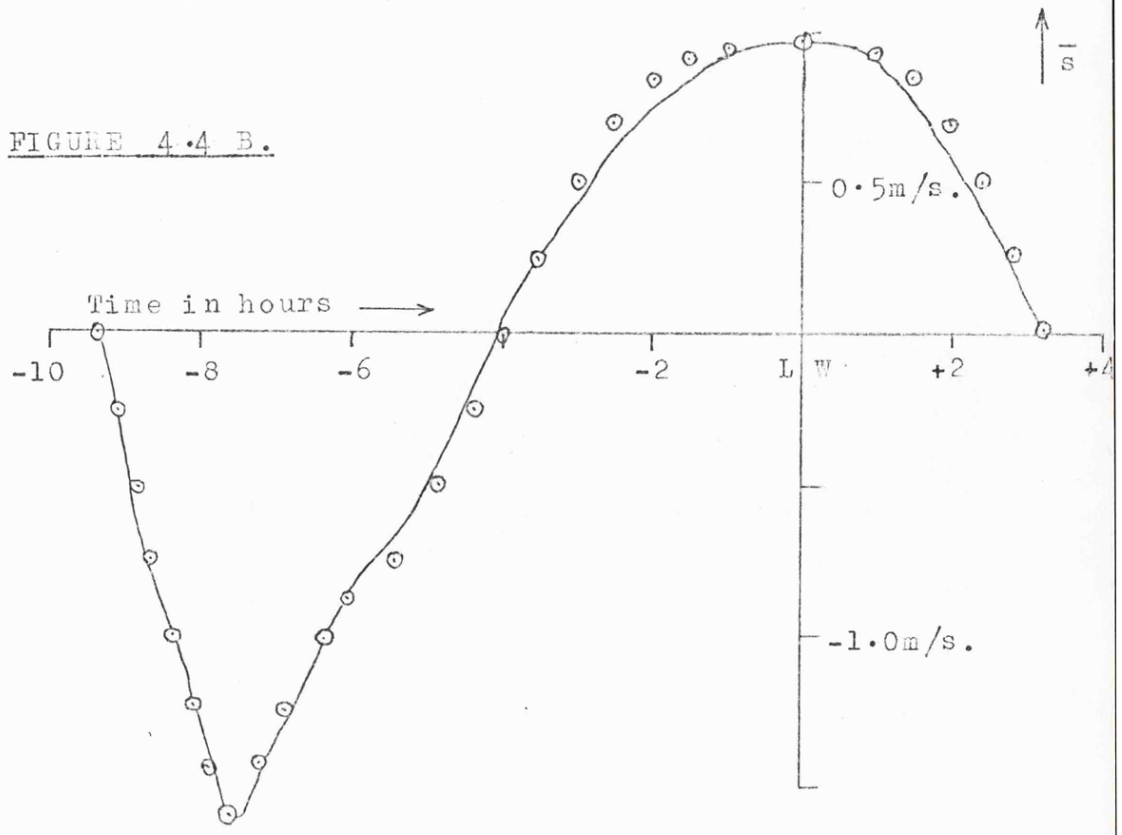

FIGURE 4·4 B.

TIDAL RANGE SCALING OF SPEED CYCLES.

FIGURES 4·4.

POSITION D.

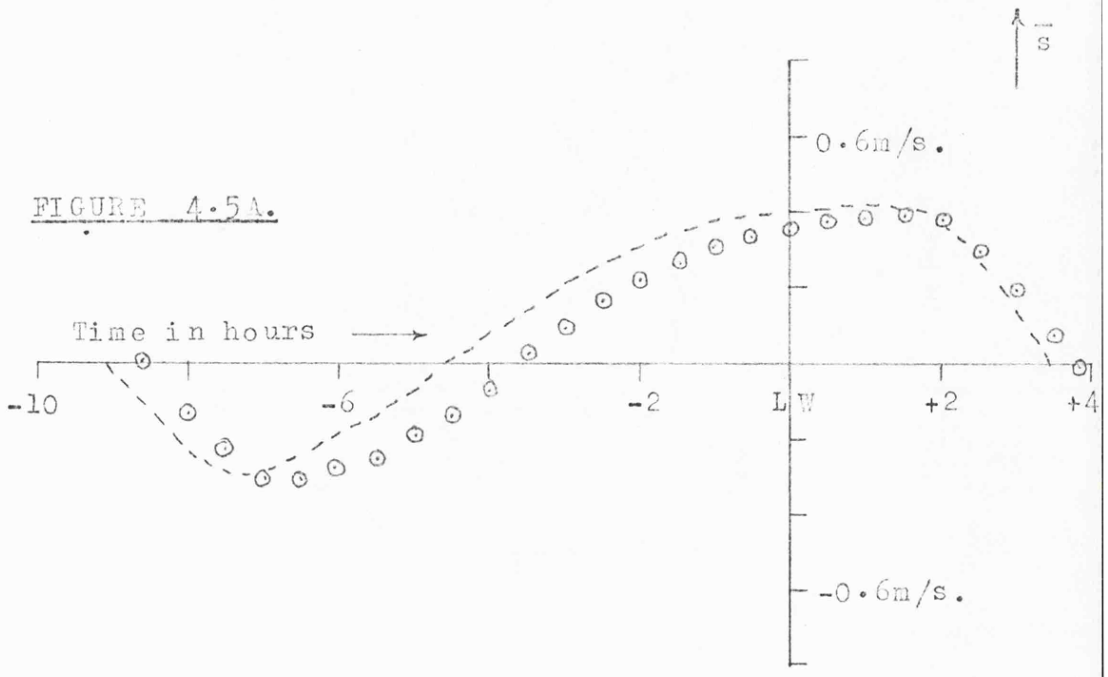

FIGURE 4·5A.

Tidal Range = 2·7 metres.

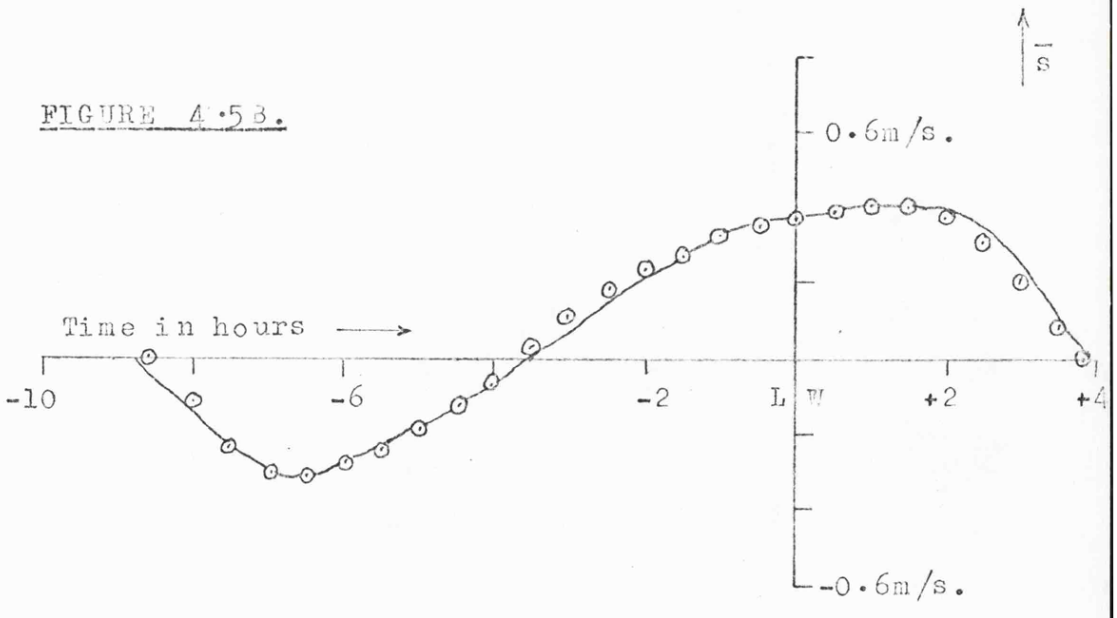

FIGURE 4·5B.

TIDAL RANGE SCALING OF SPEED CYCLES.

FIGURES 4·5.

POSITION E.

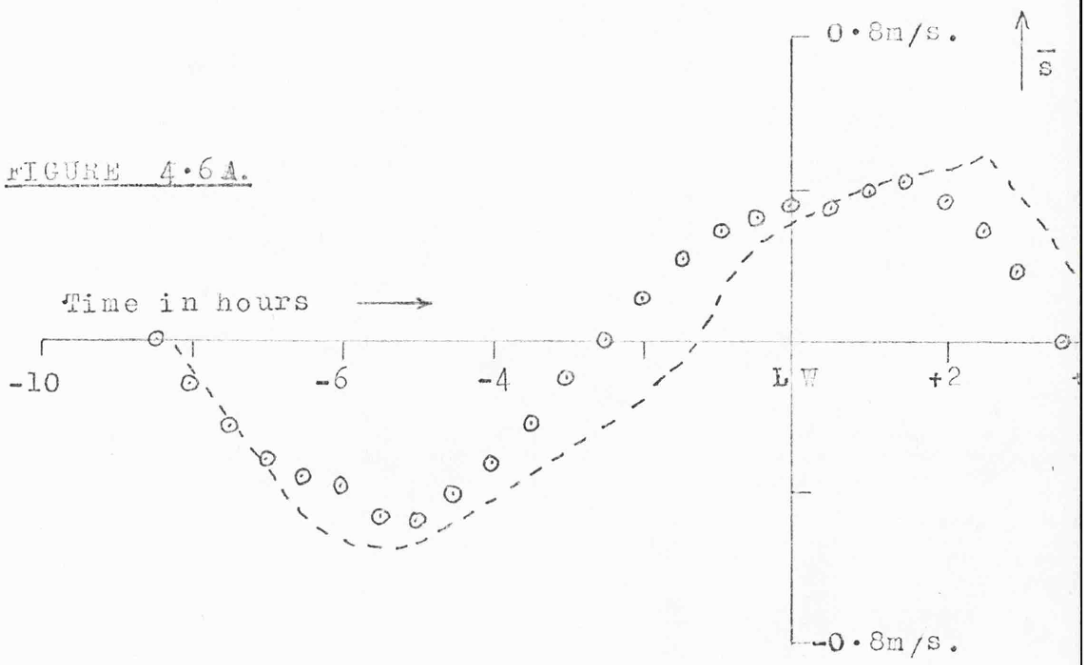

FIGURE 4·6A.

Tidal Range = 3·60 metres.

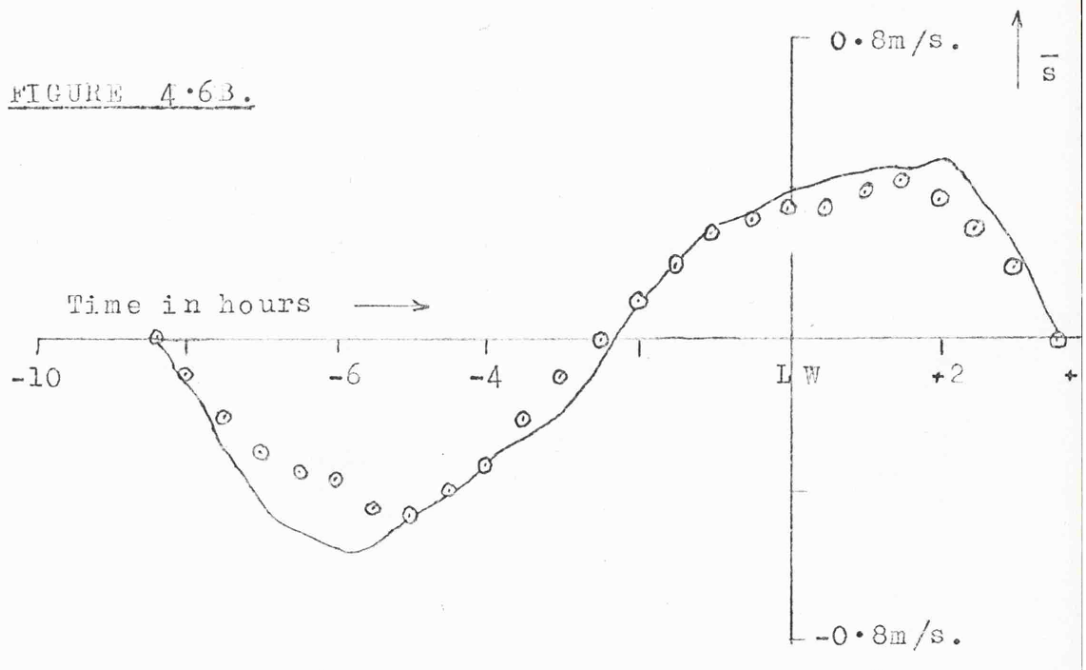

FIGURE 4·6B.

TIDAL RANGE SCALING OF SPEED CYCLES.

FIGURES 4·6.

VARIATION OF CURRENT DIRECTION CYCLES WITH TIDAL RANGE.

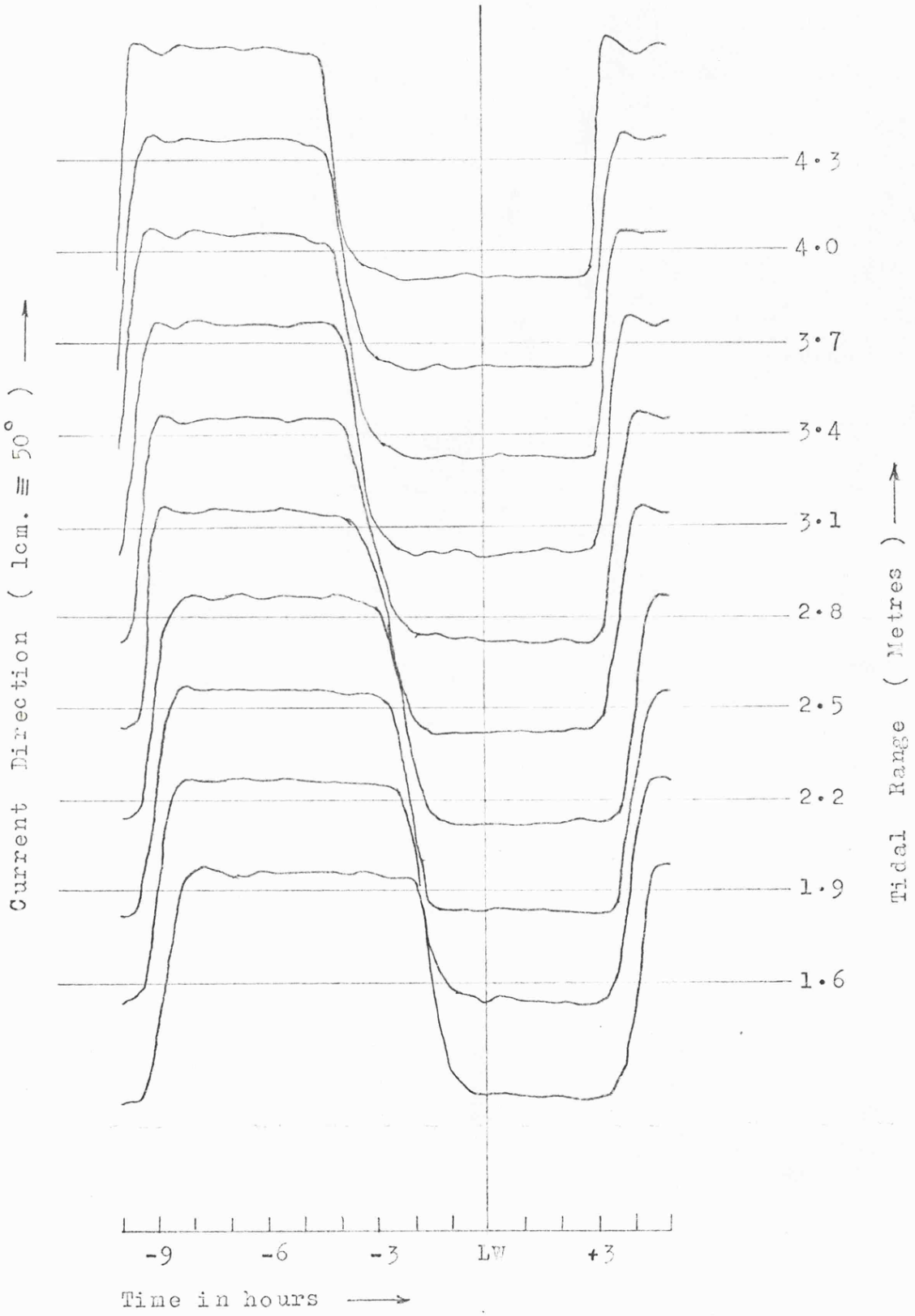

FIGURE 4·7.

POSITION O.

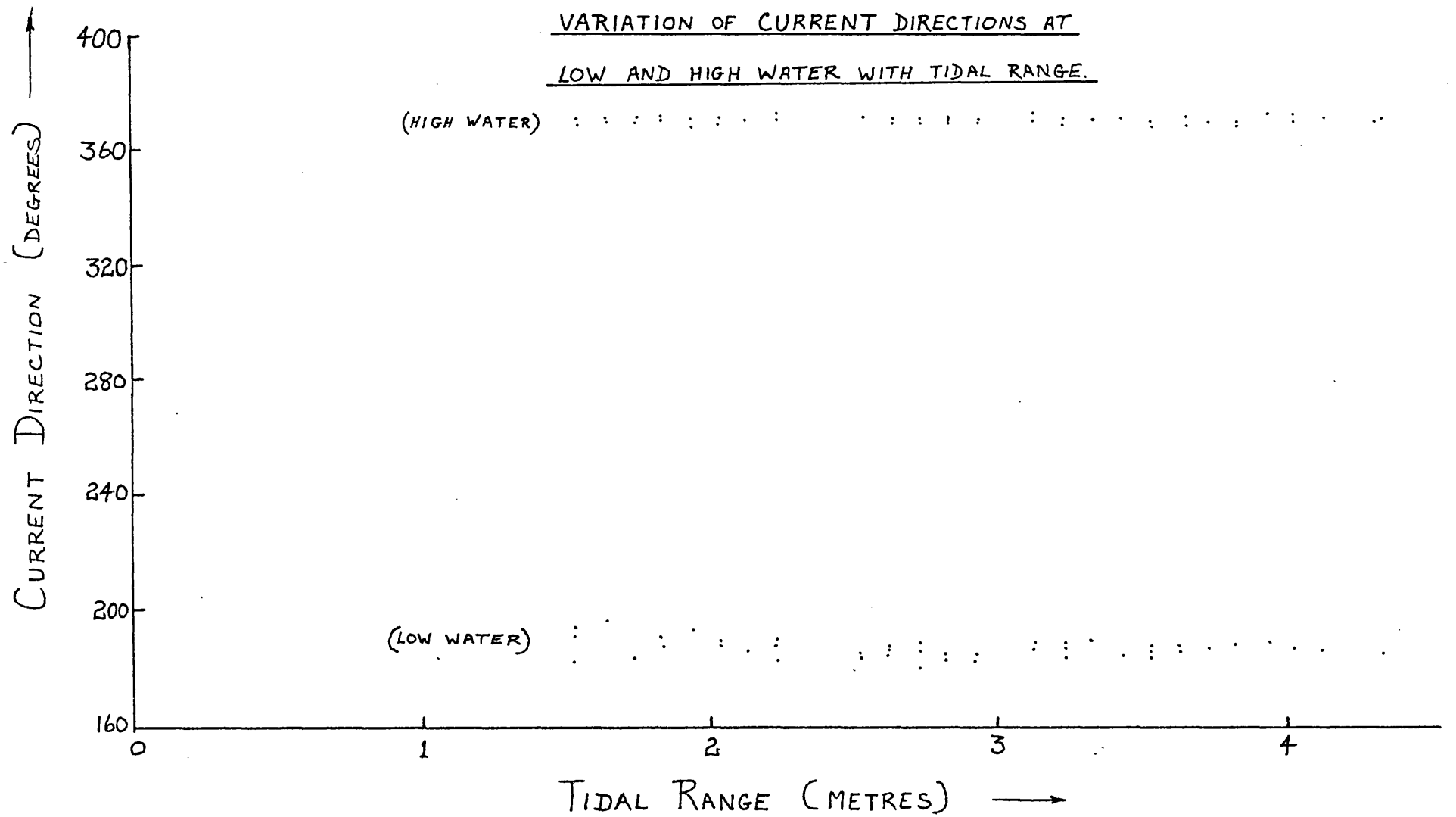

FIGURE 4.8

POSITION O.

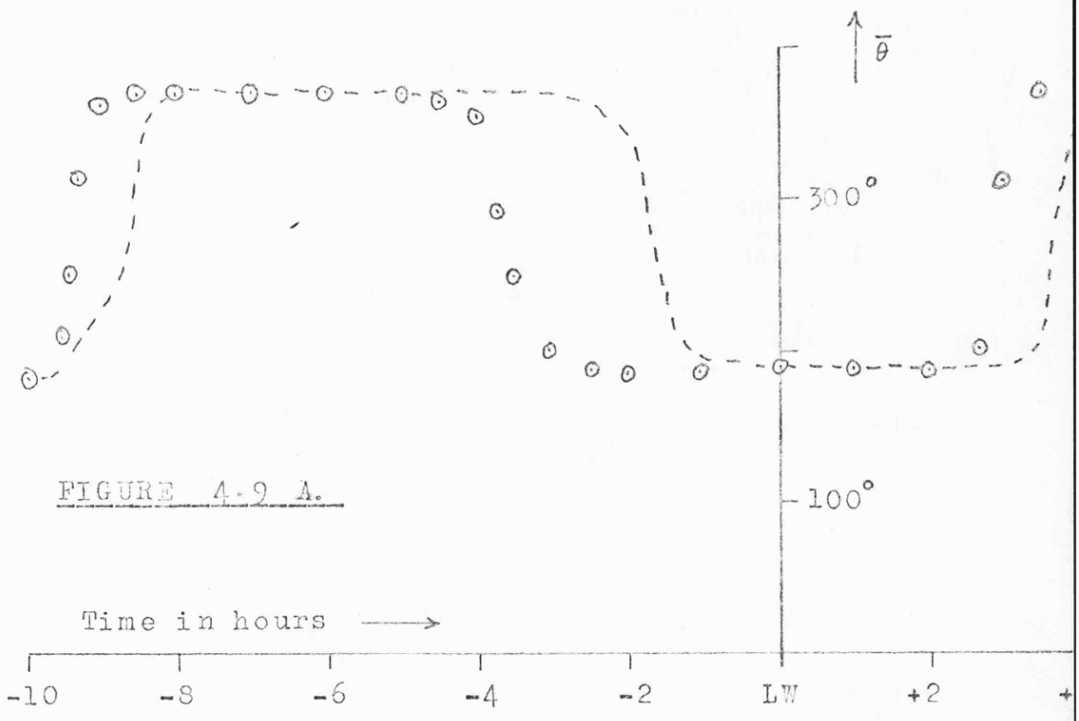

FIGURE 4.9 A.

Tidal Range = 4.00 metres.

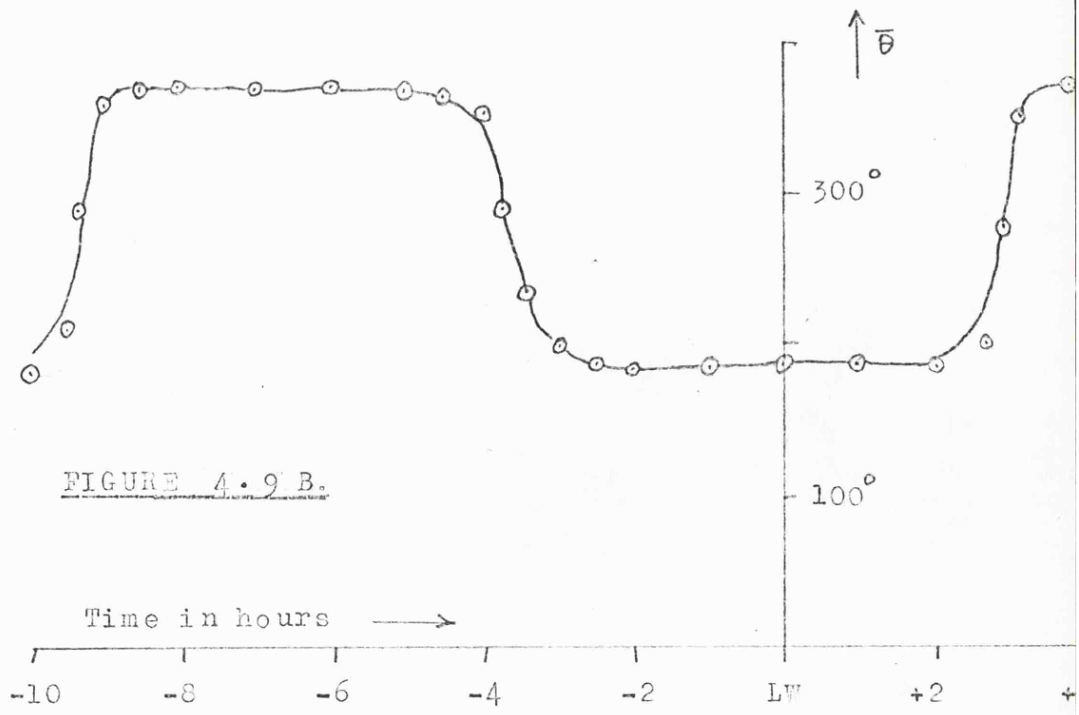

FIGURE 4.9 B.

TIDAL RANGE SCALING OF DIRECTION CYCLES.

FIGURE 4.9.

POSITION A.

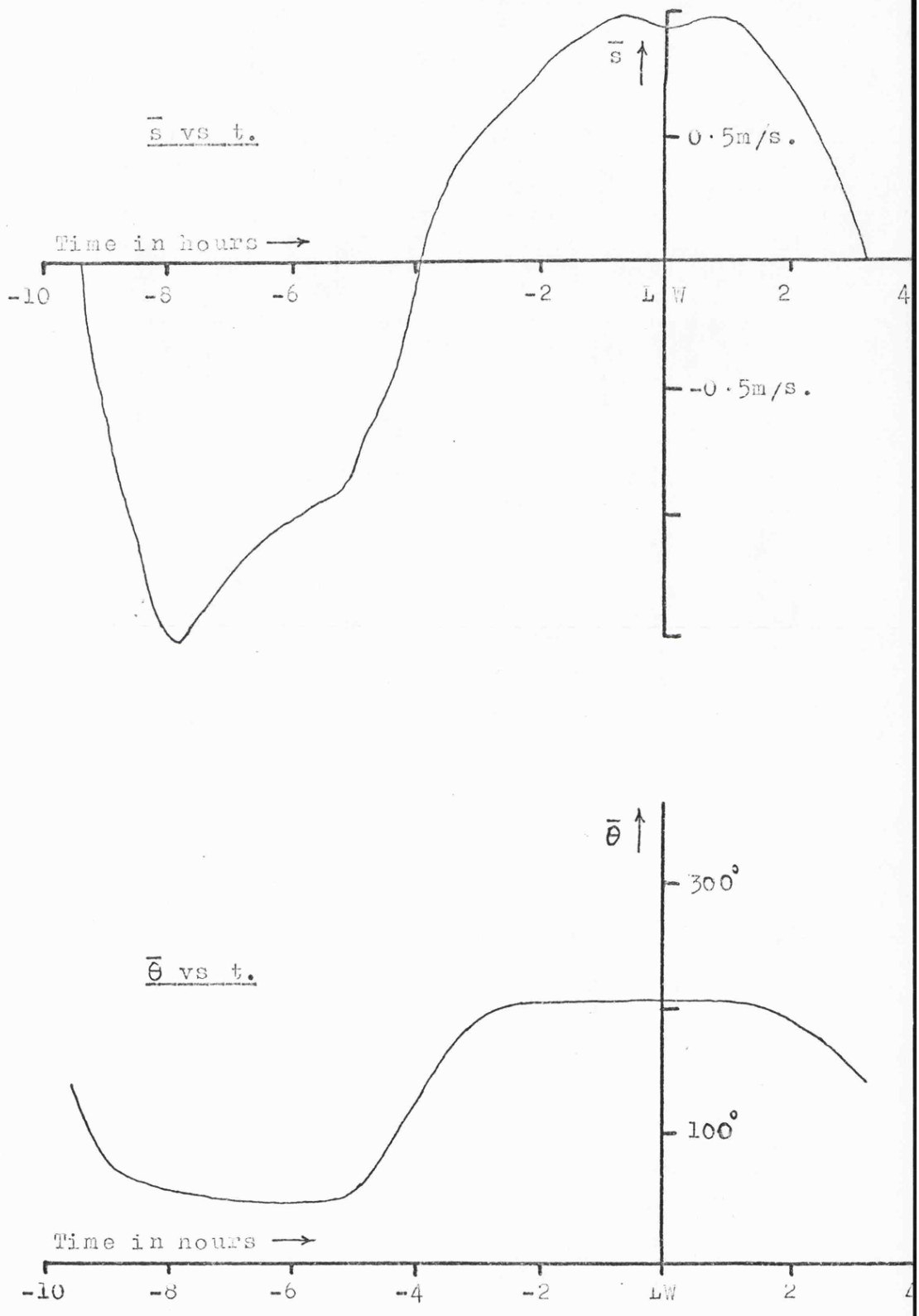

Cycles of depth-averaged tidal current speed and direction corrected to refer to a tidal range of 4·00 metres.

FIGURE 4.10.

POSITION D.

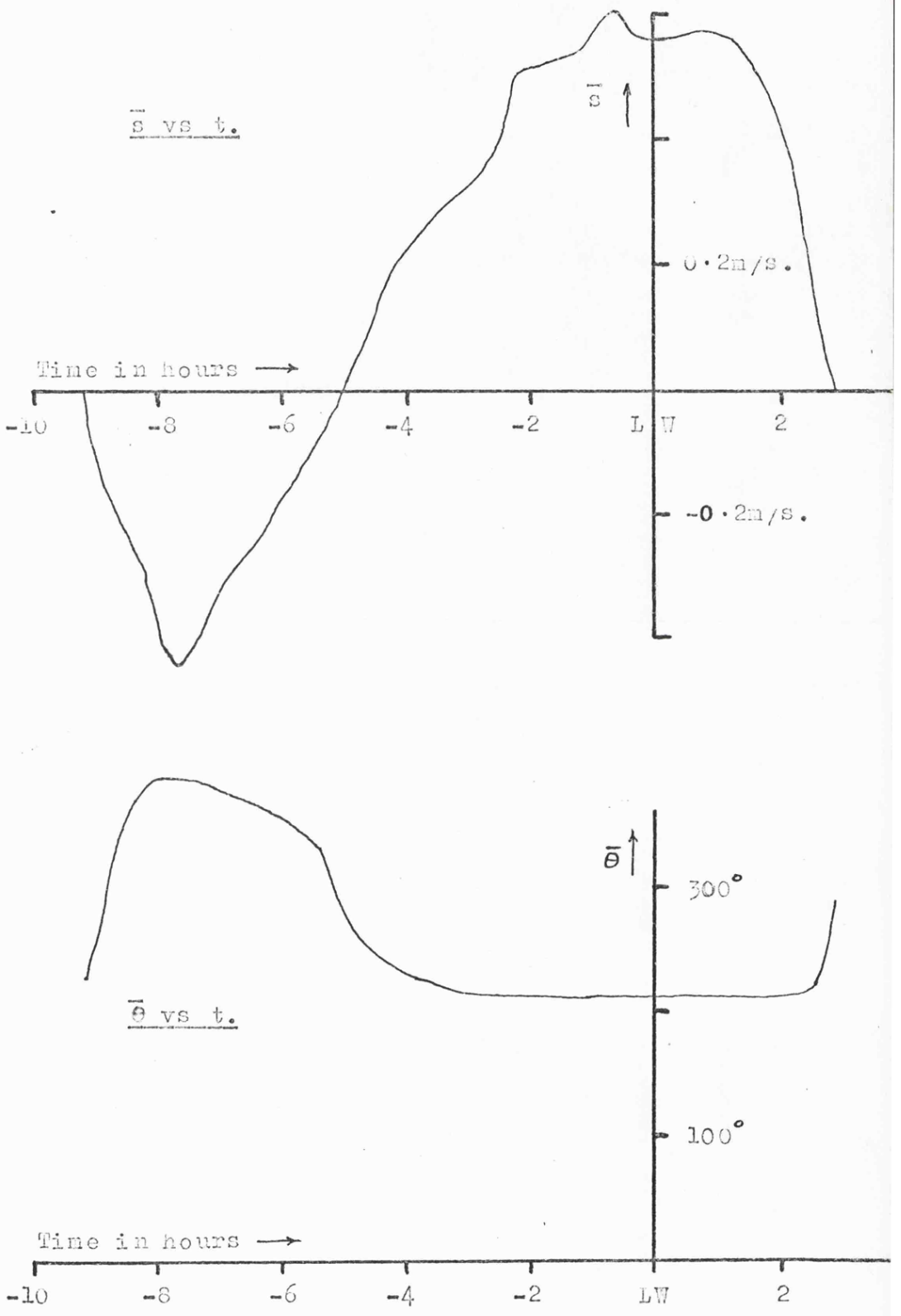

Cycles of depth-averaged tidal current speed and direction corrected to refer to a tidal range of 4·00 metres.

FIGURE 4.11.

POSITION D'.

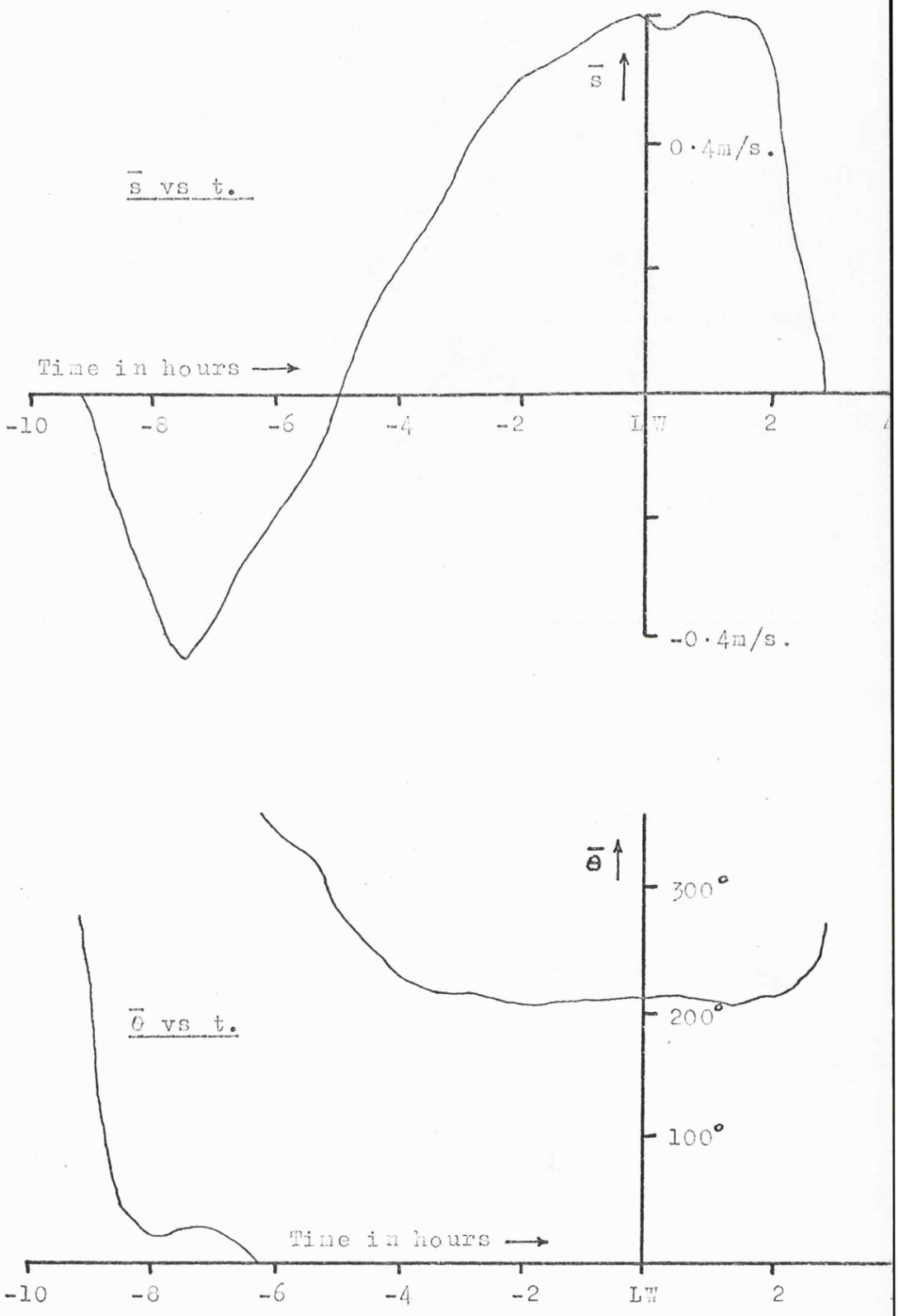

Cycles of depth-averaged tidal current speed and direction corrected to refer to a tidal range of 4·00 metres.

FIGURE 4.12.

POSITION J.

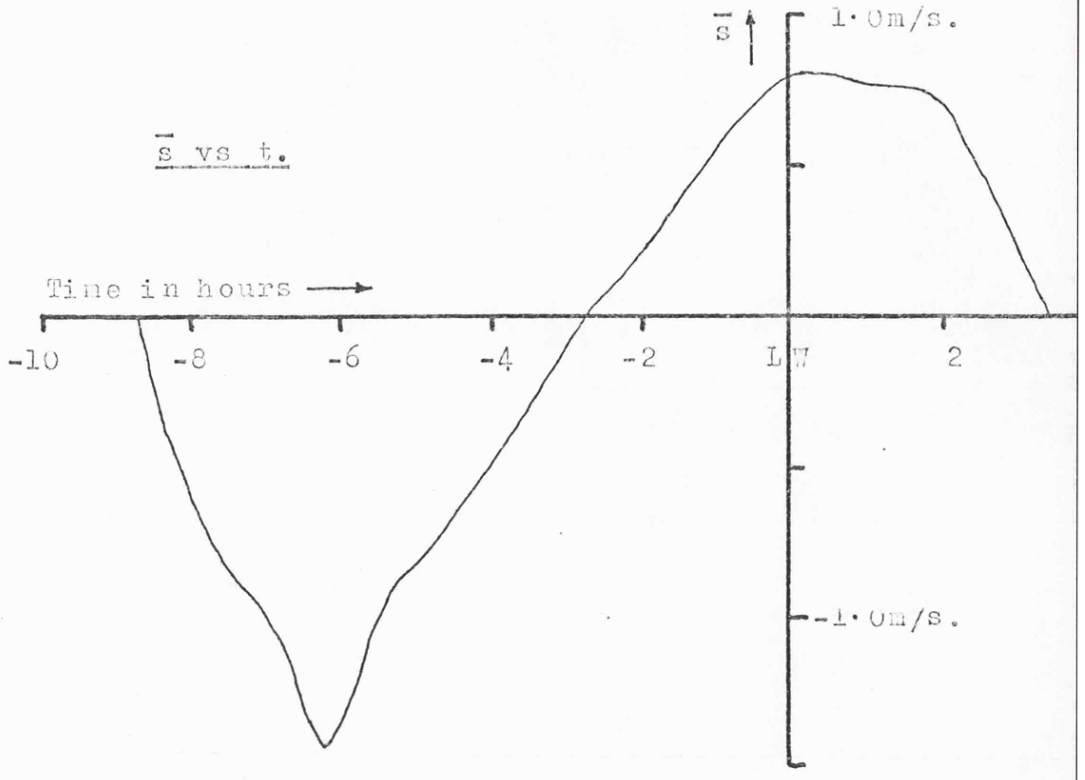

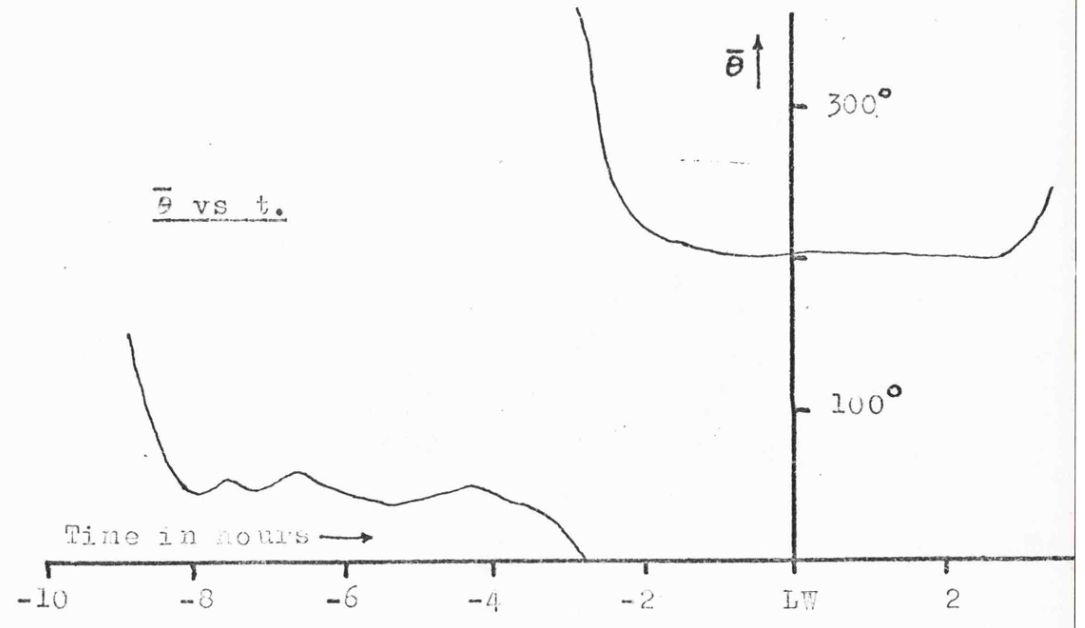

Cycles of depth-averaged tidal current speed and direction corrected to refer to a tidal range of 4·00 metres.

FIGURE 4.13.

POSITION K.

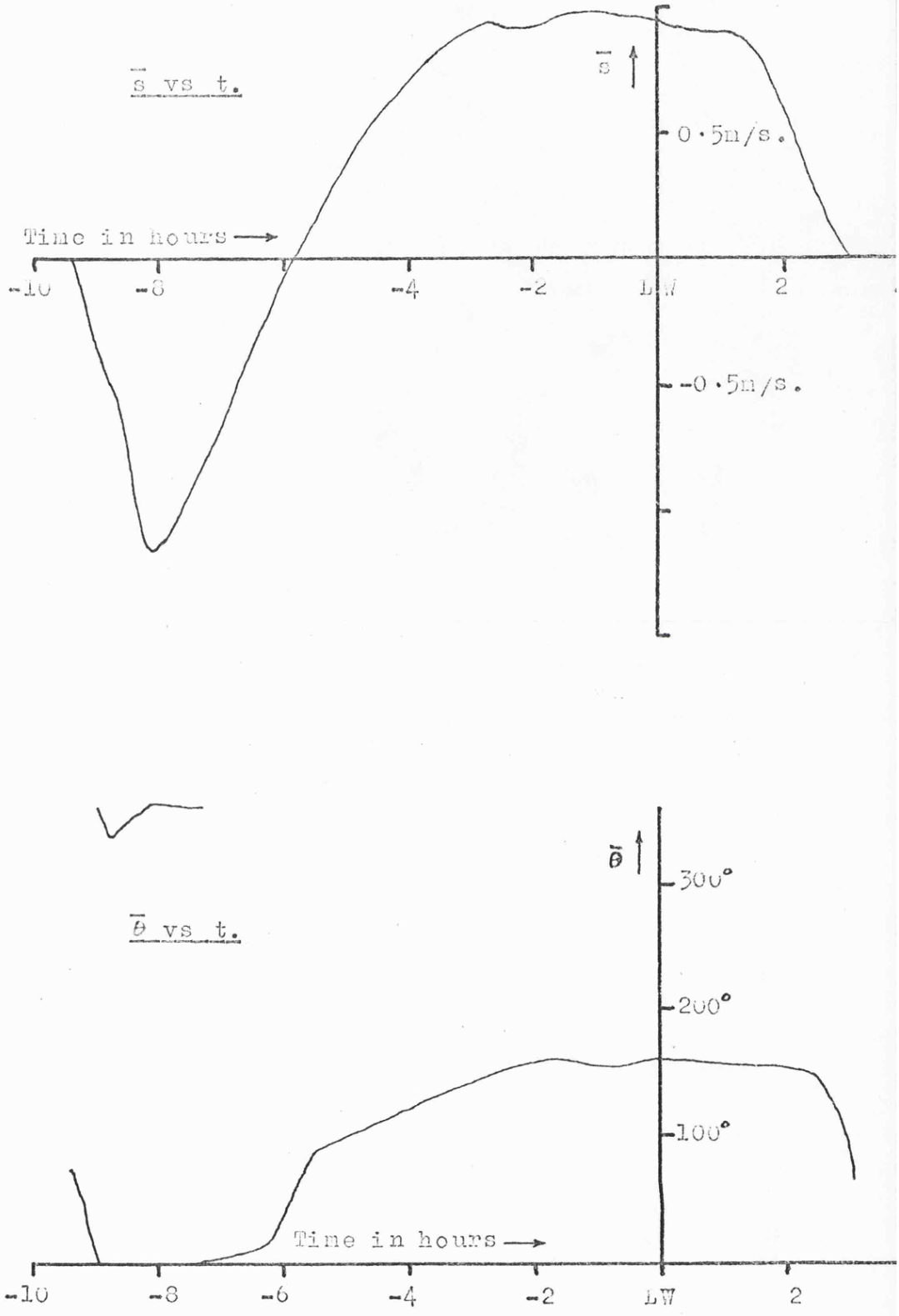

Cycles of depth-averaged tidal current speed and direction corrected to refer to a tidal range of 4·00 metres.

FIGURE 4.14.

POSITION N.

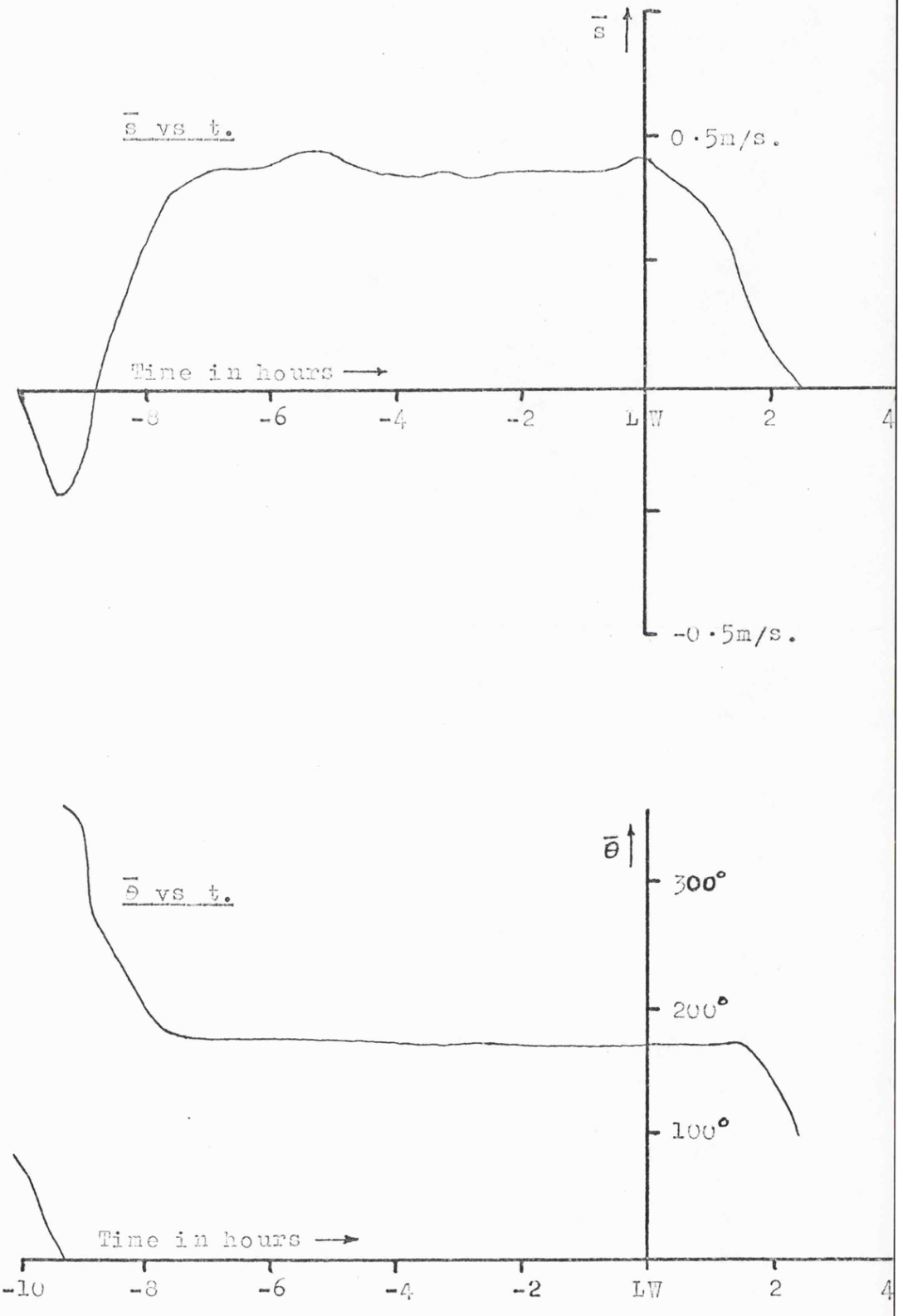

Cycles of depth-averaged tidal current speed and direction corrected to refer to a tidal range of 4·00 metres.

FIGURE 4.15.

POSITION 0.

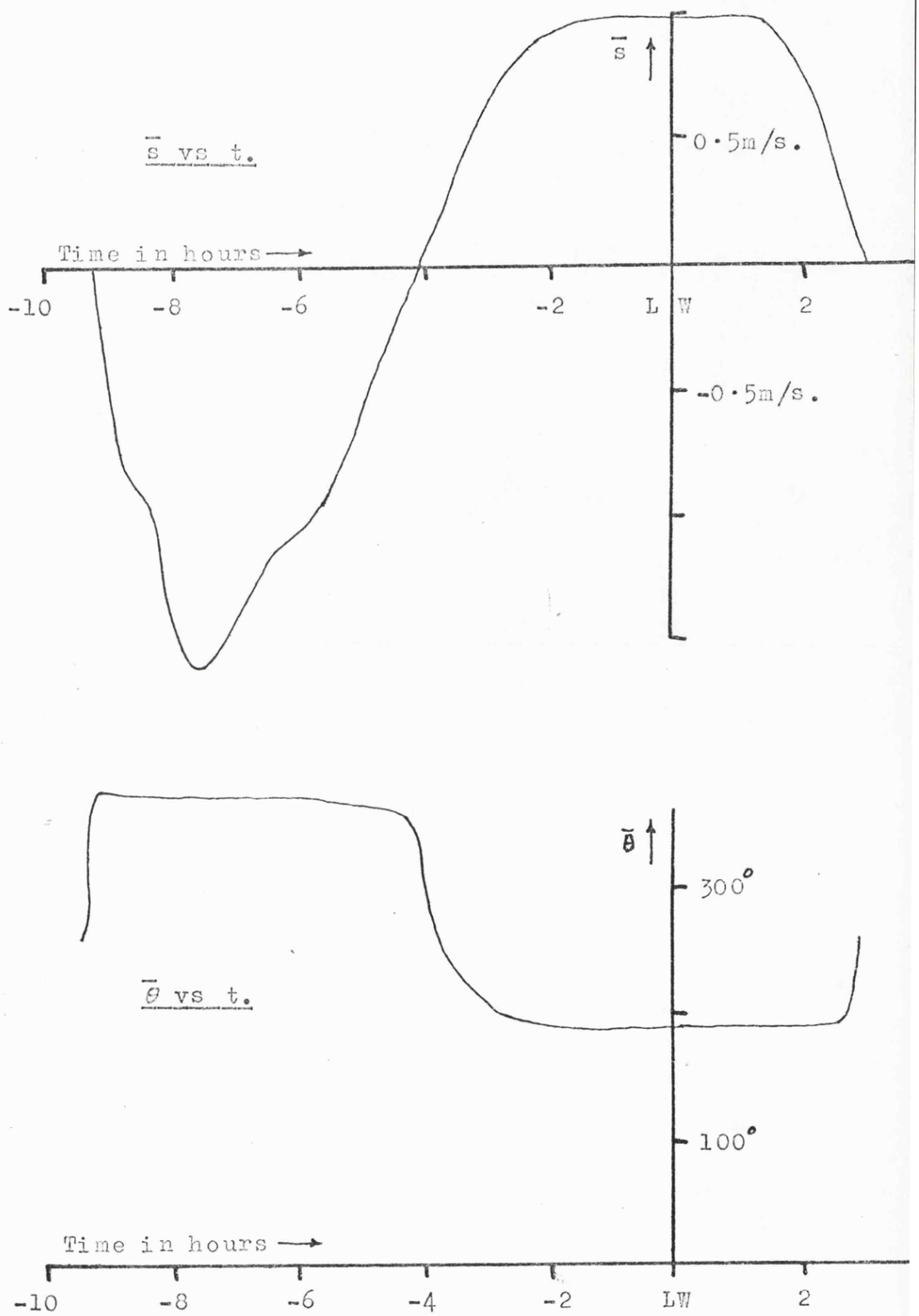

Cycles of depth-averaged tidal current speed and direction corrected to refer to a tidal range of 4·00 metres.

FIGURE 4.16.

POSITION P.

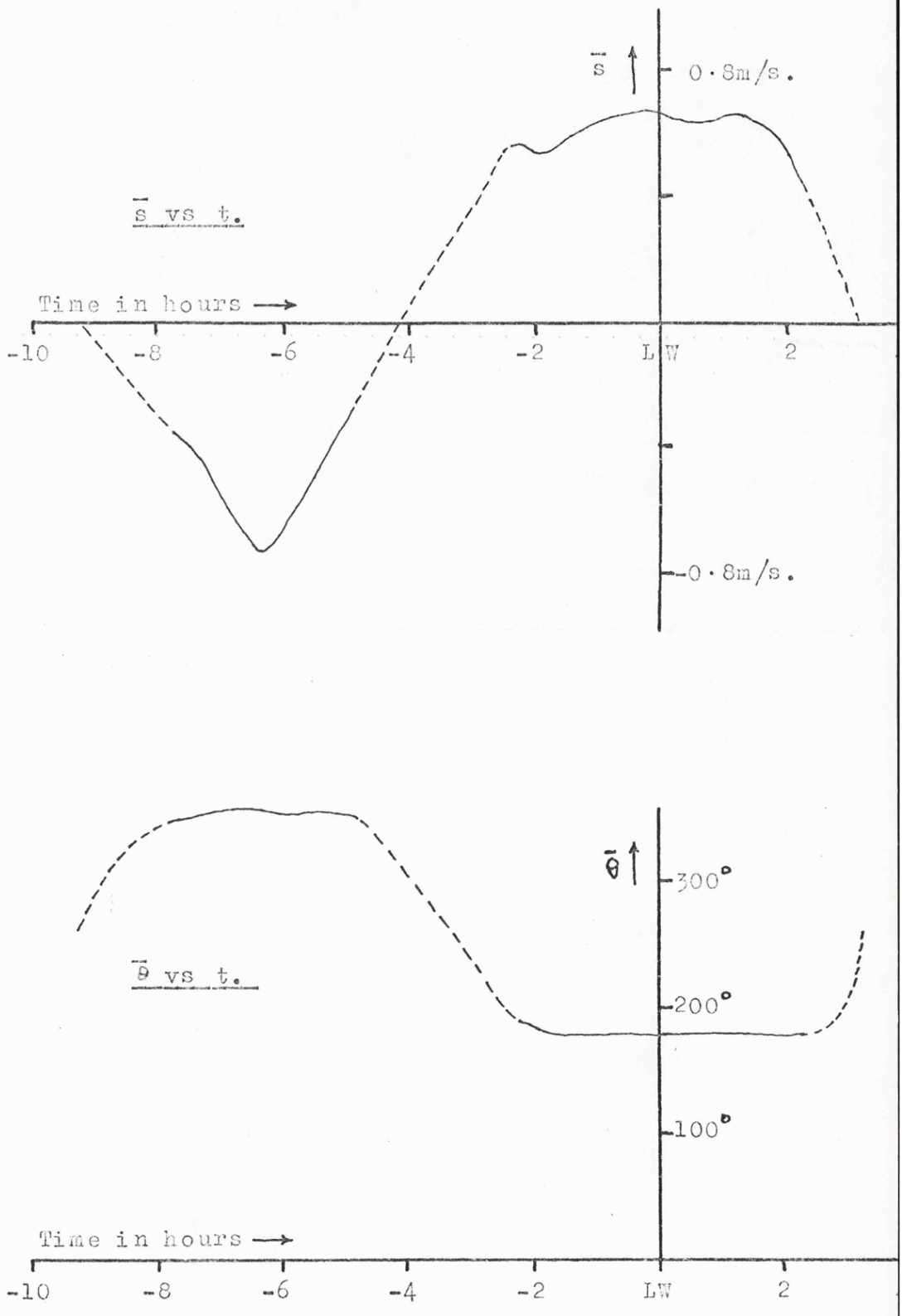

Cycles of depth-averaged tidal current speed and direction corrected to refer to a tidal range of 4·00 metres.

FIGURE 4.17.

POSITION Q.

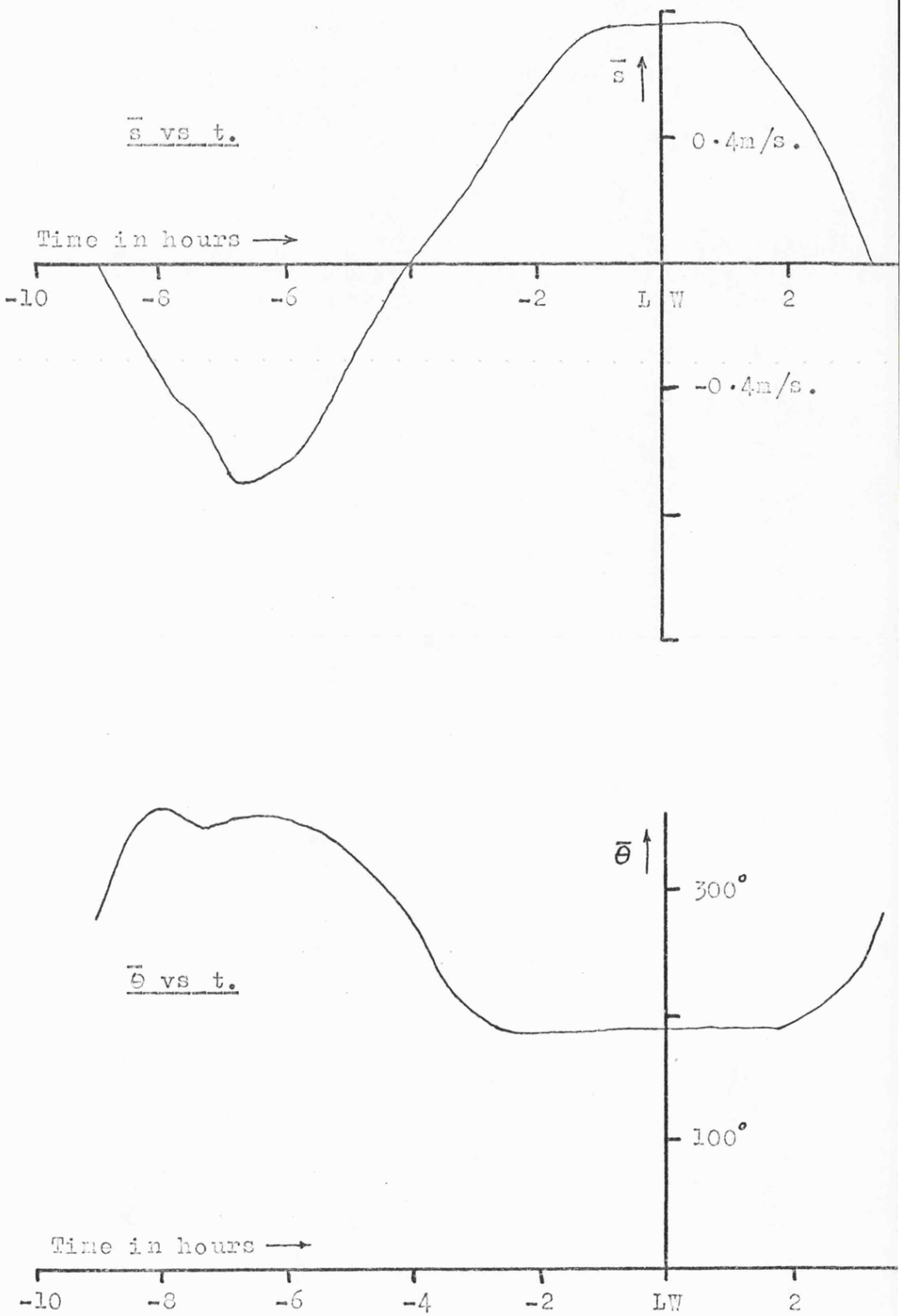

Cycles of depth-averaged tidal current speed and direction corrected to refer to a tidal range of 4·00 metres.

FIGURE 4.18.

POSITION E.

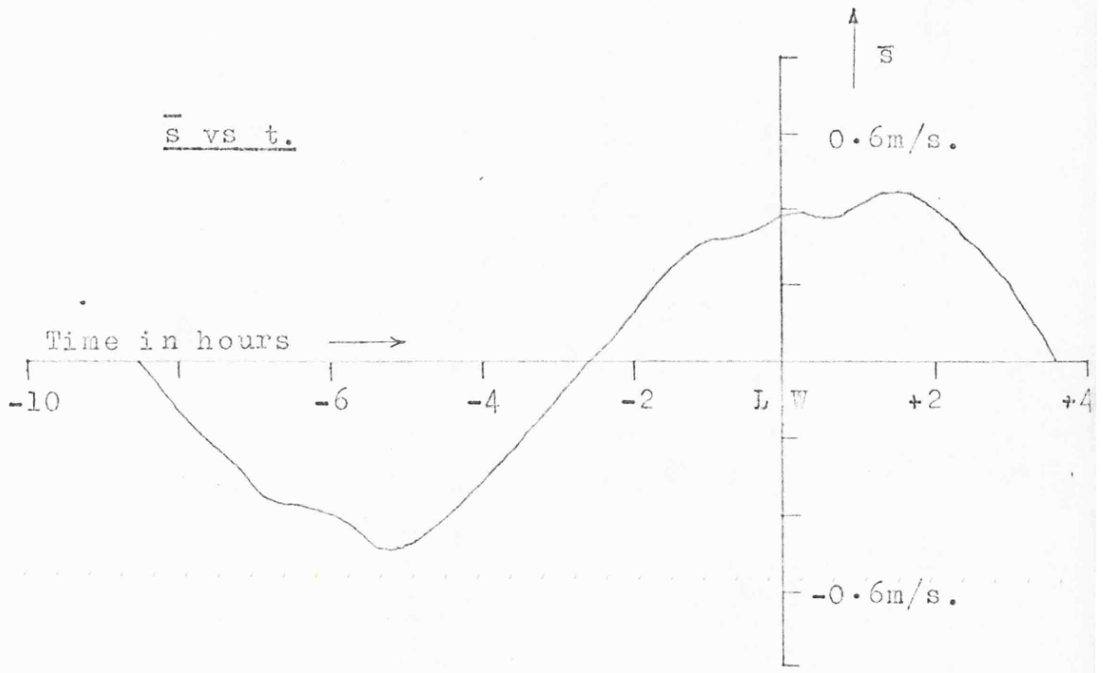

Tidal Range = 3·60 metres.

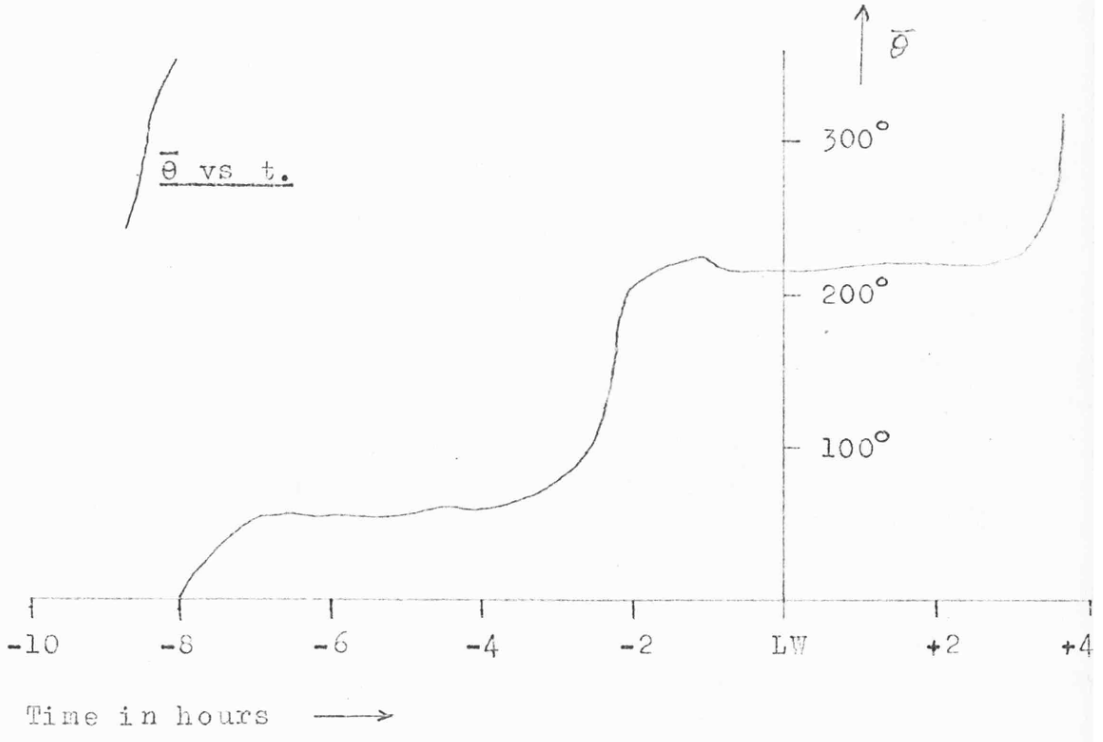

FIGURE 4·19.

POSITION H.

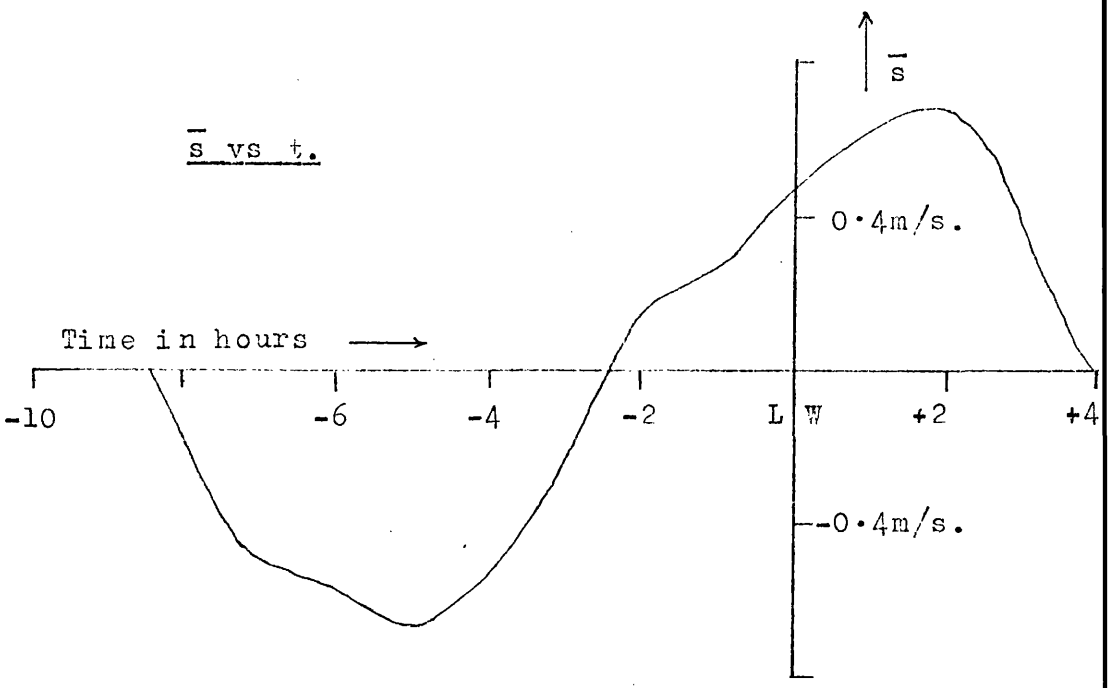

Tidal Range = 3·60 metres.

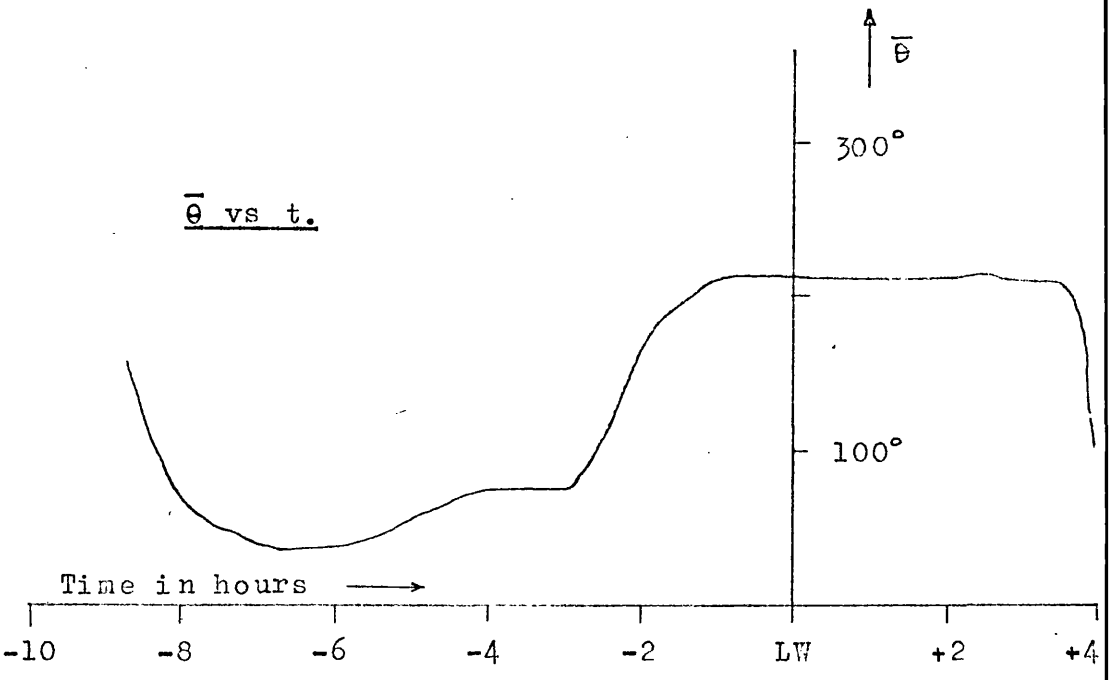

FIGURE 4·20.

POSITION M.

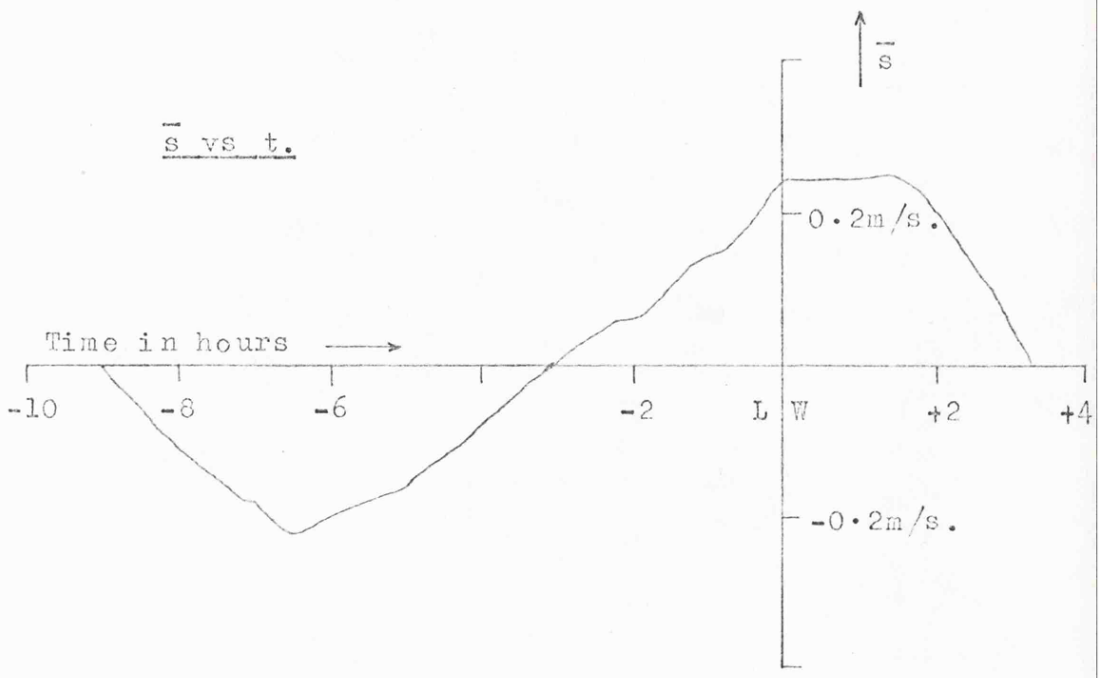

Tidal Range = 3·05 metres.

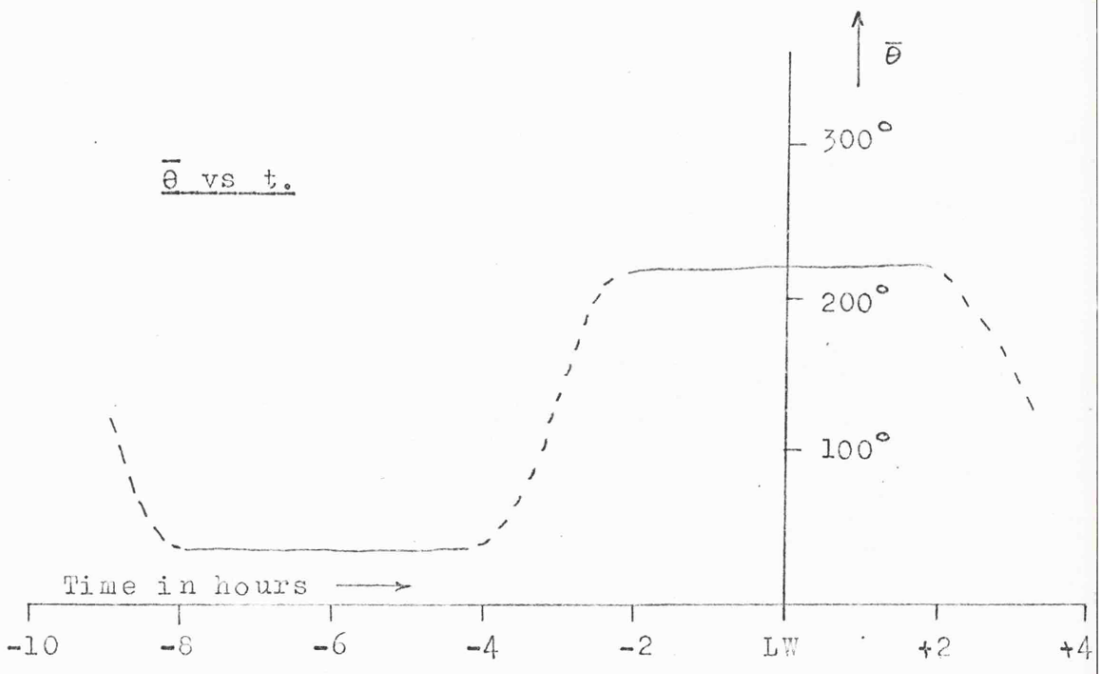

FIGURE 4.21.

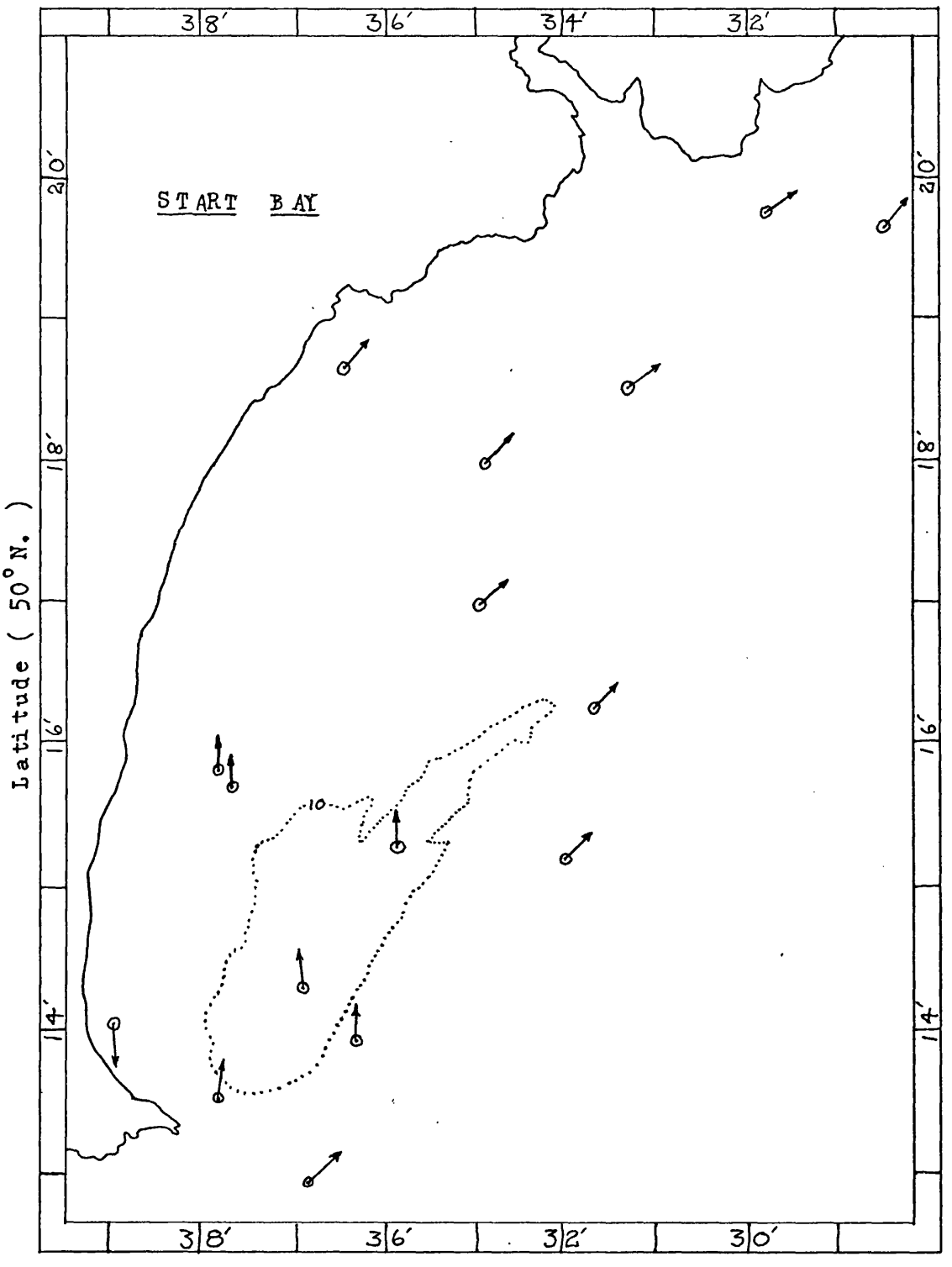

CURRENT DIRECTIONS AT HIGH WATER.

FIGURE 5.1.

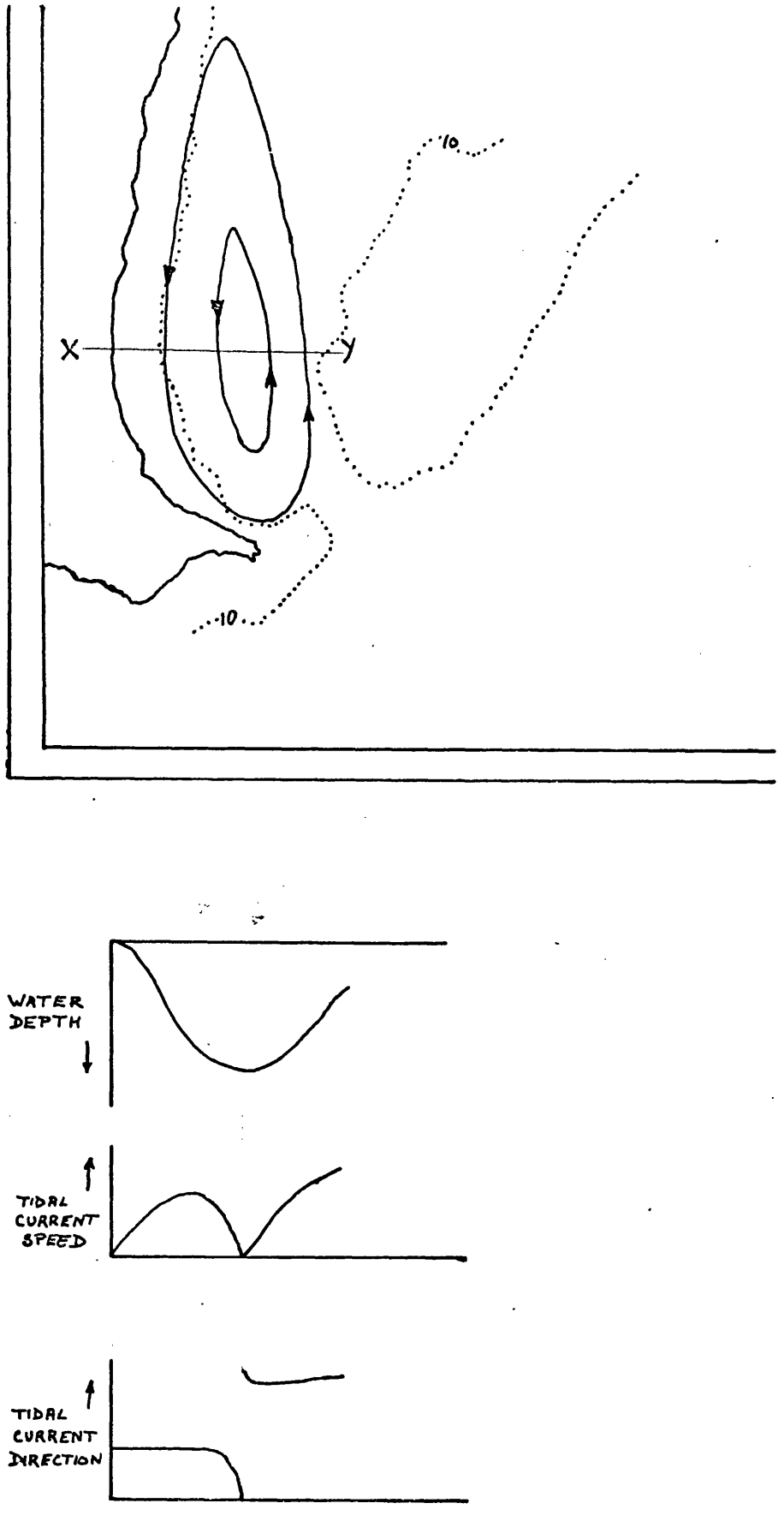

PROBLEMS ASSOCIATED WITH INTERPOLATING ACROSS AN EDDY.

FIGURE 6·1

FIGURE 7.1 Hydraulic model arranged for solution of the ebb flow.
The grid corresponds to 1 minute intervals of latitude and longitude

FIGURE 7.2 A typical float track

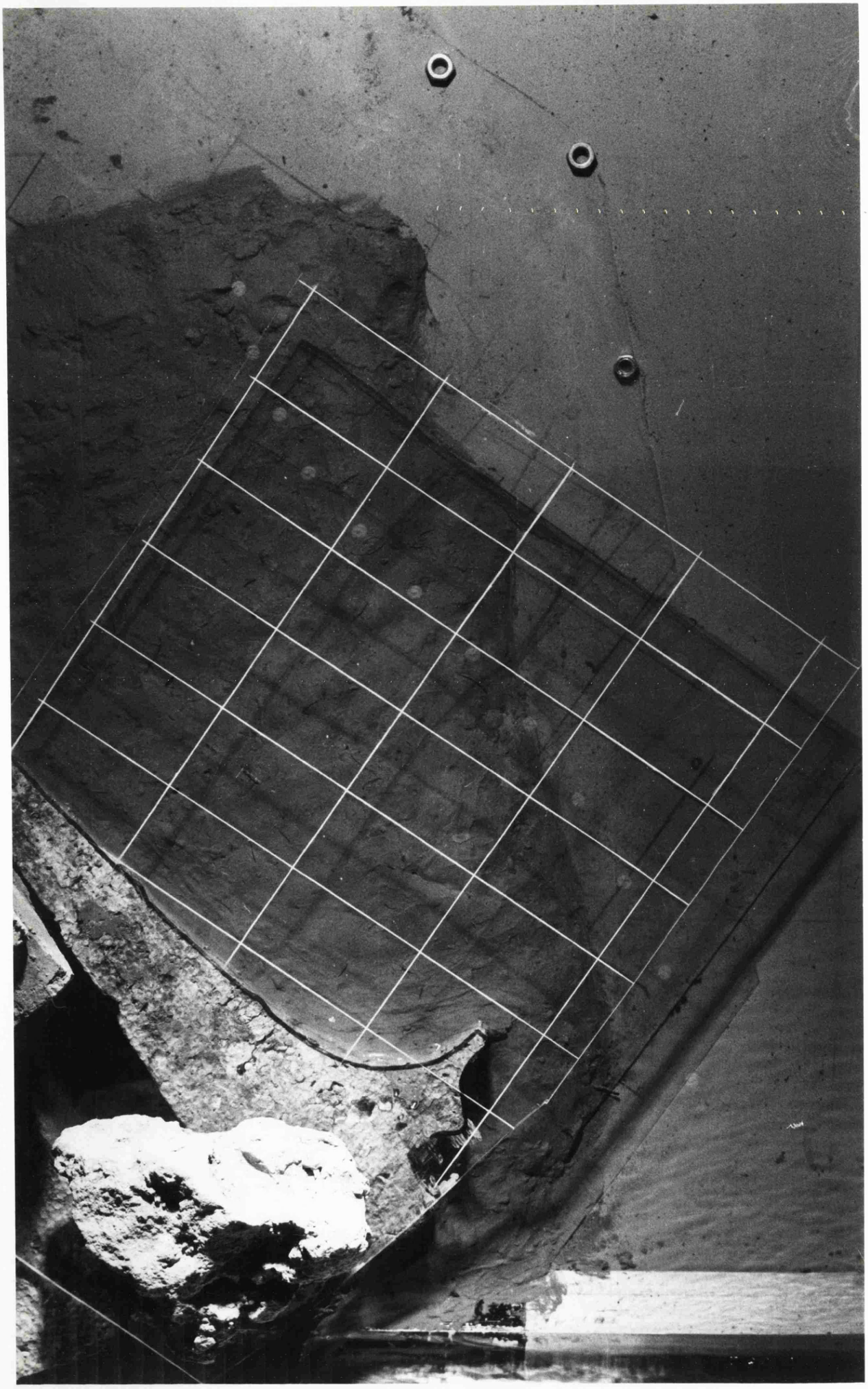

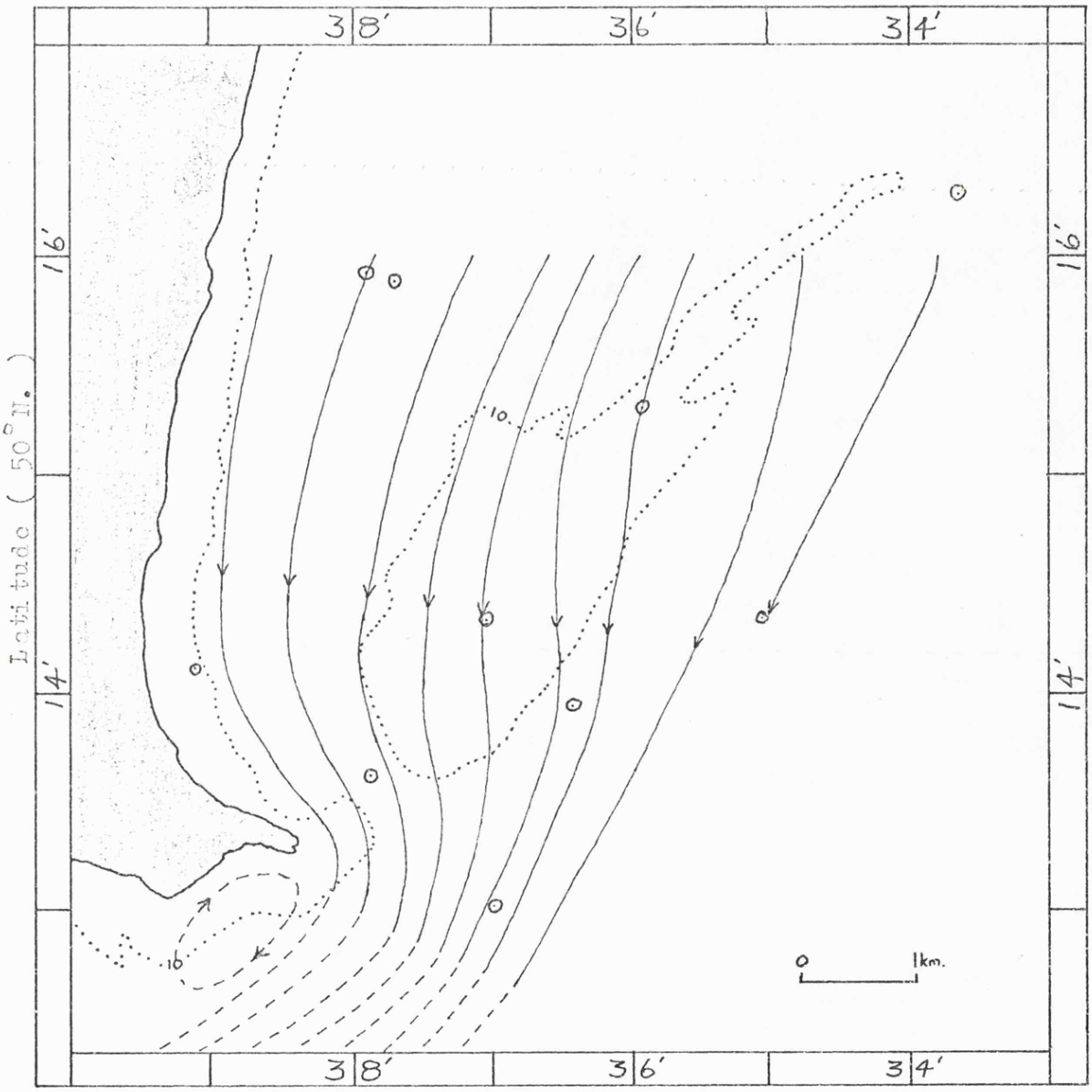

THE EBB FLOW PATTERN AT LOW WATER

FOR A TIDAL RANGE OF 4.00 METRES.

FIGURE 7.3.

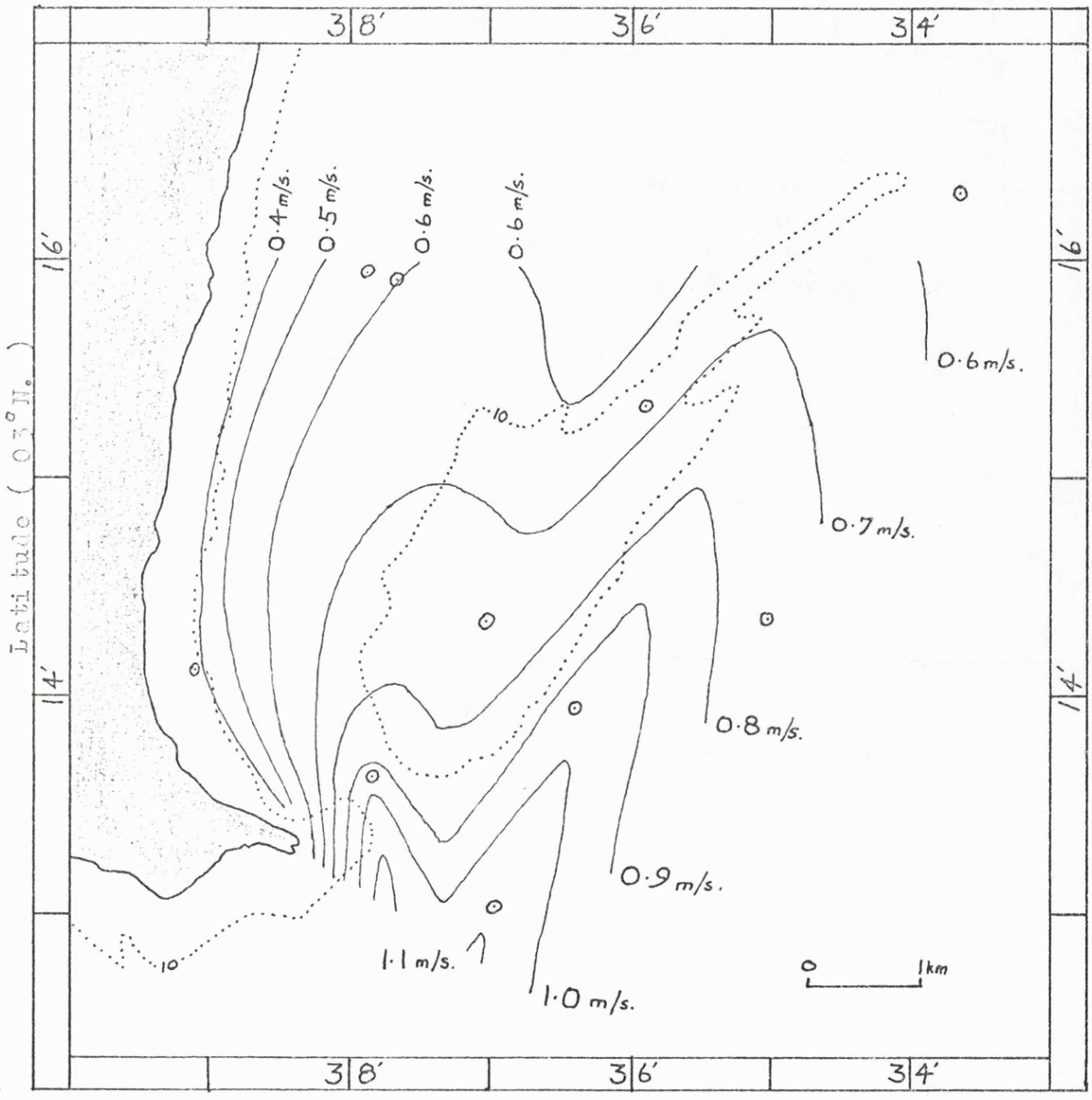

Longitude (50° W.)

THE EBB CURRENT SPEED CONTOURS AT LOW WATER FOR A TIDAL RANGE OF 4.00 METRES.

FIGURE 7.4.

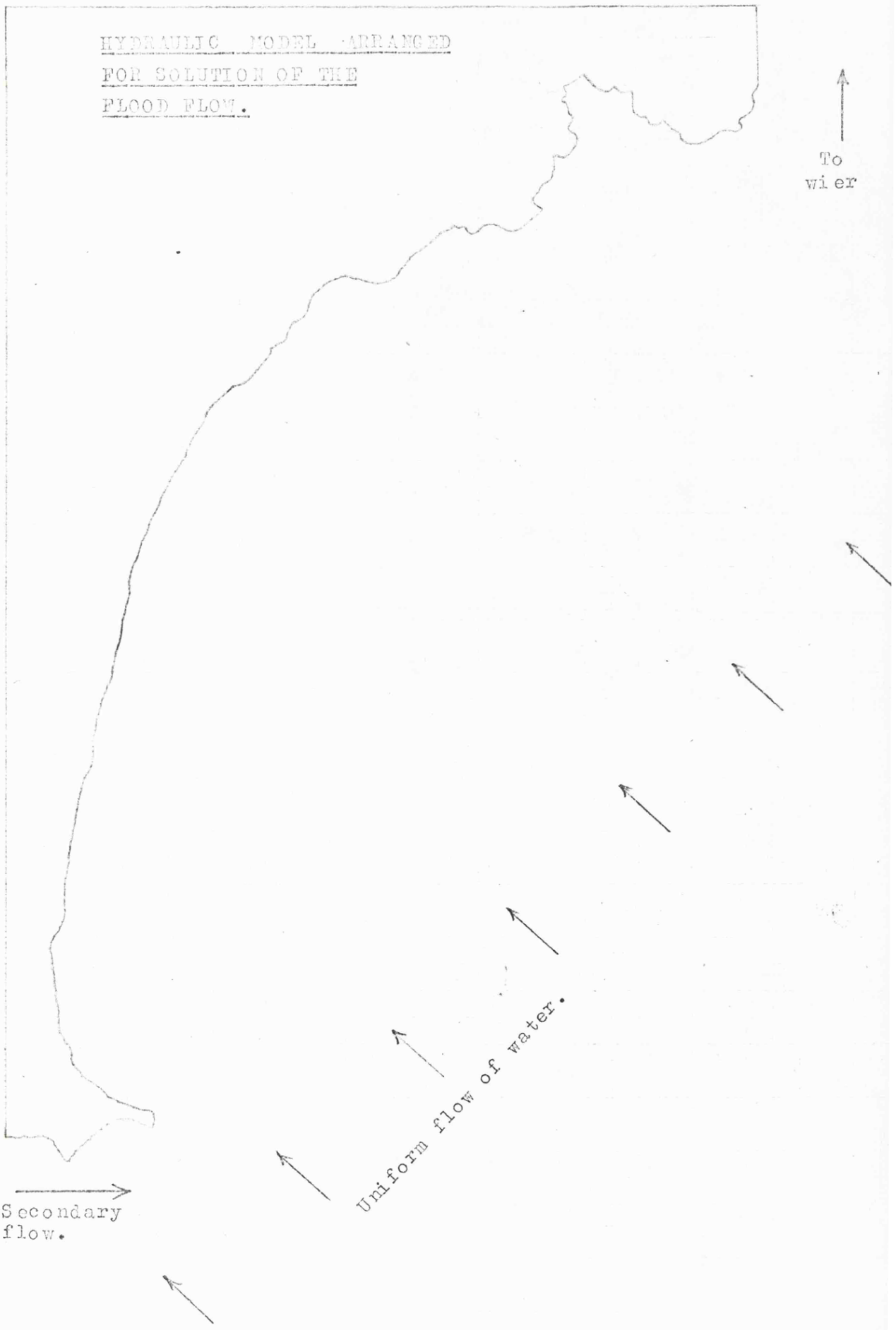
HYDRAULIC MODEL ARRANGED
FOR SOLUTION OF THE
FLOOD FLOW.
To
wier
Uniform flow of water.
Secondary
flow.

FIGURE 7·5.

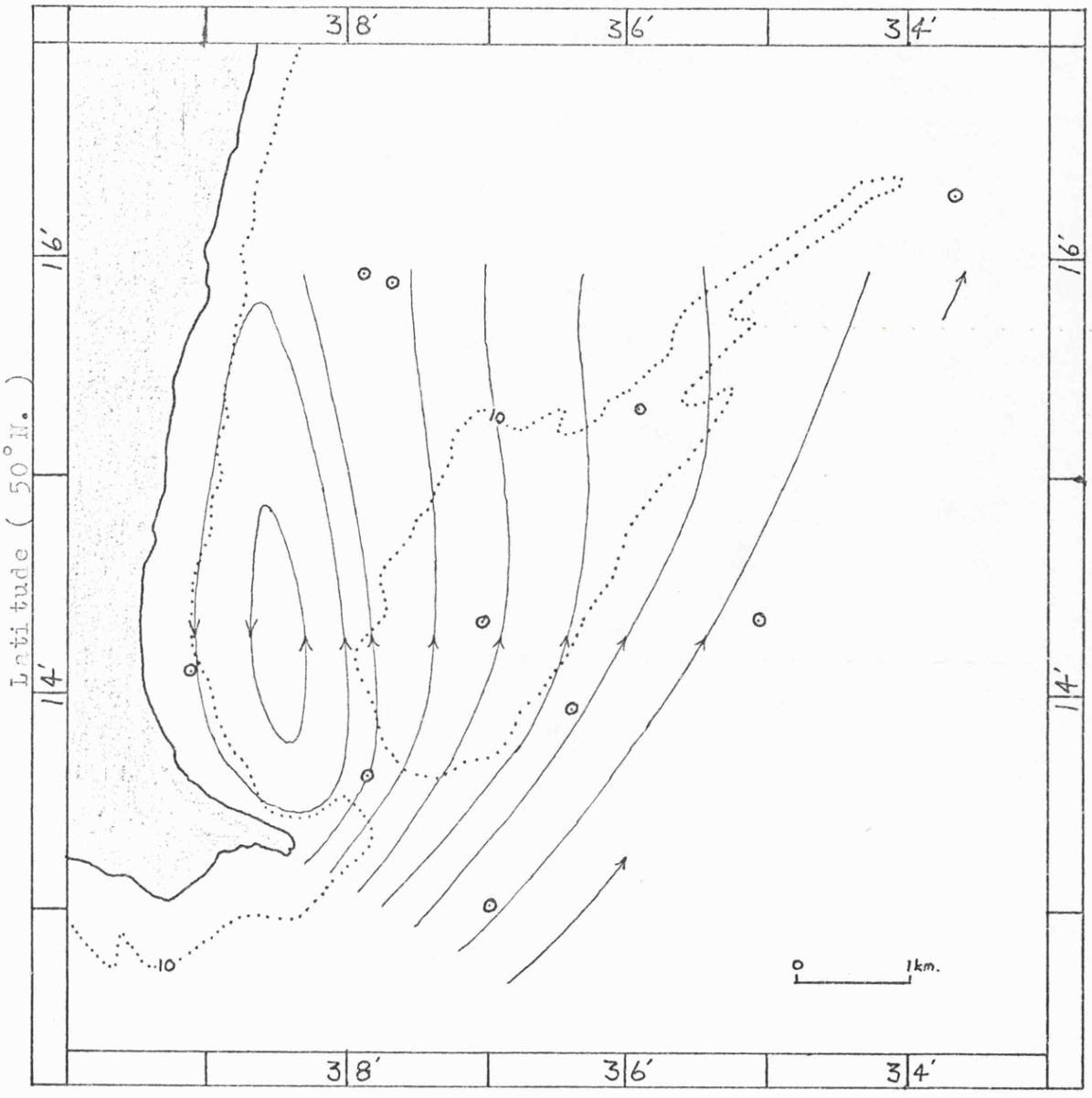

THE FLOOD FLOW PATTERN AT HIGH WATER

FOR A TIDAL RANGE OF 4.00 METRES.

FIGURE 7.6.

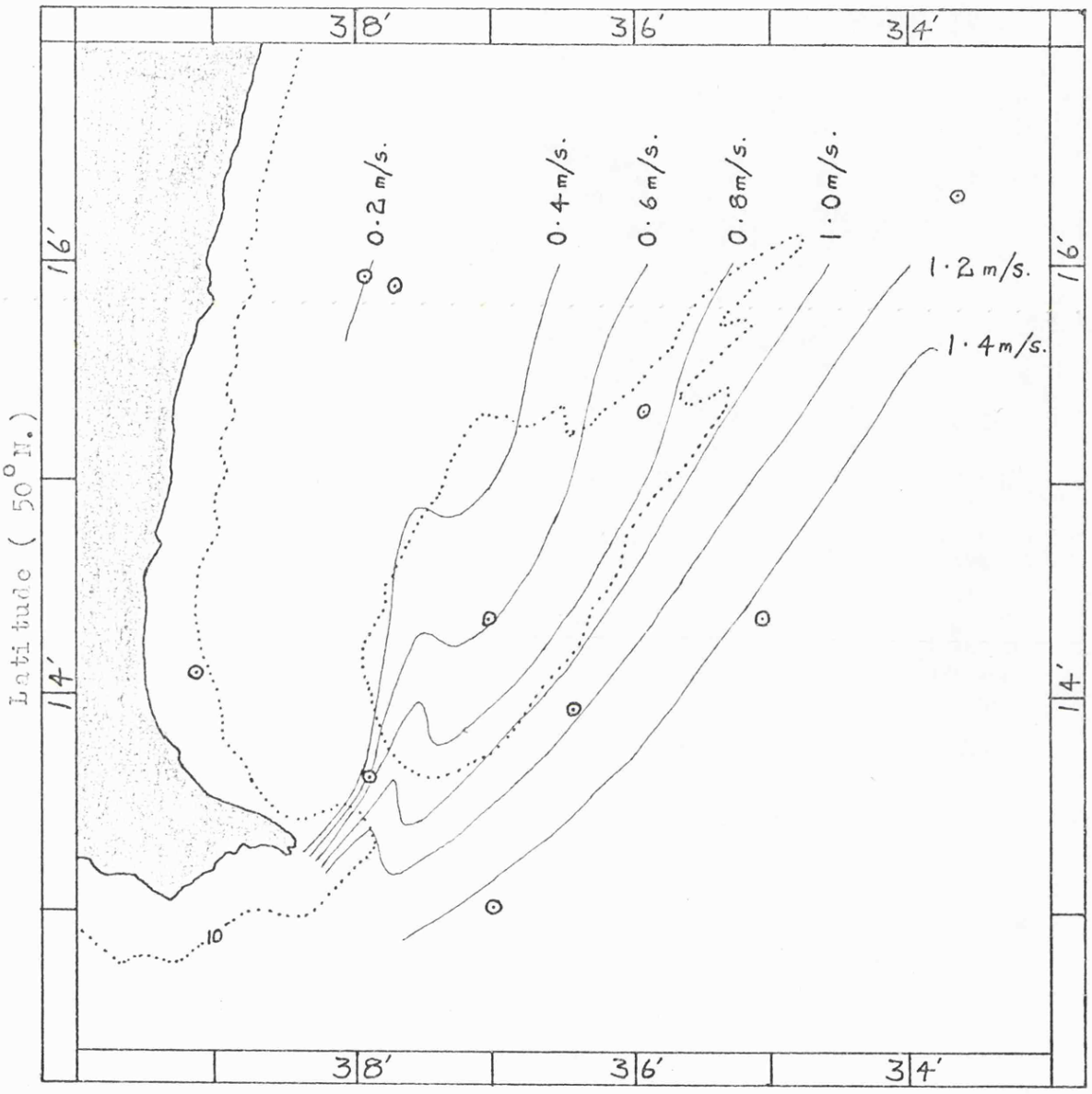

THE FLOOD CURRENT SPEED CONTOURS AT HIGH WATER FOR A TIDAL RANGE OF 4.00 METRES.

FIGURE 7.7.

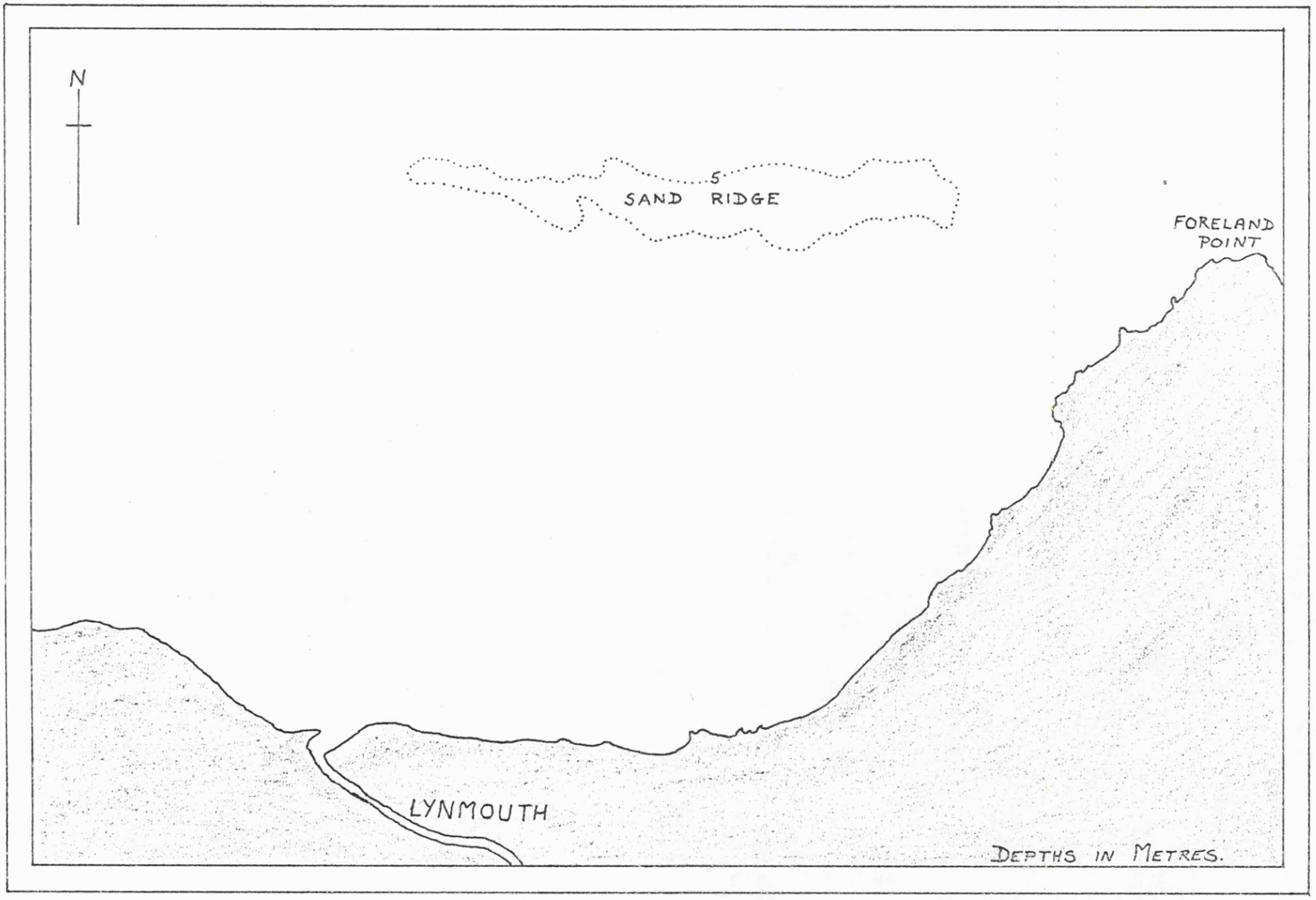

LYNMOUTH BAY.

FIGURE 8-1.

POSITION K.

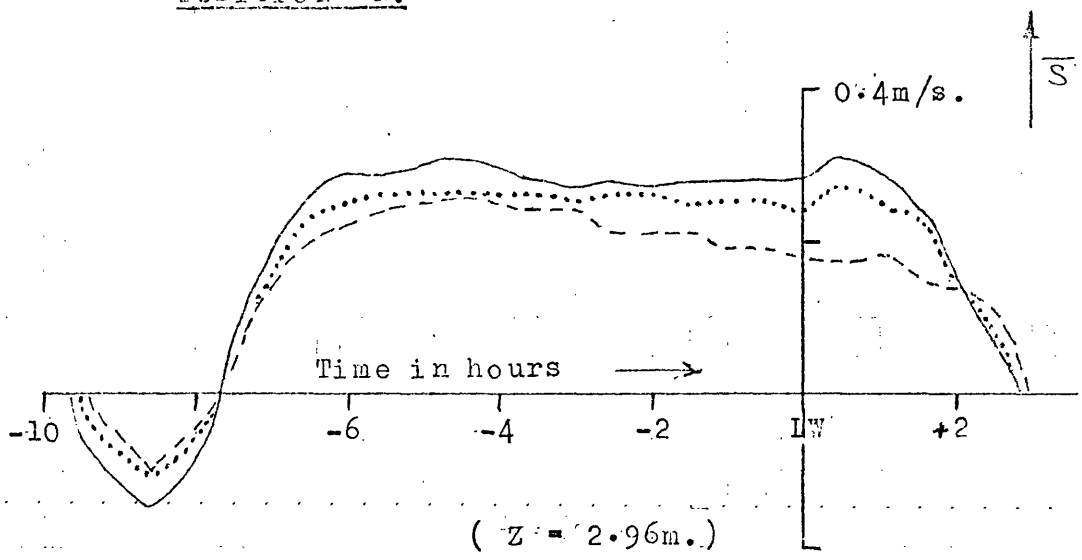

---- 1½ metre reading.

····· 3 metre reading.

—— 6 metre reading.

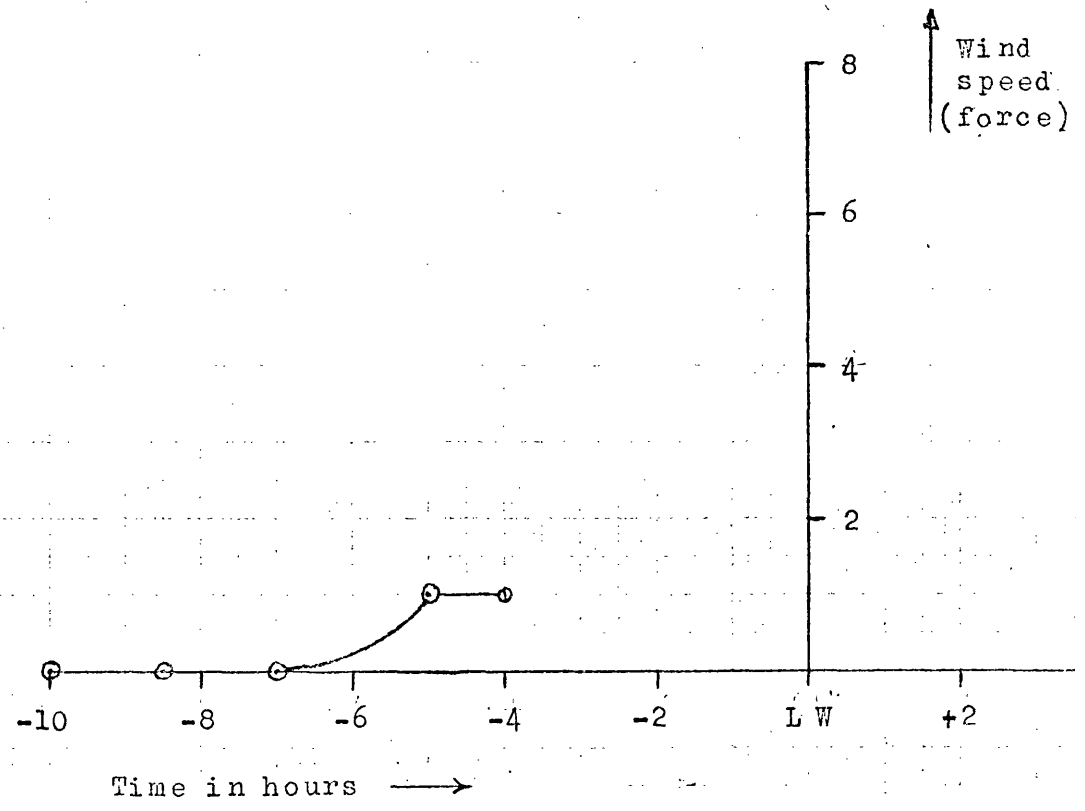

FIGURE App. 1·1A.

POSITION N.

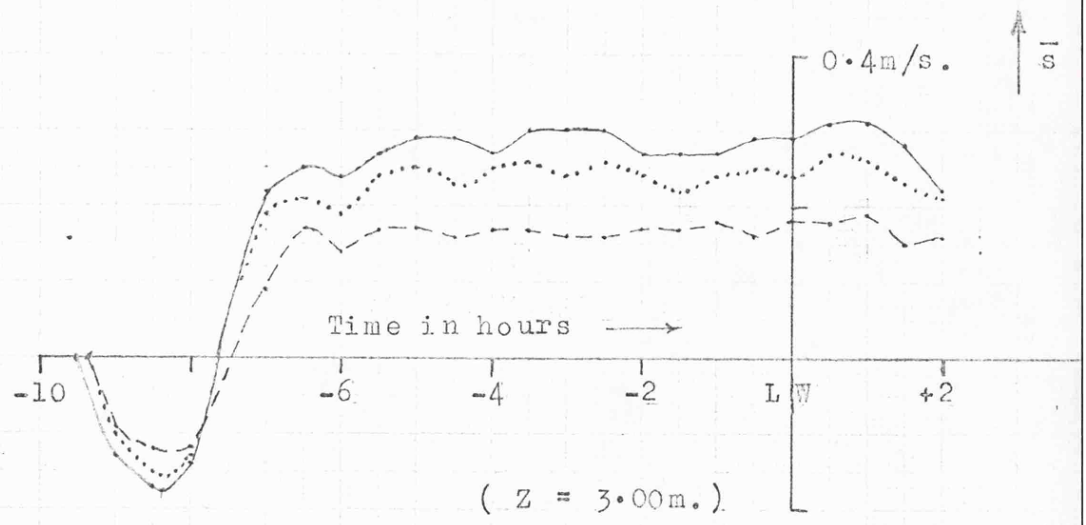

---- 1½ metre reading.

····· 3 metre reading.

—— 6 metre reading.

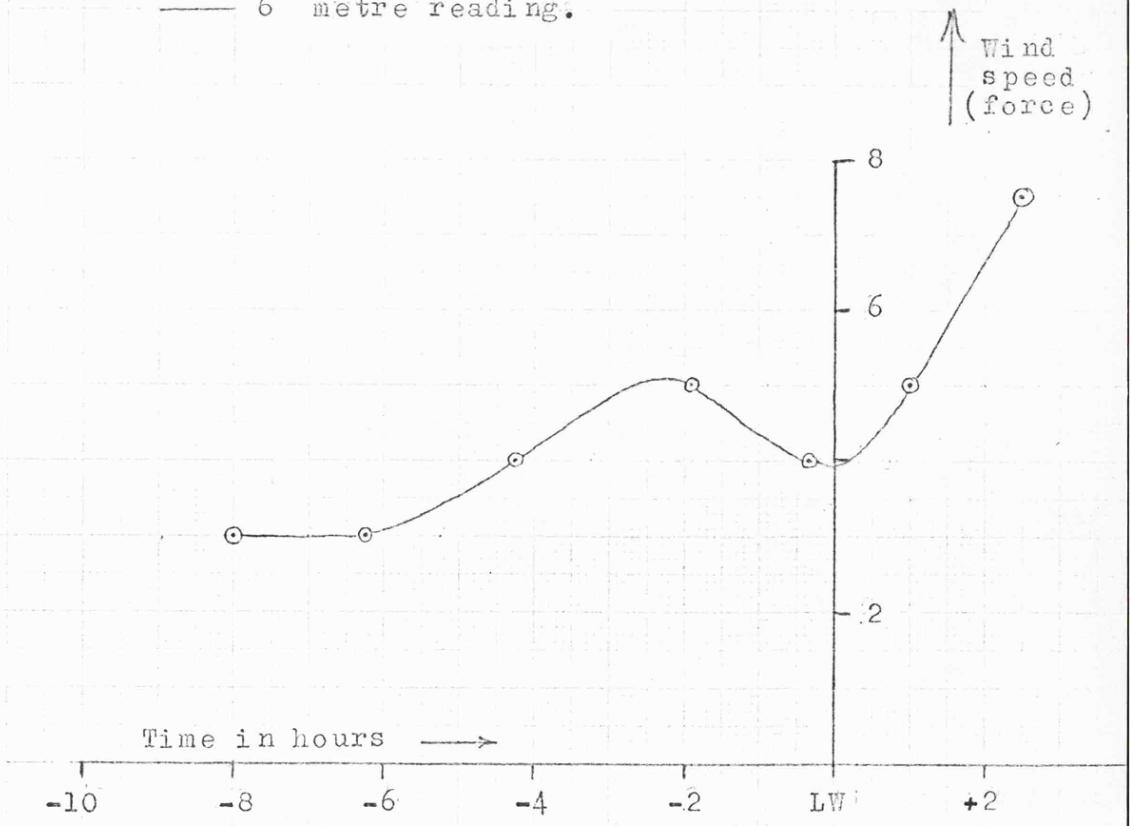

FIGURE App. 1·13.

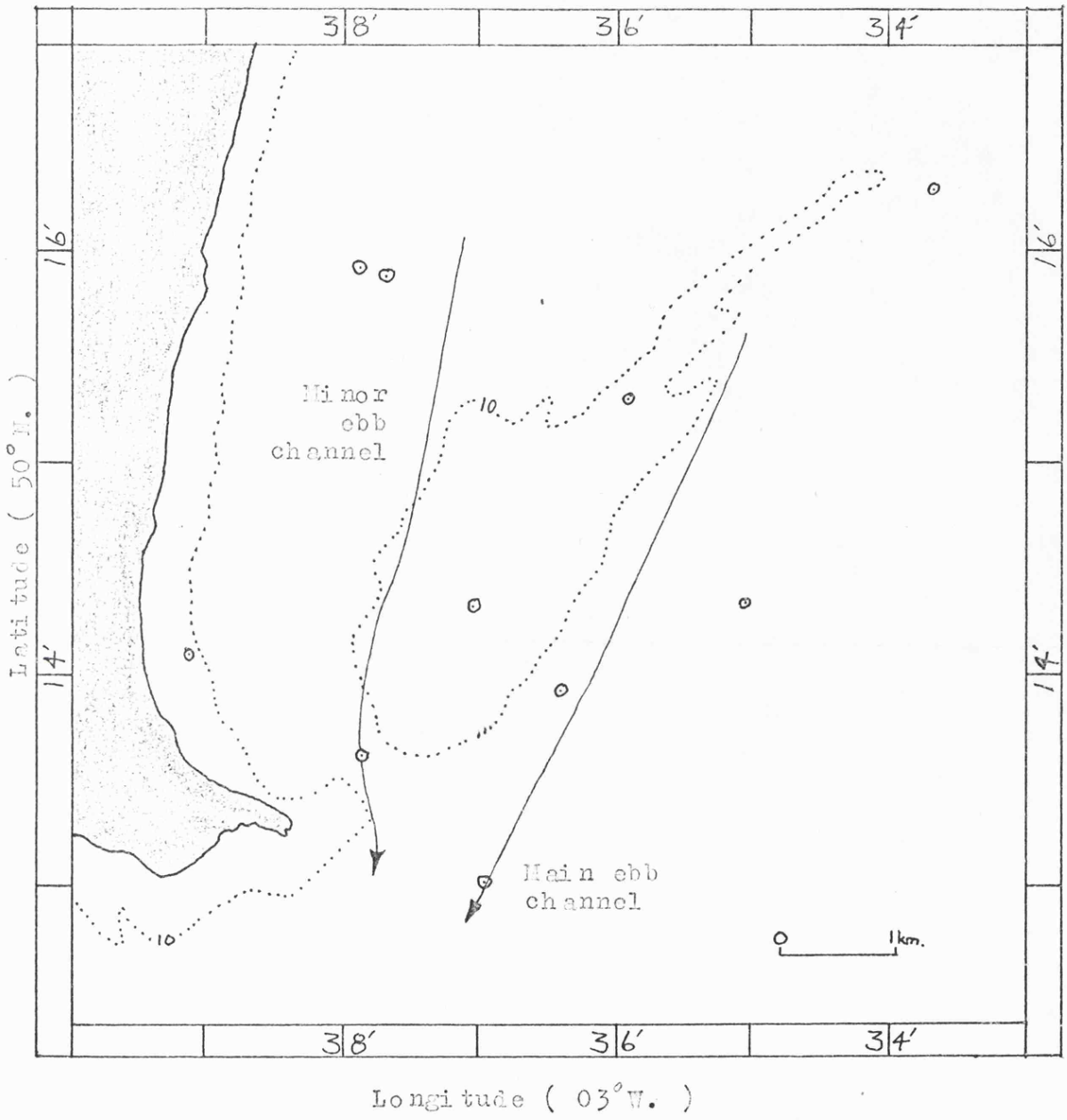

THE EBB FLOW CHANNELS AT LOW WATER.

FIGURE App. 3.1.

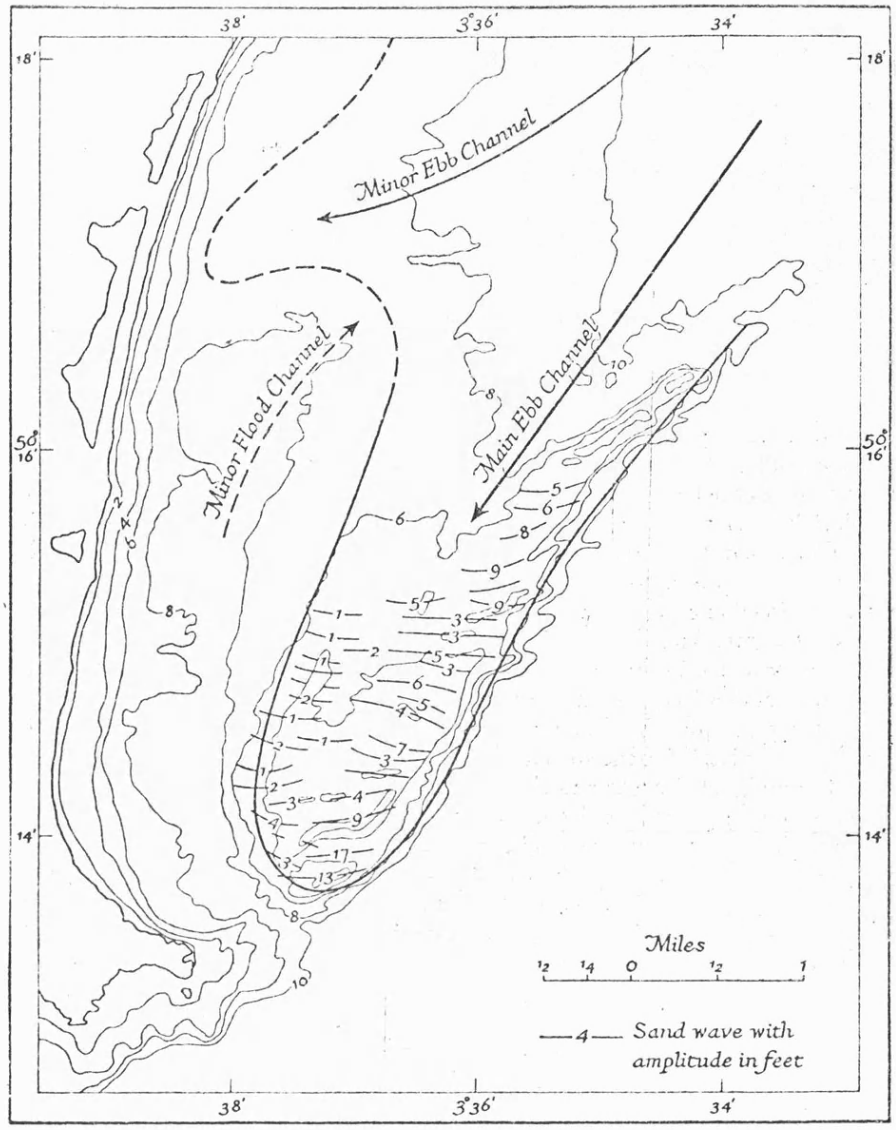

Fig. 6. Ebb-flood pattern of banks and channels in the southern part of Start Bay; associated sand waves of the Skerries Bank are also shown

REPRODUCTION OF ROBINSON'S

FIGURE 6.

FIGURE App. 3.2.

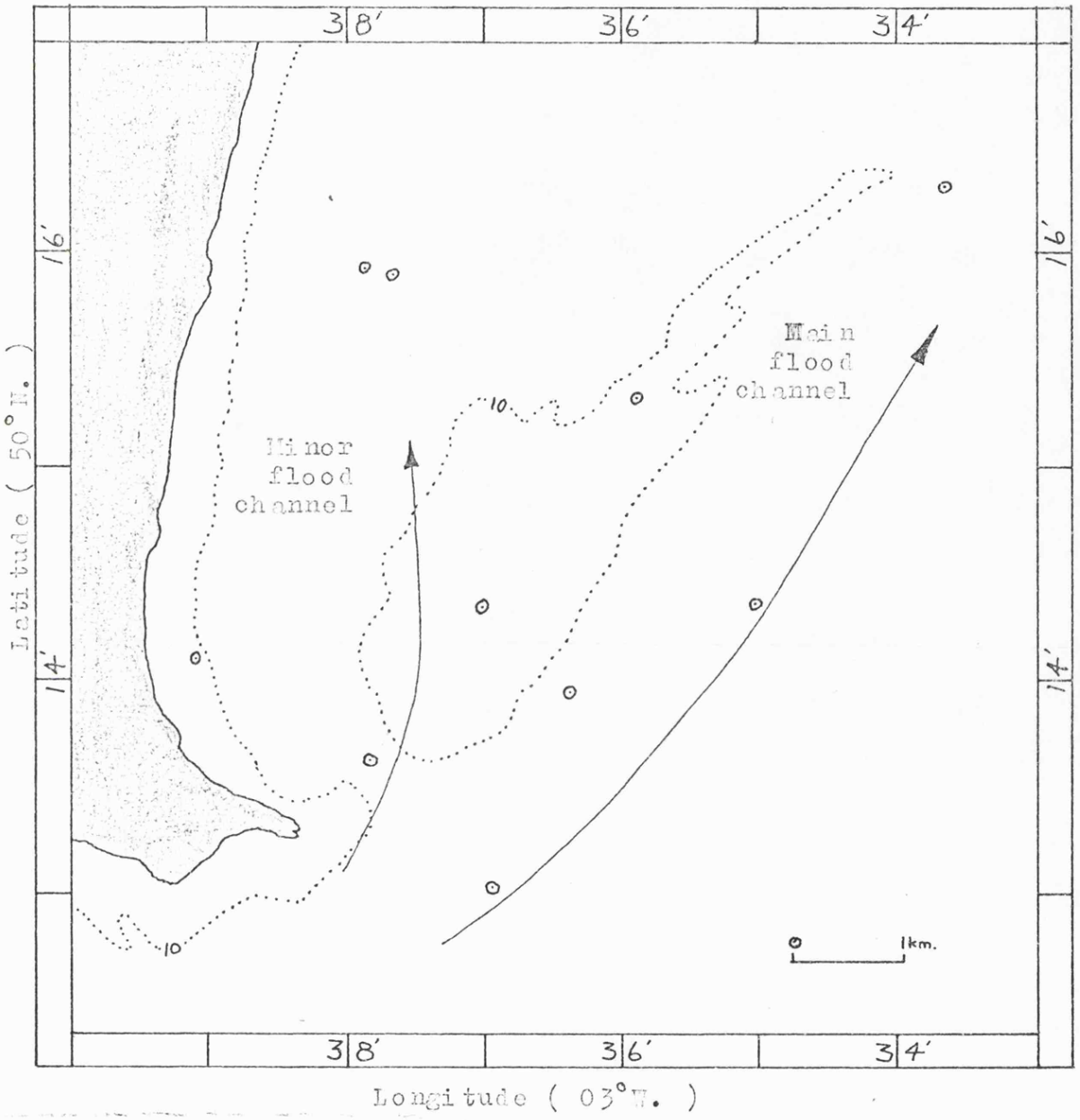

THE FLOOD FLOW CHANNELS AT HIGH WATER.

FIGURE App. 3.3.

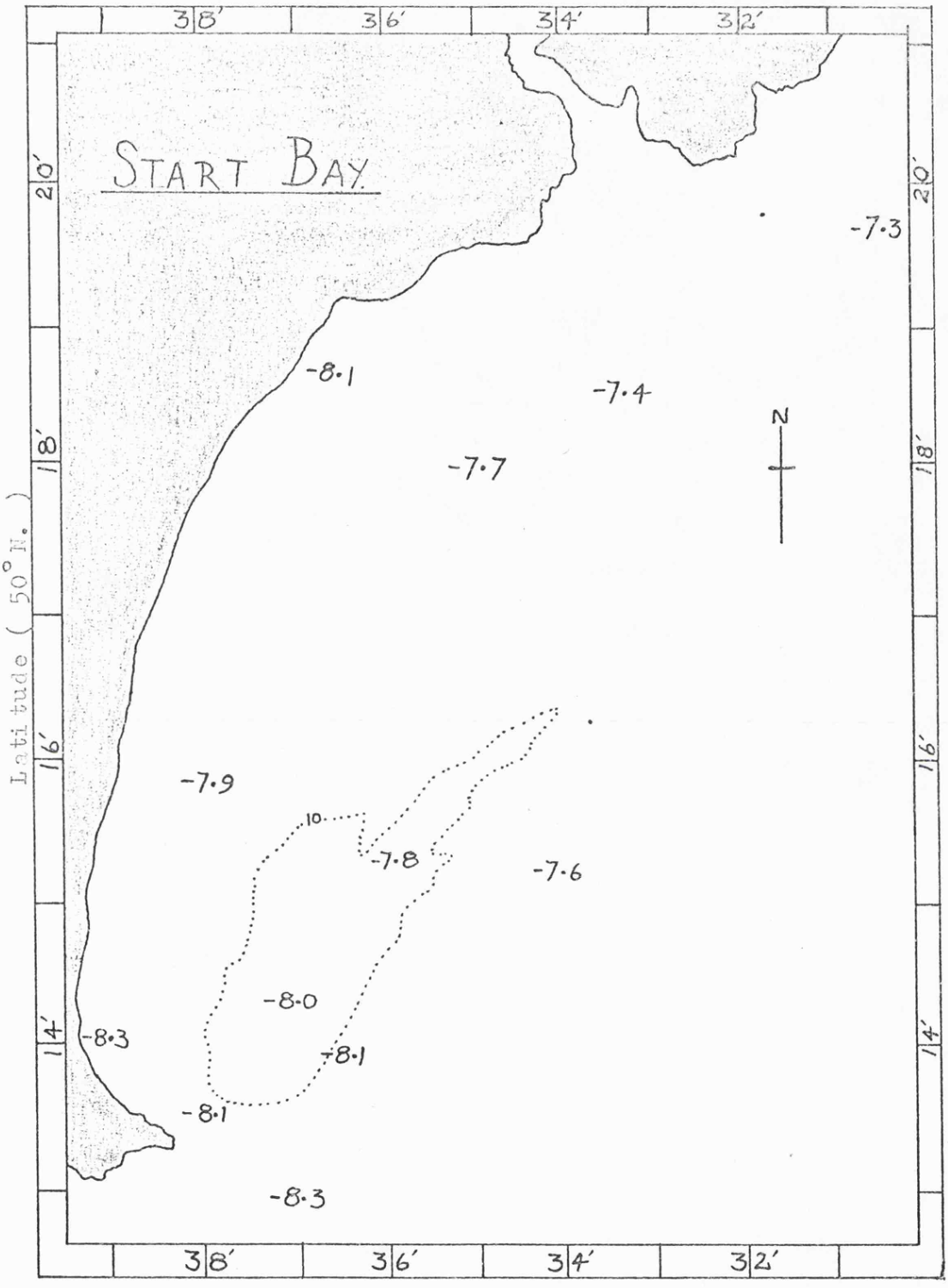

VALUES OF p. (hours)

FIGURE App. 3.4.

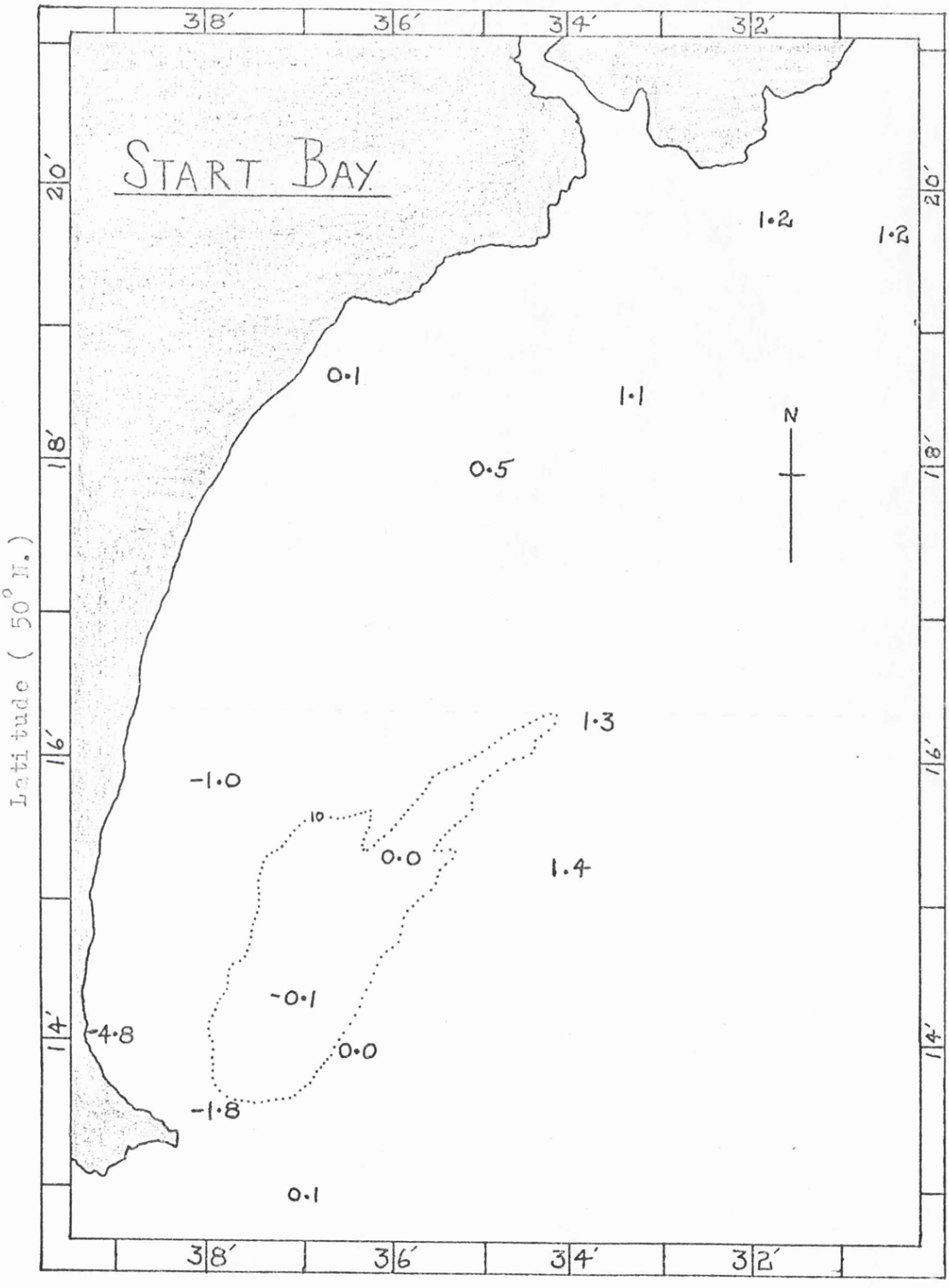

VALUES OF q. (hours)

FIGURE App. 3.5.

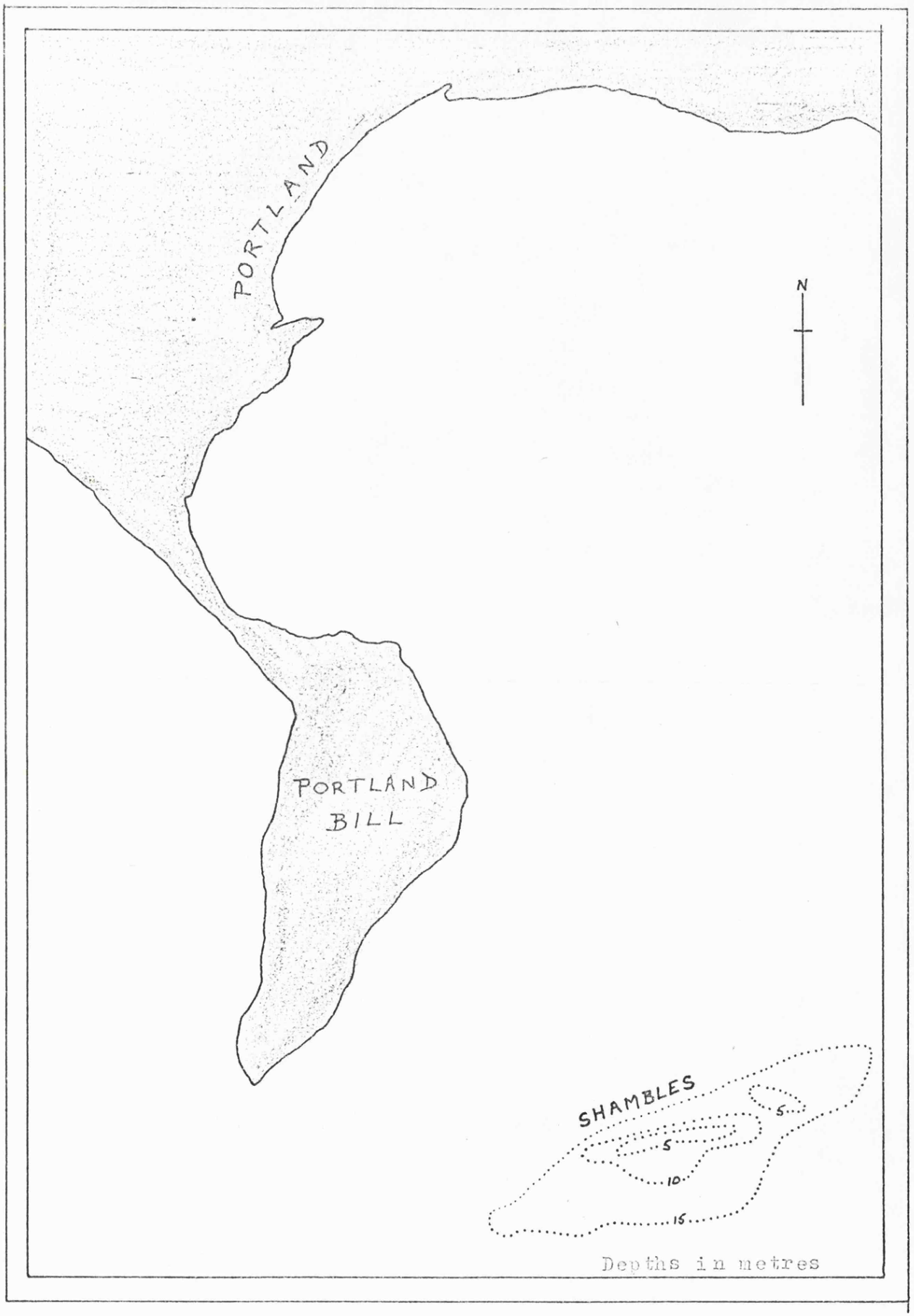

THE SHAMBLES.

FIGURE App. 3.6.